Lepton Flavor Violation in Supersymmetric Seesaw III Models

Diplomarbeit

von

Christof Weiß

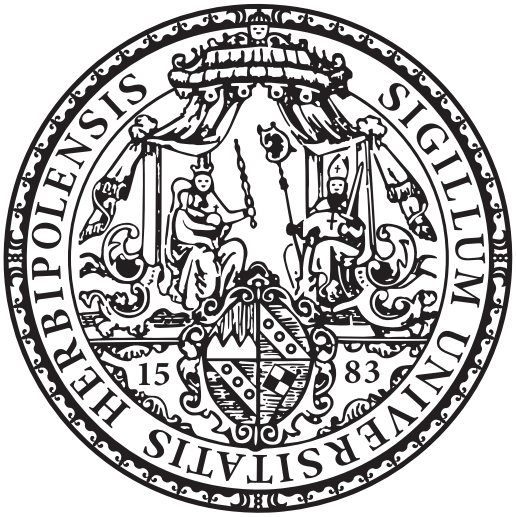

vorgelegt bei

Prof. Dr. Werner Porod

1. März 2012

Lehrstuhl für Theoretische Physik II
Institut für Theoretische Physik und Astrophysik
Julius-Maximilians-Universität Würzburg

Zusammenfassung

Seit der Beobachtung von Flavor-Oszillationen zwischen den drei Generationen von Neutrinos sind teilchenphysikalische Modelle mit masselossen Neutrinos nicht mehr mit experimentellen Daten vereinbar. Eine vielversprechende Möglichkeit, die benötigten sehr kleinen Massen zu erklären, ist der Seesaw-Mechanismus, der zusätzliche schwere Teilchen einführt. Diese können als Eichsingulett (Seesaw Typ I), skalares Eichtriplett (Typ II) oder fermionisches Eichtriplett (Typ III) unter der elektroschwachen $SU(2)_L$ Eichgruppe realisiert werden. Der letztergenannte Fall wird in dieser Arbeit behandelt.

Im experimentell gut bestätigten Standardmodell der Teilchenphysik treten allerdings noch weitere Schwierigkeiten auf, wozu unter anderem das Hierarchieproblem, die Vereinigung der Eichkopplungen sowie die Problematik der Dunklen Materie zählen. Ein viel diskutierter Ansatz zur Lösung dieser Probleme ist die Supersymmetrie, die in ihrer minimalen Realisierung zu jedem Teilchen des Standardmodells einen supersymmetrischen Partner mit unterschiedlichem Spin postuliert. In der vorliegenden Arbeit wird die Einbettung des Seesaw Mechanismus Typ III in dieses minimale supersymmetrische Standardmodell diskutiert.

Dabei werden besonders die phänomenlogischen Eigenschaften im Hinblick auf Lepton-Flavor verletzende Prozesse untersucht. Die Verzweigungsraten für solche Zerfälle im Niederenergiebereich sind stark beschränkt durch die bisher erfolglose Suche in entsprechenden Experimenten. Unter Berücksichtigung dieser Beschränkungen wird zunächst der Parameterraum des Modells untersucht. Im zweiten Schritt werden für geeignete Parameterkonstellationen die Lepton-Flavor verletzenden Zerfälle der supersymmetrischen Teilchen – besonders des zweitleichtesten Neutralinos – betrachtet und ihr Entdeckungspotential am derzeit leistungsstärksten Teilchenbeschleuniger LHC diskutiert.

Contents

1 Introduction **1**

2 Neutrino physics **3**
2.1 Neutrino masses and flavor oscillations 3
2.2 Neutrino oscillation experiments 4
2.3 The tri-bi-maximal mixing matrix 5

3 Supersymmetry **6**
3.1 Motivation 6
3.2 Basic concepts 7
3.3 The MSSM 8
3.4 Supersymmetry breaking and unification 10
3.5 Particle content 11
3.5.1 Neutralinos 11
3.5.2 Charginos 12
3.5.3 Sleptons and squarks 12
3.5.4 Gluino 13
3.6 R-parity 14

4 The supersymmetric seesaw mechanism **15**
4.1 Seesaw type I 16
4.2 Seesaw type II 18
4.3 Seesaw type III 19
4.3.1 Three **24**-plets 20
4.3.2 Two **24**-plets 21
4.4 Effects on the mass spectrum 23

5 Rare lepton decays **24**
5.1 Experimental low energy constraints 24
5.2 Lepton flavor violation in the slepton sector 25
5.3 Mass insertion approximation 26

6 Studies of the parameter space **29**
6.1 Effects of the seesaw scale 30
6.2 The reactor angle θ_{13} and the Dirac phase δ 32
6.3 Influence of the R matrix 35
6.3.1 Real case 36
6.3.2 Complex case 43
6.4 Three-body decays 44
6.5 Other low energy observables 45

7 LHC phenomenology of lepton flavor violating decays **46**
7.1 Lepton flavor violating decays of the $\widetilde{\chi}_2^0$ 46
7.2 Parameter scans at fixed BR($\mu \to e\gamma$) 49
7.3 Branching ratios and cross sections 53
7.4 Monte Carlo study 55

8 Summary and outlook **60**

A Input file **63**

References **64**

List of Figures **72**

List of Tables **75**

Chapter 1

Introduction

At the present time promising progress is taking place in particle physics, especially due to new experimental explorations in energy ranges never reached before which are being performed by the Large Hadron Collider (LHC) [1] at CERN in Geneva, Switzerland. In the first run, it collides protons at total center of mass energies of $\sqrt{s} = 7$ TeV and 8 TeV, while in the second period from late 2014 on it will be run at $\sqrt{s} = 14$ TeV with the aim to collect data up to an integrated luminosity of 100 fb^{-1}. The motivation to explore these energy ranges is, on the one hand, to complete the picture of the well-tested Standard Model (SM) of particle physics by the discovery of the Higgs boson. On the other hand, since this model still has some theoretical problems, different extensions are under discussion. The search for physics beyond the Standard Model is the second main purpose of the LHC and of the two universal detectors ATLAS [2] and CMS [3]. In particular, a promising candidate for this extension is supersymmetry (SUSY), which relates fermionic and bosonic degrees of freedom, postulating superpartners with different spin properties to the SM particles, and provides a solution to many open questions. Among these are the hierarchy problem, the unification of gauge couplings and the dark matter issue [4].

Besides the LHC, other experiments are in search of new physics, too: Since the first observation of neutrino flavor oscillations by several experiments [5–9], neutrinos cannot be considered massless anymore. To describe neutrino masses within the context of the SM or minimal realizations of SUSY, these models have to be extended. A natural way to explain the tiny neutrino masses is the so-called seesaw mechanism [10–13], which introduces additional heavy particles. One of the three possible realizations is the seesaw type III [14] where these new particles are fermionic triplets under the $SU(2)_L$ gauge group.

In general, there is no reason why such flavor mixing should not appear among the charged leptons since they are isodoublet partners of the neutrinos. However, when we implement neutrino masses into the SM, only the neutrinos carry the flavor mixing information. Therefore, the rare lepton decays like $\mu \to e\gamma$ are proportional to the small neutrino masses over the masses of the W bosons, leading to tiny branching ratios. In supersymmetric models, the situation is different: The diagrams including

superpartners of leptons enhance these branching ratios drastically, since their mass parameters can obtain flavor violating entries induced by the seesaw mechanism.

The rare lepton decays are probed by several experiments [15–18] which have not found any signal yet, so that there are strong constraints on models where large branching ratios appear. If the ongoing searches for such lepton flavor violating (LFV) decays find events and determine the branching ratios, this would be a considerable hint to physics beyond the SM. In seesaw models, the specific input parameters could be determined more precisely, since the branching ratios depend on these quantities. If the searches remain unsuccessful, there will be even tighter constraints leading to strong limitations right up to exclusions of some of the models.

In this thesis we consider an implementation of the type III seesaw mechanism into a minimal supersymmetric framework. Inspired by [19], we study the parameter space to find regions in accordance with the experimental low energy constraints. After this, we look at possible lepton flavor violating decays of the supersymmetric particles. Finally, we check interesting parameter points with respect to their phenomenology to get an estimate on whether such decays can be seen at the LHC.

The work is organized as follows: Chapter 2 shows the current status of neutrino oscillation data. In chapter 3, the main aspects of supersymmetry are summarized and all relevant parameters of our model are introduced. Chapter 4 shows the implementation of the seesaw mechanism within this model and the influence on the mass spectrum, while chapter 5 treats the current experimental constraints from rare lepton decays as well as an approximate description of them. The results of the extensive parameter study are exhibited in chapter 6; the final chapter 7 discusses possible lepton flavor violating processes and their LHC phenomenology.

Chapter 2

Neutrino physics

2.1 Neutrino masses and flavor oscillations

To receive conservation of energy and momentum in the description of the radioactive β-decay, W. Pauli postulated the existence of the neutrinos in 1930. From measurements ot these decays, only an upper mass limit could be determined. In 1957, B. Pontecorvo proposed for the first time the idea of neutrino flavor oscillations [20], which are explained by the existence of the neutrinos in three mass eigenstates ν_i ($i = 1, 2, 3$) and three different flavor eigenstates ν_α ($\alpha = e, \mu, \tau$). If the leptonic Yukawa matrix Y_e (cf. Eq. 3.12) is diagonal, we can write the unitary transformation relating these bases as

$$|\nu_\alpha\rangle = U^{-1}_{\alpha i}|\nu_i\rangle \qquad \text{and} \qquad |\nu_i\rangle = U_{i\alpha}|\nu_\alpha\rangle. \tag{2.1}$$

The matrix U is usually parametrized in the following way [21]:

$$\begin{aligned} U &= \begin{pmatrix} 1 & 0 & 0 \\ 0 & c_{23} & -s_{23}e^{i\delta} \\ 0 & s_{23} & c_{23} \end{pmatrix} \times \begin{pmatrix} c_{13} & 0 & -s_{13} \\ 0 & 1 & 0 \\ s_{13}e^{-i\delta} & 0 & c_{13} \end{pmatrix} \times \begin{pmatrix} c_{12} & -s_{12} & 0 \\ s_{12} & c_{12} & 0 \\ 0 & 0 & 1 \end{pmatrix} \times A \\ &= \begin{pmatrix} c_{12}c_{13} & s_{12}c_{13} & s_{13}e^{-i\delta} \\ -s_{12}c_{23} - c_{12}s_{23}s_{13}e^{i\delta} & c_{12}c_{23} - s_{12}s_{23}s_{13}e^{i\delta} & s_{23}c_{13} \\ s_{12}s_{23} - c_{12}c_{23}s_{13}e^{i\delta} & -c_{12}s_{23} - s_{12}c_{23}s_{13}e^{i\delta} & c_{23}c_{13} \end{pmatrix} \times A \end{aligned} \tag{2.2}$$

with the majorana phase matrix

$$A = \begin{pmatrix} e^{-i\alpha_1/2} & 0 & 0 \\ 0 & e^{-i\alpha_2/2} & 0 \\ 0 & 0 & 1 \end{pmatrix} \tag{2.3}$$

where $c_{ij} = \cos(\theta_{ij})$, $s_{ij} = \sin(\theta_{ij})$. The Dirac phase δ contains information about CP violation, α_1 and α_2 are Majorana phases that only appear in the case of Majorana neutrinos. U is the so-called Pontecorvo-Maki-Nakagawa-Sakata (PMNS) matrix.

2.2 Neutrino oscillation experiments

Beginning in the late 1960s, several experiments started exploring neutrino physics. One of the first was the Homestake experiment [5], which measured the solar neutrino flux arriving at the earth and observed only a fraction of the predicted value. Other experiments also measured the flux of atmospheric [6], reactor [7] and accelerator [9, 22] neutrinos and obtained similar results. From a fit to the measured neutrino fluxes, only the squared mass differences $\Delta m^2_{ij} = m^2_i - m^2_j$ are accessible with additional hints on the Dirac phase δ. The latest best-fit values are listed in Tab. 2.1. θ_{12} is the solar neutrino mixing angle, θ_{23} the atmospheric angle and θ_{13} the reactor angle, as they appear in the PMNS matrix (Eq. 2.2), $\Delta m^2_{21} = \Delta m^2_{sol}$ is the solar, $\Delta m^2_{32} = \Delta m^2_{31} - \Delta m^2_{21} = \Delta m^2_{atm}$ the atmospheric squared mass difference.

Parameter	Best-fit $\pm 1\sigma$	
$\sin^2(\theta_{12})$	$0.312^{+0.017}_{-0.015}$	
$\sin^2(\theta_{23})$	$0.52^{+0.06}_{-0.07}$	$[\ 0.52 \pm 0.06\ ]$
$\sin^2(\theta_{13})$	$0.013^{+0.007}_{-0.005}$	$[\ 0.016^{+0.008}_{-0.006}\ ]$
$\Delta m^2_{21}/(10^{-5}\mathrm{eV}^2)$	$7.59^{+0.20}_{-0.18}$	
$\Delta m^2_{31}/(10^{-3}\mathrm{eV}^2)$	$2.50^{+0.09}_{-0.16}$	$[\ -(2.40^{+0.08}_{-0.09})\ ]$
δ	$(-0.61^{+0.75}_{-0.65})\pi$	$[\ (-0.41^{+0.65}_{-0.70})\pi\ ]$

Table 2.1: Experimental best-fit values of global neutrino data from ref. [23]; see also [24]. The values in brackets are deviations for inverse mass hierarchy.

There are two possible hierarchies for the neutrino mass spectrum: The normal hierarchy $m_1 < m_2 < m_3$ and the inverse hierarchy $m_3 < m_1 < m_2$ (Fig. 2.1). Furthermore, the value of the smallest neutrino mass is not determined yet, so that, depending on the hierarchy, $m_1 = 0$ resp. $m_3 = 0$ is still possible. As we will see later on, this case allows different physical descriptions because only two massive neutrinos have to be considered.

Assuming a small $m_1 \approx 0$, this results in neutrino masses

$$m_2 = \sqrt{\Delta m^2_{21}} \approx 8.71 \cdot 10^{-3}\ \mathrm{eV},\ m_3 = \sqrt{\Delta m^2_{31}} \approx 5.00 \cdot 10^{-2}\ \mathrm{eV}, \qquad (2.4)$$

for normal hierarchy. Using $m_3 \approx 0$, we get

$$m_2 = \sqrt{\Delta m^2_{21} - \Delta m^2_{31}} \approx 4.98 \cdot 10^{-2}\ \mathrm{eV},\ m_1 = \sqrt{-\Delta m^2_{31}} \approx 4.90 \cdot 10^{-2}\ \mathrm{eV}, \quad (2.5)$$

for inverse hierarchy.

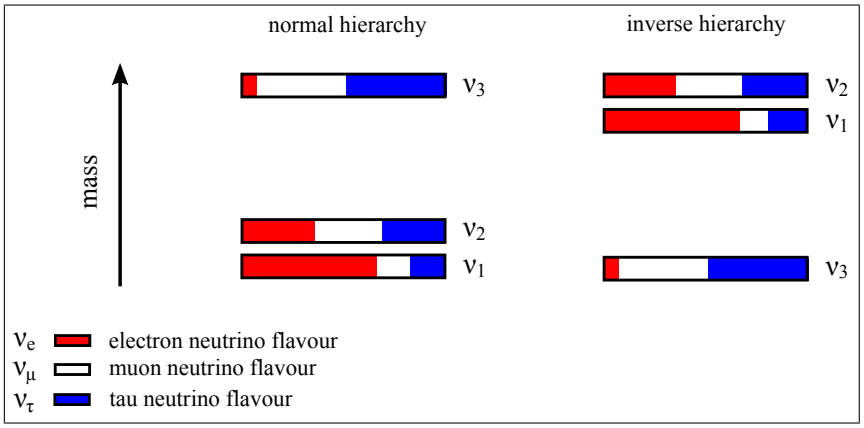

Figure 2.1: The possible neutrino mass hierarchies and their flavor composition [25].

2.3 The tri-bi-maximal mixing matrix

Before recent experimental hints to a non-zero reactor mixing angle θ_{13} were published in June 2011 [22, 23], there had only been an upper limit to that angle. Hence, the tri-bi-maximal form of the PMNS matrix given by Eq. 2.6 had been a promising realization:

$$U_{tbm} = \begin{pmatrix} \sqrt{\frac{2}{3}} & \frac{1}{\sqrt{3}} & 0 \\ -\frac{1}{\sqrt{6}} & \frac{1}{\sqrt{3}} & \frac{1}{\sqrt{2}} \\ \frac{1}{\sqrt{6}} & -\frac{1}{\sqrt{3}} & \frac{1}{\sqrt{2}} \end{pmatrix} \tag{2.6}$$

This specific form was first proposed in [26] and is the probably most interesting one of various special PMNS matrix realizations. There might be fundamental symmetries that generate this structure of the PMNS matrix which hopefully will be tested in the near future by experiments [27]. We will use the respective values of the mixing angles for most of the later calculations.

Chapter 3

Supersymmetry

3.1 Motivation

The $SU(3)_C \times SU(2)_L \times U(1)_Y$ Standard Model of particle physics achieved large succcess in explaining fundamental particle physics in the last decades. It consists of a combination of quantum chromodynamics to describe the strong interaction in the $SU(3)_C$ gauge group picture and the Glashow-Salam-Weinberg-Theory [28–30] for the description of the electroweak interactions according to the $SU(2)_L \times U(1)_Y$ gauge group. However, there are a couple of problems left which require an extension. One of the most convincing arguments is the so called hierarchy problem [31]: To explain the masses of the SM particles a non-vanishing vacuum expectation value (VEV) of the neutral Higgs component is required, which is experimentally determined by the W boson mass to $\langle H \rangle \approx 174$ GeV [31]. The 1-loop diagram in Fig. 3.1 of a fermionic particle f coupling to the Higgs field by the Langrangian term $-\lambda_f H \bar{f} f$ yields potentially large corrections to the Higgs squared mass. These corrections are proportional to an ultraviolet momentum cutoff Λ squared which is at least at a scale where new physcis appears:

$$\Delta m_H^2 \propto -\frac{|\lambda_f|^2}{8\pi^2}\Lambda^2 + ... \tag{3.1}$$

To avoid this problem without the requirement of any special fine tuning of the counter terms, a scalar particle S coupling to the Higgs field like $\lambda_S |H|^2 |S|^2$ could

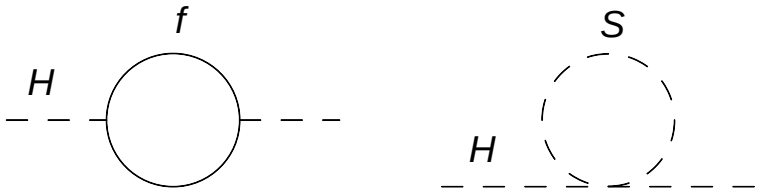

Figure 3.1: One-loop graphs for the quantum corrections to the Higgs squared mass by a fermion f (left) resp. a scalar S (right).

be introduced producing a correction

$$\Delta m_H^2 \propto \frac{\lambda_S}{16\pi^2}\Lambda^2 + ... \tag{3.2}$$

A symmetry with $\lambda_S = |\lambda_f|^2$ which introduces a bosonic partner to every SM fermion and vice versa is called a supersymmetry (SUSY) and provides a natural cancellation of the loop corrections of order Λ^2 [4].

Another deficiency of the SM is the absence of a candidate particle to explain the nature of dark matter. Assuming a special symmetry called R-Parity (cf. 3.3) that forbids the decay of the lightest supersymmetric particle (LSP), one can construct supersymmetric theories containing a neutral and stable dark matter candidate. One additional appealing feature of SUSY is the ability to construct grand unification theories (GUT) where all gauge couplings g_1, g_2, g_3 meet at a specific GUT scale M_{GUT}, which is in the minimal models usually of order $\mathcal{O}(10^{16}\text{ GeV})$.

A profound discussion of the basic properties of SUSY as well as the formalism of Weyl spinor objects can be found in many basic works like [31–35] and will not be repeated in this thesis. In the following only the features and formulas relevant for our discussions are mentioned, mostly following [31, 36]. Moreover, we will specify the precise model and the SUSY breaking mechanism used in this work and motivate the relevant parameters which will be of importance later.

3.2 Basic concepts

In order to describe SUSY, one introduces an operator Q (in general N distinct copies) that generates supersymmetry transformations of the form

$$Q|\text{Boson}\rangle = |\text{Fermion}\rangle, \qquad Q|\text{Fermion}\rangle = |\text{Boson}\rangle. \tag{3.3}$$

which fulfill the following algebra [34]

$$\begin{aligned} \left\{Q_\alpha, Q^\dagger_{\dot\beta}\right\} &= 2\sigma^\mu_{\alpha\dot\beta} P_\mu \\ \{Q_\alpha, Q_\beta\} &= \left\{Q^\dagger_{\dot\alpha}, Q^\dagger_{\dot\beta}\right\} = 0 \\ [Q_\alpha, P_\mu] &= \left[Q^\dagger_{\dot\beta}, P_\mu\right] = 0. \end{aligned} \tag{3.4a}$$

with $\sigma^\mu = (\mathbb{1}, \sigma_i)$ where σ_i are the Pauli matrices and $\alpha, \beta, \dot\alpha, \dot\beta \in \{1, 2\}$ if Q is a 2-component Weyl spinor. A supermultiplet contains corresponding single particle states which are irreducible representations of the SUSY algebra. Since Q commutes with the four-momentum squared generator $P^\mu P_\mu$, all states within a supermultiplet – called superpartners – have the same masses as long as SUSY is unbroken. In $N = 1$ SUSY, Q also commutes with the generators of the SM gauge transformations; in this case the superpartners carry the same gauge quantum numbers. One can show

that for each supermultiplet the number of bosonic and fermionic degrees of freedom must be equal [31]. The simplest realization is a chiral supermultiplet containing a two-component Weyl fermion ψ_i and two real scalars or one complex scalar ϕ_i. Additionally, an auxiliary field F_{aux} is required so that the SUSY algebra closes off-shell. The other relevant type is a vector supermultiplet with a spin-1 vector boson A^a_μ and a spin-1/2 Weyl fermion λ^a. This case also requires an auxiliary field D^a_{aux} is necessary.

We introduce the superpotential

$$W = \frac{1}{2}M^{ij}\phi_i\phi_j + \frac{1}{6}y^{ijk}\phi_i\phi_j\phi_k \tag{3.5}$$

with the fermion mass matrix M^{ij}, the Yukawa couplings y^{ijk} and the derivatives

$$W^{ij} = \frac{\delta^2}{\delta\phi_i\delta\phi_j}W, \qquad W^i = \frac{\delta}{\delta\phi_i}W \tag{3.6}$$

which can in a more general way also be expressed as the same function of the superfields Φ_i instead of the scalar fields ϕ_i. For details concerning the common superfield formalism see e. g. [33–35].

Using the equations of motions for the auxiliary fields

$$F_i = -W^*_i, \qquad F^{*i} = -W^i, \qquad D^a = -g(\phi^* T^a \phi) \tag{3.7}$$

the Langrangian for a renormalizable supersymmetric theory can be written in the following way according to [31]:

$$\mathcal{L} = \mathcal{L}_{\text{chiral}} + \mathcal{L}_{\text{gauge}} + \mathcal{L}_{\text{extra}} = \tag{3.8a}$$

$$(D^\mu\phi_i)^\dagger(D_\mu\phi_i) + i\psi^{\dagger i}\bar{\sigma}^\mu D_\mu\psi_i - \frac{1}{2}(W^{ij}\psi_i\psi_j + W^{*ij}\psi^\dagger_i\psi^\dagger_j) - W^iW^*_i \tag{3.8b}$$

$$-\frac{1}{4}F^a_{\mu\nu}F^{a\mu\nu} + i\lambda^{a\dagger}\bar{\sigma}^\mu D_\mu\lambda^a - \frac{1}{2}g^2(\phi^{*i}T^a\phi_i)(\phi^{*j}T^a\phi_j) \tag{3.8c}$$

$$-\sqrt{2}g(\phi^{*i}T^a\psi_i)\lambda^a - \sqrt{2}g\lambda^{\dagger a}(\psi^{\dagger i}T^a\phi_i) \tag{3.8d}$$

Here, D_μ is the covariant derivative for the respective fields and T^a are the gauge group generators.

3.3 The MSSM

The Minimal Supersymmetric Standard Model (MSSM) is minimal in the sense that there is exactly one superpartner to each SM particle. To obtain an anomaly free electroweak theory, at least two Higgs doublets H_u and H_d are necessary, which after electroweak symmetry breaking give the masses to the up-type and the down-type fields, respectively. The VEVs of their neutral components are used in the convention

$$\langle H^0_u\rangle = \frac{v_u}{\sqrt{2}}, \qquad \langle H^0_d\rangle = \frac{v_d}{\sqrt{2}} \tag{3.9}$$

and related to the Z mass and the electroweak gauge couplings as [35]

$$v_u^2 + v_d^2 = v^2 = \frac{2m_Z^2}{g^2 + g'^2} \approx (246 \text{ GeV})^2; \tag{3.10}$$

their ratio is written as

$$\tan(\beta) = \frac{v_u}{v_d}. \tag{3.11}$$

In the superfield formalism the superpotential of the MSSM is given by

$$W_{\text{MSSM}} = U^c Y_u Q \cdot H_u - D^c Y_d Q \cdot H_d - E^c Y_e L \cdot H_d + \mu H_u \cdot H_d \tag{3.12}$$

where $A \cdot B = A_1 B_2 - A_2 B_1$ is the $SU(2)$ invariant product and the summations over family and color indices are suppressed. Y_f are the respective Yukawa couplings and μ is the mass parameter of the higgs doublets. Tab. 3.1 shows the chiral supermultiplets corresponding to the chiral superfields in Eq. 3.12. In Tab. 3.2 the gauge supermultiplets of the MSSM are listed.

Name		spin 0	spin 1/2	$SU(3)_C, SU(2)_L, U(1)_Y$
squarks, quarks	Q	$(\widetilde{u}_L \quad \widetilde{d}_L)$	$(u_L \quad d_L)$	$(\mathbf{3}, \mathbf{2}, \frac{1}{6})$
(3 families)	U^c	$\widetilde{u}_R^*$	$u_R^\dagger$	$(\overline{\mathbf{3}}, \mathbf{1}, -\frac{2}{3})$
	D^c	$\widetilde{d}_R^*$	$d_R^\dagger$	$(\overline{\mathbf{3}}, \mathbf{1}, \frac{1}{3})$
sleptons, leptons	L	$(\widetilde{\nu} \quad \widetilde{e}_L)$	$(\nu \quad e_L)$	$(\mathbf{1}, \mathbf{2}, -\frac{1}{2})$
(3 families)	E^c	$\widetilde{e}_R^*$	$e_R^\dagger$	$(\mathbf{1}, \mathbf{1}, 1)$
Higgs, higgsinos	H_u	$(H_u^+ \quad H_u^0)$	$(\widetilde{H}_u^+ \quad \widetilde{H}_u^0)$	$(\mathbf{1}, \mathbf{2}, +\frac{1}{2})$
	H_d	$(H_d^0 \quad H_d^-)$	$(\widetilde{H}_d^0 \quad \widetilde{H}_d^-)$	$(\mathbf{1}, \mathbf{2}, -\frac{1}{2})$

Table 3.1: Chiral supermultiplets in the MSSM [31].

Name	spin 1/2	spin 1	$SU(3)_C, SU(2)_L, U(1)_Y$
gluino, gluon	$\widetilde{g}$	g	$(\mathbf{8}, \mathbf{1}, 0)$
winos, W bosons	$\widetilde{W}^\pm \quad \widetilde{W}^0$	$W^\pm \quad W^0$	$(\mathbf{1}, \mathbf{3}, 0)$
bino, B boson	$\widetilde{B}^0$	B^0	$(\mathbf{1}, \mathbf{1}, 0)$

Table 3.2: Gauge supermultiplets in the MSSM [31].

3.4 Supersymmetry breaking and unification

The fact that mass degenerate superpartners of the SM particles have not been found indicates that SUSY has to be broken spontaneously in the vacuum state. Claiming SUSY to be a solution to the hierarchy problem, only couplings of positive mass dimension are allowed in the Lagrangian, and the soft breaking terms have to be at a typical mass scale m_{soft} not higher than of TeV range. They are given for the MSSM as [33, 36]

$$\begin{aligned}
-\mathcal{L}_{\text{soft}}^{\text{MSSM}} =& \frac{1}{2}(M_1 \widetilde{B}\widetilde{B} + M_2 \widetilde{W}^a \widetilde{W}^a + M_3 \widetilde{g}^a \widetilde{g}^a + h.c.) \\
&+ m_Q^2(\widetilde{u}_L^* \widetilde{u}_L + \widetilde{d}_L^* \widetilde{d}_L) + m_u^2 \widetilde{u}_R^* \widetilde{u}_R + m_d^2 \widetilde{d}_R^* \widetilde{d}_R \\
&+ m_L^2(\widetilde{e}_L^* \widetilde{e}_L + \widetilde{\nu}_L^* \widetilde{\nu}_L) + m_e^2 \widetilde{e}_R^* \widetilde{e}_R \\
&+ m_{H_u}^2 |H_u|^2 + m_{H_d}^2 |H_d|^2 + (B\mu H_u H_d + h.c.) \\
&+ (A_u H_u \widetilde{u}_R^* \widetilde{q}_L + A_d H_d \widetilde{d}_R^* \widetilde{q}_L + A_e H_d \widetilde{e}_R^* \widetilde{l}_L + h.c.)
\end{aligned} \tag{3.13}$$

with complex parameters M_1, M_2, M_3, B, real parameters $m_{H_u}^2$, $m_{H_d}^2$, Hermitian 3×3 matrices m_Q^2, m_u^2, m_d^2, m_L^2, m_e^2 and complex matrices A_u, A_d, A_e in family space. All of the scales are roughly of the order m_{soft}.

After redefining the phases and the flavor basis for the multiplets, there are more than 100 new parameters – a number that makes general studies impossible. To reduce this number we restrict all parameters to be real and all matrices to be diagonal, assuming only small CP violation and flavor changing effects. Furthermore it is common to choose a specific breaking scheme where the origin of SUSY breaking takes place in a hidden sector by the VEV of an auxiliary field F and is mediated to the visible sector by flavor-blind interactions. In the case of the minimal supergravity (mSUGRA) scheme used in this work these interactions are of gravitational strength yielding the rough approximation

$$m_{\text{soft}} \approx \frac{\langle F \rangle}{M_{\text{Planck}}} \tag{3.14}$$

with the Planck scale $M_{\text{Planck}} = \mathcal{O}(10^{19}\ \text{GeV})$.

A nice property of supersymmetric models is the unification of the SM gauge couplings g_1, g_2, g_3 due to the running of the renormalization group equations (RGEs). Compared to the SM they have larger coefficients b_a because of the additional particles in the loops. At 1-loop level they are given by [31]

$$\begin{aligned}
&\beta_{g_a} \equiv \frac{d}{dt} g_a = \frac{1}{16\pi^2} b_a g_a^3 \\
&\text{with} \quad (b_1, b_2, b_3) = \left(\frac{33}{5}, 1, -3\right) \quad \text{and} \quad t = \ln\left(\frac{Q}{Q_0}\right)
\end{aligned} \tag{3.15}$$

with the renormalization group (RG) scale Q. In our model, the gauge groups unify to a $SU(5)$ which is broken to $SU(3)_C \times SU(2)_L \times U(1)_Y$ below the GUT scale $M_{\mathrm{GUT}} = \mathcal{O}(10^{16}\ \mathrm{GeV})$. In a minimal realization of mSUGRA, we also assume a unification of several soft breaking parameters and thus postulate a common gaugino mass $m_{1/2}$, a common scalar mass m_0 as well as the trilinear coupling parameter A_0. Together with $\tan(\beta)$ specified in Eq. 3.11, the parameter space is defined by four real parameters and the sign of the μ parameter $\mathrm{sgn}(\mu)$:

$$\begin{aligned} &M_1 = M_2 = M_3 = m_{1/2} \\ &m_{H_u}^2 = m_{H_d}^2 = m_0^2 \\ &m_Q^2 = m_u^2 = m_d^2 = m_L^2 = m_e^2 = m_0^2 \mathbb{1} \\ &A_u = A_0 Y_u\ ,\ A_d = A_0 Y_d\ ,\ A_e = A_0 Y_e \end{aligned} \tag{3.16}$$

3.5 Particle content

Since the MSSM contains two Higgs doublets, the generation of masses by electroweak symmetry breaking becomes more complicated than in the SM. This will not be discussed in this work, for further information see e. g. [33–35]. In this section, only the mixings of the fields with identical quantum numbers will be introduced, with a focus on the particles relevant for the following considerations.

3.5.1 Neutralinos

The neutral higgsinos and the neutral gauginos mix to form four neutralino mass eigenstates. From the superpotential Eq. 3.12 one can derive the neutralino mass matrix in the basis $\psi^0 = (\widetilde{B}^0, \widetilde{W}^0, \widetilde{H}_d^0, \widetilde{H}_u^0)$ as

$$M_{\widetilde{\chi}^0} = \begin{pmatrix} M_1 & 0 & -g' v_d/2 & g' v_u/2 \\ 0 & M_2 & g v_d/2 & -g v_u/2 \\ -g' v_d/2 & g v_d/2 & 0 & -\mu \\ g' v_u/2 & -g v_u/2 & -\mu & 0 \end{pmatrix} \tag{3.17}$$

where M_1 and M_2 are the gaugino mass parameters from Eq. 3.13 and the products of the electroweak couplings and the Higgs VEVs can be expressed in terms of the Weinberg angle θ_W, β and the Z boson mass m_Z. Diagonalizing $M_{\widetilde{\chi}^0}$ by the unitary mixing matrix N provides mass eigenstates

$$\widetilde{\chi}_i^0 = N_{ij} \psi_j^0 \tag{3.18}$$

yielding

$$N^* M_{\widetilde{\chi}^0} N^{-1} = diag(m_{\widetilde{\chi}_1^0}, m_{\widetilde{\chi}_2^0}, m_{\widetilde{\chi}_3^0}, m_{\widetilde{\chi}_4^0}). \tag{3.19}$$

In many supersymmetric models and also in most regions of the parameter space of the model under consideration, the lightest neutralino $\widetilde{\chi}_1^0$ is the lightest supersymmetric particle (LSP). This will play an important role in the later chapters.

3.5.2 Charginos

In a similar way, also the charged higgsino and wino components are mixing to the two chargino mass eigenstates. In the basis $\psi^{\pm} = (\widetilde{W}^+, \widetilde{H}_u^+, \widetilde{W}^-, \widetilde{H}_d^-)$, the mass matrix is given by

$$M_{\widetilde{\chi}^{\pm}} = \begin{pmatrix} 0 & X^T \\ X & 0 \end{pmatrix} \qquad \text{with} \qquad X = \begin{pmatrix} M_2 & gv_u/\sqrt{2} \\ gv_d/\sqrt{2} & \mu \end{pmatrix} \tag{3.20}$$

and can be diagonalized as

$$\begin{pmatrix} \widetilde{\chi}_1^+ \\ \widetilde{\chi}_2^+ \end{pmatrix} = V \begin{pmatrix} \widetilde{W}^+ \\ \widetilde{H}_u^+ \end{pmatrix}, \qquad \begin{pmatrix} \widetilde{\chi}_1^- \\ \widetilde{\chi}_2^- \end{pmatrix} = U \begin{pmatrix} \widetilde{W}^- \\ \widetilde{H}_d^- \end{pmatrix}, \tag{3.21}$$

providing mass eigenstates $\widetilde{\chi}_i^{\pm}$ so that

$$U^* X V^{-1} = \mathrm{diag}(m_{\widetilde{\chi}_1^{\pm}}, m_{\widetilde{\chi}_2^{\pm}}). \tag{3.22}$$

3.5.3 Sleptons and squarks

Via the soft breaking terms, in general all the up-type resp. down-type squarks as well as the charged sleptons resp. sneutrinos can mix with each other, obtaining their mass eigenstates by diagonalizing three 6×6 matrices and one 3×3 matrix. However, we assume most of the mixing angles to be small due to the flavor-blindness of the soft parameters specified in Eq. 3.16, so that in a good approximation only the third-family sparticles show a left-right mixing in pairs, originating from their large Yukawa and soft couplings.

In our mSUGRA scenario specified in section 3.4 all scalar sparticles have the common squared mass m_0^2 at the GUT scale. The squared masses at the electroweak scale are determined by the RGE running which provides contributions proportional to the gaugino squared mass $m_{1/2}^2$ [31]. Since these contributions depend on the relative size of the gauge couplings, the squarks are in general expected to be heavier than the sleptons because of the contributing RGE effects of the strong coupling.

The equations for the first and second generation masses can be looked up in [31, 33], for instance. For the aforementioned left-right coupling of the stau, the squared mass matrix is given by [33]

$$m_{\widetilde{\tau}}^2 = \begin{pmatrix} m_{\widetilde{\tau}_L}^2 + m_\tau^2 + \Delta_{\widetilde{\tau}_L} & m_\tau(A_\tau - \mu \tan(\beta)) \\ m_\tau(A_\tau - \mu \tan(\beta)) & m_{\widetilde{\tau}_R}^2 + m_\tau^2 + \Delta_{\widetilde{\tau}_R} \end{pmatrix} \tag{3.23}$$

$$\text{with} \quad \Delta_{\widetilde{\tau}_L} = \left(-\frac{1}{2} + \sin^2(\theta_W)\right) m_Z^2 \cos(2\beta) \tag{3.24}$$

$$\text{and} \quad \Delta_{\widetilde{\tau}_R} = \frac{1}{3} + \sin^2(\theta_W) m_Z^2 \cos(2\beta) \tag{3.25}$$

Similar squared mass matrices can be specified for the top and the bottom squarks. They can be diagonalized by unitary matrices to generate mass eigenstates. Since the MSSM does not contain right-handed neutrinos, of course there are no superpartners to them. Therefore, a left-right mixing is not possible for sneutrinos. However, like for the squarks and charged sleptons, the first- and second-generation particles of the sneutrinos $\widetilde{\nu}_e$ and $\widetilde{\nu}_\mu$ are nearly degenerate, while $\widetilde{\nu}_\tau$ can be significantly lighter [31]. The introduction of the seesaw mechanism can change this situation because of the additional heavy particles and the corresponding neutrino Yukawa couplings. Furthermore, it will lead to larger off-diagonal entries in the charged slepton and sneutrino mass matrices. These effects will be discussed in chapter 5.

3.5.4 Gluino

Together with its superpartner, the gluino, the gluon forms the only color octet supermultiplet in the MSSM. Therefore no mixing with other particles is possible. The gluino mass parameter M_3 specified in Eq. 3.13 is determined at the GUT scale by Eq. 3.16 and driven by the RG evolution similar to the bino and wino mass parameters M_1, M_2. Using these relations one can show that, at the TeV scale, the parameters behave roughly like

$$M_3 : M_2 : M_1 \approx 6 : 2 : 1. \tag{3.26}$$

Thus we suspect the gluino to be among the heaviest sparticles.

3.6 R-parity

In general it is possible to introduce terms into the superpotential given by Eq. 3.12 that violate baryon number B or lepton number L. Since this has not been observed by experiment yet – e. g. in the case of proton decay – , an additional symmetry is necessary to forbid these terms while still permitting the terms of W_{MSSM}. This is usually done by defining a multiplicative quantum number

$$R = (-1)^{3(B-L)+2S} \tag{3.27}$$

with the spin S. This discrete symmetry is called R-parity and has the nice feature that all SM particle carry $R = +1$ while their superpartners carry $R = -1$.

In the MSSM, we assume conservation of R-parity. This leads to interesting phenomenological consequences:

- The lightest supersymmetric particle (LSP) is stable. In many regions of the mSUGRA parameter space, this is the lightest neutralino $\widetilde{\chi}_1^0$, which is neutral, massive and only weakly interacting, thus constituting an interesting candidate to solve the dark matter problem.

- The number of supersymmetric particles in any interaction vertex must be even, so that sparticles can only be produced in pairs at collider experiments. Moreover they can decay only into an odd number of sparticles generating final states with an even number of LSPs in the collider processes.

Chapter 4

The supersymmetric seesaw mechanism

Neither the Standard Model nor the MSSM allow the neutrinos to be massive. However, as the experimental results point to at least two non-zero neutrino masses, one has to include a theoretical framework to explain these small masses. This can be done in an elegant way via the seesaw mechanism [10–13] by introducing new mediator particles at a very high scale that couple to the left-handed lepton fields as well as to the Higgs fields via neutrino Yukawa couplings. If implemented in a non-supersymmetric model there will arise another hierarchy problem because of radiative corrections to the Higgs mass [37]. Since in a supersymmetric framework also the superpartners of the new particles with a similar mass couple to the Higgs field, this problem is avoided naturally. Furthermore, all the nice features of supersymmetry as discussed in chapter 3 are maintained. The common derivation of the typical SUSY seesaw properties presented in the following is in accordance with [19, 36–38].

As neutrinos do not carry electric charge they can possibly be Majorana particles. In this case tiny neutrino masses can be obtained by introducing the effective dimension-5 Weinberg operator [39–41]:

$$\frac{f_{\alpha\beta}}{\Lambda}(H_u L_\alpha)(H_u L_\beta) \quad \Rightarrow \quad (m^\nu)_{\alpha\beta} = \frac{f_{\alpha\beta} v_u^2}{2\Lambda} \tag{4.1}$$

Λ is at the scale of the mediator particles M, and $f_{\alpha\beta}$ is a combination of different Yukawa couplings and thus can go up to $\mathcal{O}(1)$, requiring $\Lambda \lesssim \mathcal{O}(10^{15})$ GeV to obtain the neutrino masses predicted by experiment. This principle clarifies the name "seesaw". Fig. 4.1 shows the possible realizations of the effective Weinberg operator which is obtained by integrating out the heavy degrees of freedom.

Since two doublets can be decomposed into a triplet and a singlet as $\mathbf{2} \otimes \mathbf{2} = \mathbf{3} \oplus \mathbf{1}$, the gauge structure only allows three ways to obtain the Weinberg operator at tree-level [10] because the symmetry properties at the vertices of the right diagram in Fig. 4.1 do not allow the realization with a scalar singlet mediator. The three possible types of seesaw mechanisms will be presented in the following sections.

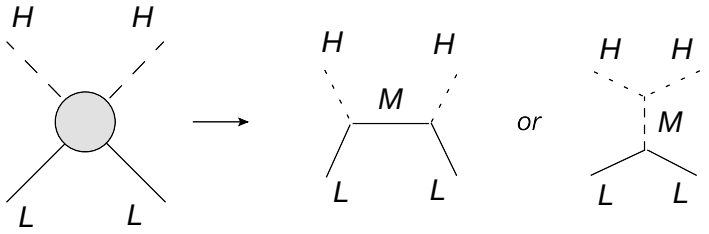

Figure 4.1: Principle of the seesaw mechanism [41].

As gauge coupling unification is one of the most interesting properties of supersymmetric theories (cf. section 3.4), we will take care to maintain this quality while introducing the new states. This will be done by embedding them in complete $SU(5)$ representations [41–43].

4.1 Seesaw type I

In the seesaw type I, the left-handed leptons couple to the higgs field by the exchange of a heavy virtual fermion [12, 13, 44]. This right-handed neutrino N^c is a singlet under all Standard Model gauge groups. We postulate three of them to generate three light neutrino masses.

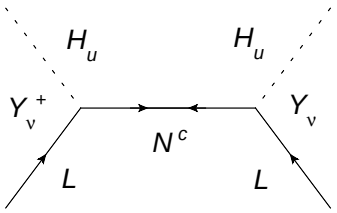

Figure 4.2: Seesaw type I.

After the $SU(5)$ breaking at the GUT scale one obtains the superpotential [19, 37, 41]

$$W_{\mathrm{I}} = W_{\mathrm{MSSM}} + W_{\nu} \tag{4.2}$$

with the usual MSSM part shown in Eq. 3.12 and the additional part

$$W_{\nu} = N^c Y_{\nu} L \cdot H_u + \frac{1}{2} N^c M_R N^c \tag{4.3}$$

where M_R is the 3×3 mass matrix of the heavy right-handed neutrino and Y_{ν} the neutrino Yukawa coupling. Below the scale of the lightest N^c, all the heavy fields are integrated out, yielding an effective superpotential [37]

$$W_{\mathrm{I,eff}} = W_{\mathrm{MSSM}} + \frac{1}{2} (Y_{\nu} L \cdot H_u)^T M_R^{-1} (Y_{\nu} L \cdot H_u). \tag{4.4}$$

Electroweak symmetry breaking leads to the following mass matrix for the light neutrinos:

$$m_\nu = -\frac{v_u^2}{2} Y_\nu^T M_R^{-1} Y_\nu \tag{4.5}$$

This is the famous seesaw formula which like Eq. 4.1 clearly shows the seesaw principle. As it is complex and symmetric the neutrino mass matrix m_ν can be diagonalized in flavor space by the already known 3×3 PMNS matrix U (Eq. 2.2):

$$\widehat{m}_\nu = U^T m_\nu U \tag{4.6}$$

Additionally, we can choose to work in a basis of the right-handed neutrinos where M_R is also diagonal:

$$\widehat{M}_R = \mathrm{diag}\,(M_1, M_2, M_3) := M_R \tag{4.7}$$

Thus it is possible to invert Eq. 4.5 in the following way [37]:

$$\widehat{m}_\nu = -\frac{v_u^2}{2} U^T Y_\nu^T M_R^{-1} Y_\nu U \tag{4.8}$$

Multiplication from both sides by the matrix

$$\sqrt{\widehat{m}_\nu^{-1}} = \mathrm{diag}\left(\frac{1}{\sqrt{m_1}}, \frac{1}{\sqrt{m_2}}, \frac{1}{\sqrt{m_3}}\right) \tag{4.9}$$

yields

$$\mathbb{1} = -\frac{v_u^2}{2}\left(\sqrt{M_R^{-1}} Y_\nu U \sqrt{\widehat{m}_\nu^{-1}}\right)^T \left(\sqrt{M_R^{-1}} Y_\nu U \sqrt{\widehat{m}_\nu^{-1}}\right) = R^T R \tag{4.10}$$

where we introduced the complex orthogonal matrix

$$R = -i\frac{v_u}{\sqrt{2}} \sqrt{M_R^{-1}} Y_\nu U \sqrt{\widehat{m}_\nu^{-1}} \tag{4.11}$$

which expresses our ignorance of which right-handed neutrino generates the mass of which left-handed neutrino. With this matrix we can express the Yukawa couplings as

$$Y_\nu = i\frac{\sqrt{2}}{v_u} \sqrt{M_R} R \sqrt{\widehat{m}_\nu} U^\dagger \tag{4.12}$$

Further properties of R like a possible parametrization will be discussed in section 4.3 for the similar type III case.

4.2 Seesaw type II

In the case of type II seesaw the coupling of the leptons to the Higgs field is realized by the exchange of a scalar $SU(2)_L$ triplet T [45, 46]. As the leptons L carry hypercharge $-\frac{1}{2}$ the scalar T carries hypercharge 1 and thus must be embedded in a **15**-plet to obtain a complete $SU(5)$ representation. After breaking $SU(5)$, it decomposes under $SU(3)_C \times SU(2)_L \times U(1)_Y$ to [42, 47]

$$\mathbf{15} = S + T + Z \sim \left(6, 1, -\frac{2}{3}\right) + (1, 3, 1) + \left(3, 2, \frac{1}{6}\right). \tag{4.13}$$

To explain the light neutrino masses and to avoid chiral anomalies, two **15**-plets 15 and $\overline{15}$ are necessary.

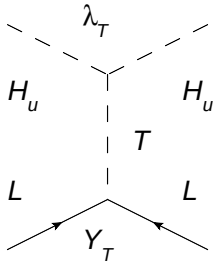

Figure 4.3: Seesaw type II.

Below the GUT scale the parts of the superpotential needed for the implementation of the seesaw in the MSSM reads[1]

$$W_{\text{II}} = W_{\text{MSSM}} + \frac{1}{\sqrt{2}}\left(LY_T TL + \lambda_T H_d T H_d + \lambda_{\overline{T}} H_u \overline{T} H_u\right) + M_T T\overline{T} \tag{4.14}$$

which after integrating out the heavy states and electroweak symmetry breaking yields

$$m_\nu = \frac{v_u^2}{2}\frac{\lambda_{\overline{T}}}{M_T} Y_T. \tag{4.15}$$

Like in type I, m_ν and thus also Y_T are diagonalized by the matrix U. This means that the Yukawa couplings are fixed at known neutrino data up to a constant. The other components of the **15**-plet also lead to additional Yukawa couplings Y_S and Y_Z which in principle also contribute. At the GUT scale they are all required to be equal. As the seesaw type II is not of main interest in this work, further properties of this mechanism are not discussed here.

[1] For the full operator and field content, see appendix E of [41] and [42].

4.3 Seesaw type III

The third possible realization of the seesaw mechanism is the seesaw type III which is in general very similar to type I. In this scenario the fermionic $SU(2)_L$ singlet is replaced by a fermionic triplet Σ_R with zero hypercharge belonging to the adjoint representation of $SU(2)_L$ [14].

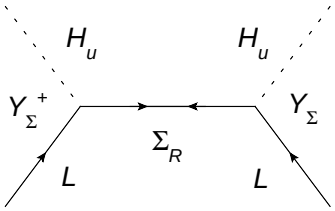

Figure 4.4: Seesaw type III.

To maintain gauge coupling unification, we embed the new fermions in a **24**-plet obtaining a complete $SU(5)$ representation. The decomposition under the Standard Model gauge group $SU(3)_C \times SU(2)_L \times U(1)_Y$ after breaking the $SU(5)$ is [19]

$$\begin{aligned} \mathbf{24}_M &= B_M + W_M + G_M + X_M + \overline{X}_M \\ &\sim (1,1,0) + (1,3,0) + (8,1,0) + \left(3,2,-\frac{5}{6}\right) + \left(3^*,2,\frac{5}{6}\right). \end{aligned} \tag{4.16}$$

As the quantum numbers of the first two parts are the same as in the fermionic $SU(2)_L$ singlet N^c and the triplet Σ_R, respectively, in the $\mathbf{24}_M$ always appears a combination of seesaw type I and type III.

Breaking $SU(5)$ leads to the following superpotential below the GUT scale [19, 41]:

$$\begin{aligned} W_{\text{III}} = W_{\text{MSSM}} &+ H_u \left(W_M Y_W - \sqrt{\frac{3}{10}} B_M Y_B \right) L + H_u \overline{X}_M Y_X D^c \\ &+ \frac{1}{2} B_M M_B B_M + \frac{1}{2} G_M M_G G_M + \frac{1}{2} W_M M_W W_M + X_M M_X \overline{X}_M \end{aligned} \tag{4.17}$$

Since we want to achieve unification the boundary conditions $M_B = M_W = M_G = M_X$ and $Y_B = Y_W = Y_X$ are used at the GUT scale. For the implementation of the seesaw in the MSSM, only B_M and W_M fields are necessary. By integrating out the mediators at the seesaw scale we obtain the effective superpotential

$$\begin{aligned} W_{\text{III,eff}} = W_{\text{MSSM}} + \frac{1}{2} \Bigg(& \frac{3}{10} (Y_B L \cdot H_u)^T M_B^{-1} (Y_B L \cdot H_u) \\ & + \frac{1}{2} (Y_W L \cdot H_u)^T M_W^{-1} (Y_W L \cdot H_u) \Bigg). \end{aligned} \tag{4.18}$$

By electroweak symmetry breaking we obtain the neutrino mass matrix

$$m_\nu = -\frac{v_u^2}{2}\left(\frac{3}{10}Y_B^T M_B^{-1} Y_B + \frac{1}{2}Y_W^T M_W^{-1} Y_W\right). \tag{4.19}$$

Unlike the type I seesaw formula Eq. 4.5, the type III equivalent has two contributions, originating from the $SU(2)_L$ singlet and the $SU(2)_L$ triplet part of the superpotential, respectively. In this situation, the calculation of the Yukawa couplings becomes more complicated in general. It can be simplified by the following approximation: As we postulate identical masses and couplings at the GUT scale and the seesaw scale still is quite high, we can assume that $M_B \cong M_W$ and $Y_B \cong Y_W$ is still approximately true at $\mathcal{O}(M_{\text{seesaw}})$. In this case Eq. 4.19 reduces to

$$m_\nu = -\frac{2}{5}v_u^2 Y_W^T M_W^{-1} Y_W \tag{4.20}$$

which coincides with the type I seesaw formula 4.5 up to a factor $\frac{4}{5}$. Thus we can make the same inversion as in the type I case to express the Yukawa couplings. In the following, this will be done both for the case of three as well as for the case of two generations of the **24**-plet.

4.3.1 Three 24-plets

To describe three non-zero neutrino masses, we have to introduce three copies of the **24**-plet corresponding to three right-handed neutrinos in the seesaw type I. m_ν can then be diagonalized in the same way by the 3×3 PMNS matrix U (Eq. 2.2):

$$\widehat{m}_\nu = U^T m_\nu U \tag{4.21}$$

With a chosen M_W-diagonal basis for the **24**-plets

$$\widehat{M_W} = \text{diag}(M_1, M_2, M_3) := M_W, \tag{4.22}$$

Eq. 4.20 can be inverted according to Eqs. 4.8 and 4.10 [37]:

$$\widehat{m}_\nu = -\frac{2}{5}v_u^2 U^T Y_W^T M_W^{-1} Y_W U, \tag{4.23}$$

$$\mathbb{1} = -\frac{2}{5}v_u^2\left(\sqrt{M_W^{-1}}Y_W U\sqrt{\widehat{m}_\nu^{-1}}\right)^T\left(\sqrt{M_W^{-1}}Y_W U\sqrt{\widehat{m}_\nu^{-1}}\right) = R^T R, \tag{4.24}$$

with $\sqrt{\widehat{m}_\nu^{-1}}$ like in Eq. 4.9 and the corresponding R matrix

$$R = -i\sqrt{\frac{2}{5}}v_u\sqrt{M_W^{-1}}Y_W U\sqrt{\widehat{m}_\nu^{-1}}. \tag{4.25}$$

By inverting this formula, the Yukawa couplings can be expressed as

$$Y_W = \sqrt{\frac{5}{2}}\frac{i}{v_u}\sqrt{M_W}R\sqrt{\widehat{m}_\nu}U^\dagger. \tag{4.26}$$

Like in type I, R is a complex orthogonal matrix. It is conveniently parametrized [37] by three complex angles ϕ_1, ϕ_2, ϕ_3 with $c_i = \cos(\phi_i)$, $s_i = \sin(\phi_i)$ which gives

$$R = \begin{pmatrix} c_2c_3 & -c_1s_3 - s_1s_2c_3 & s_1s_3 - c_1s_2c_3 \\ c_2s_3 & c_1c_3 - s_1s_2s_3 & -s_1c_3 - c_1s_2s_3 \\ s_2 & s_1c_2 & c_1c_2 \end{pmatrix}. \tag{4.27}$$

This is just a product of three rotation matrices (no reflections):

$$R = \begin{pmatrix} 1 & 0 & 0 \\ 0 & c_1 & -s_1 \\ 0 & s_1 & c_1 \end{pmatrix} \times \begin{pmatrix} c_2 & 0 & -s_2 \\ 0 & 1 & 0 \\ s_2 & 0 & c_2 \end{pmatrix} \times \begin{pmatrix} c_3 & -s_3 & 0 \\ s_3 & c_3 & 0 \\ 0 & 0 & 1 \end{pmatrix} \tag{4.28}$$

There is no specification about the masses M_i of the three **24**-plet copies. They can be chosen to be either degenerate $M_1 = M_2 = M_3 = M_{\text{seesaw}}$ or hierarchical in any possible ordering. Changing this ordering has the same effect as changing the multiplication sequence in Eq. 4.28. In this work we always fix R to the aforementioned parametrization and vary only the order of the heavy masses.

So, there are several (free) parameters in addition to the MSSM parameters: The neutrino mixing angles θ_{12}, θ_{23}, θ_{13}, the Dirac phase δ (real); the R parametrization angles ϕ_1, ϕ_2, ϕ_3 (complex) and the three **24**-plet masses M_1, M_2, M_3; further the choice of the neutrino mass hierarchy (normal or inverse) and the mass of the lightest neutrino.

4.3.2 Two 24-plets

If the lightest neutrino mass is zero (i.e. $m_1 = 0$ for normal hierarchy, $m_3 = 0$ for inverse hierarchy; cf. section 2.2), the seesaw type III is also possible with only two copies of the **24**-plet, as well as type I with two right-handed neutrinos – also called 3×2 seesaw [48]. For the type I model this was discussed in [49–51]. In this case M_W is a 2×2 matrix. Of course we can choose a basis with diagonal M_W again:

$$\widehat{M}_W = \text{diag}(M_1, M_2) := M_W \tag{4.29}$$

The diagonalized neutrino mass matrix Eq. 4.23 now has one diagonal entry zero and thus is not invertible anymore. However, we can do a similar inversion as in sections 4.1 and 4.3.1 by multiplying this equation from both sides with the matrix

$$\left(\sqrt{\widehat{m}_\nu^{-1}}\right)'_{\text{norm}} = \text{diag}\left(0, \frac{1}{\sqrt{m_2}}, \frac{1}{\sqrt{m_3}}\right) \tag{4.30}$$

for normal hierarchy ($m_1 = 0$) and

$$\left(\sqrt{\widehat{m}_\nu^{-1}}\right)'_{\text{inv}} = \text{diag}\left(\frac{1}{\sqrt{m_1}}, \frac{1}{\sqrt{m_2}}, 0\right) \tag{4.31}$$

for inverse hierarchy ($m_3 = 0$), respectively. Then, we obtain

$$\mathbb{1}' = -\frac{2}{5} v_u^2 \left(\sqrt{M_W^{-1}} Y_W U \left(\sqrt{\widehat{m}_\nu^{-1}} \right)' \right)^T \left(\sqrt{M_W^{-1}} Y_W U \left(\sqrt{\widehat{m}_\nu^{-1}} \right)' \right) = R^T R \quad (4.32)$$

with the matrix

$$\mathbb{1}' = \mathrm{diag}(1,1,0) \qquad \text{resp.} \qquad \mathbb{1}' = \mathrm{diag}(0,1,1) \quad (4.33)$$

for normal (inverse) hierarchy. In this case, the Yukawa matrix and thus also the R matrix are of 2×3 size

$$R = -i\sqrt{\frac{2}{5}} v_u \sqrt{2} \sqrt{M_W^{-1}} Y_W U \left(\sqrt{\widehat{m}_\nu^{-1}} \right)' = \begin{pmatrix} r_{11} & r_{12} & r_{13} \\ r_{21} & r_{22} & r_{23} \end{pmatrix}, \quad (4.34)$$

yielding again

$$Y_W = \sqrt{\frac{5}{2}} \frac{i}{v_u} \sqrt{M_W} R \left(\sqrt{\widehat{m}_\nu^{-1}} \right)' U^\dagger. \quad (4.35)$$

As a 2×3 matrix R can be parametrized by only one complex angle ϕ and written as a product of a 2×2 rotation matrix and a kind of 2×3 "unity matrix" that depends on the chosen hierarchy.[2] Thus, we get for normal hierarchy ($m_1 = 0$)

$$R_{\text{norm}} = \begin{pmatrix} \cos(\phi) & -\sin(\phi) \\ \sin(\phi) & \cos(\phi) \end{pmatrix} \times \begin{pmatrix} 0 & 1 & 0 \\ 0 & 0 & 1 \end{pmatrix} \quad (4.36)$$

and for inverse hierarchy ($m_3 = 0$)

$$R_{\text{inv}} = \begin{pmatrix} \cos(\phi) & -\sin(\phi) \\ \sin(\phi) & \cos(\phi) \end{pmatrix} \times \begin{pmatrix} 1 & 0 & 0 \\ 0 & 1 & 0 \end{pmatrix}. \quad (4.37)$$

Now, of course, R is not orthogonal anymore, but we obtain

$$R^T R = \mathbb{1}' \ , \quad R R^T = \mathbb{1}_{2\times 2}. \quad (4.38)$$

On the one hand, in this two **24**-plet realization of the seesaw mechanism type III the number of free parameters is reduced as there are only two seesaw masses M_1, M_2 and thus two possible orderings as well as only one complex angle ϕ left. On the other hand, this case has further nice features which will be discussed in section 6.1.

It is also possible to treat this scenario as a limit of the three generation case where one of the heavy masses is infinite. For type I, this was done in [49, 50].

[2] Since $m_2 = 0$ is excluded by experiment the third possibility of this "unity matrix" with the middle column entries all zero cannot be realized.

4.4 Effects on the mass spectrum

The additional particles of the seesaw mechanism also affect the mass spectrum of the model. As already mentioned in section 3.4 the 1-loop RGEs for the gauge couplings are given by Eq. 3.15 with the coefficents

$$(b_1, b_2, b_3) = \left(\frac{33}{5}, 1, -3\right). \tag{4.39}$$

Adding a **24**-plet to the spectrum produces a shift of $\Delta b_a = 5$. Thus the overall contribution in the two **24**-plet case is $\Delta b_a = 10$, in the three **24**-plet case $\Delta b_a = 15$. These enhanced RGE coefficients also lead to changes in the evolution of the mass parameters m_0 and $m_{1/2}$ yielding a lighter sparticle spectrum [43, 47]. The scalar masses also can be modified by some of the Yukawa couplings getting large. Compared to the other seesaw scenarios, these effects are largest in the type III case, although they depend considerably on the high scale values of m_0 and $m_{1/2}$. But especially the value of the seesaw scale has an important influence, enhancing the effects the smaller it is. Illustrations and further reflections on this can be found in [19]. In the two **24**-plet case, the effects are smaller due to the smaller Δb_a.

The large beta functions also restrict the allowed range for M_{seesaw}: The gauge couplings at the GUT scale get large (Landau pole), leading to the break down of pertubation theory below a certain value. In the seesaw type III, the effects of the 2-loop RGEs are also very important due to their large coefficients. They can be found e. g. in appendix A 4 of [19] where also possible shifts of the GUT scale are discussed. Another limit which can shift the lower limit for M_{seesaw} towards higher values than the occurence of the Landay pole is the possible appearance of negative squared masses for the scalars. This problem is avoided or at least reduced as we increase the mSUGRA parameters.

Chapter 5

Rare lepton decays

5.1 Experimental low energy constraints

Since in the Standard Model neutrinos and charged leptons are isodoublet partners with identical flavor quantum numbers, flavor violation is expected to appear also in the charged lepton sector as soon as we introduce a mechanism that generates neutrino flavor mixing. This leads to new possible rare decay processes like the two-body decays $l_i \to l_j\gamma$ and the three-body decays $l_i \to 3l_j$ [48]. From low energy experiments performed by the MEG collaboration [15], the BELLE collaboration [16] and others [17, 18], the branching ratios (BRs) for these decays are constrained to the very small values listed in Tab. 5.1. Especially the branching ratio of the LFV decay $\mu \to e\gamma$ constitutes a strong constraint on many models where a sensitivity of $\mathcal{O}(10^{-13})$ is expected in the near future.

BR	current bound
$\mu \to e\gamma$	$2.4 \cdot 10^{-12}$ [15]
$\tau \to e\gamma$	$1.2 \cdot 10^{-7}$ [18]
$\tau \to \mu\gamma$	$4.5 \cdot 10^{-8}$ [18]

BR	current bound
$\mu \to 3e$	$1.0 \cdot 10^{-12}$ [52]
$\tau \to 3e$	$2.7 \cdot 10^{-8}$ [18]
$\tau \to 3\mu$	$2.1 \cdot 10^{-8}$ [18]

Table 5.1: Current experimental bounds for the BRs of low energy two-body (left) and three-body (right) LFV decays.

Implementing neutrino masses in the SM yields only tiny values for these BRs since they are suppressed by the neutrino masses over the W boson masses as shown in the diagram of Fig. 5.1. In a supersymmetric scenario, the situation is different because new particles with lepton flavor appear; in the MSSM case these are the sleptons (cf. section 3.5.3). The mass ratios of the sparticles involved in the contributing SUSY 1-loop diagrams (Fig. 5.2) are, in general, clearly larger than the

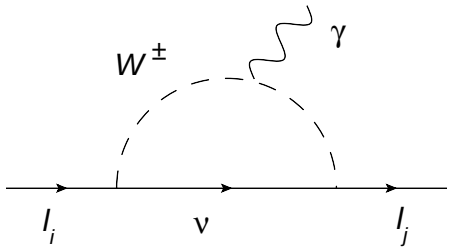

Figure 5.1: SM 1-loop graph for BR($l_i \to l_j\gamma$) mediated by neutrinos and W bosons.

one in Fig. 5.1. Since the seesaw mechanism can induce flavor violating entries in the slepton mass parameters, this can result in strongly enhanced branching ratios for the rare lepton decays [48, 53]. This is a typical property of the SUSY seesaw models and constrains them strongly, especially in the seesaw type III model as will be seen later on.

5.2 Lepton flavor violation in the slepton sector

Depending on the realized supersymmetry breaking mechanism there are different possible sources of flavor violation or combinations of these sources. In mSUGRA scenarios without additional seesaw particles we can choose to work in a basis where the 6×6 squared mass matrix of the charged sleptons M_L^2 and the 3×3 sneutrino squared mass matrix M_ν^2 are flavor diagonal (cf. section 3.5.3). This is motivated by the assumption of flavor-blind mSUGRA mediation of SUSY breaking introduced in section 3.4. The additional particles and neutrino Yukawa couplings of the seesaw mechanism change this situation: In our seesaw type III model, the non-trivial flavor structure of the Yukawa couplings Y_W induces off-diagonal entries in the slepton squared mass matrices that cannot be rotated away. Through the running of the RGEs down from the GUT scale to the seesaw scale the flavor mixing is communicated to the low energy fields [54].

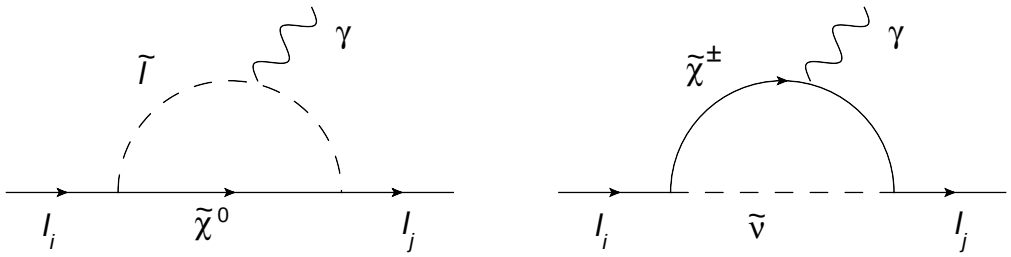

Figure 5.2: 1-loop graphs dominating BR($l_i \to l_j\gamma$) via lepton flavor violation in the slepton sector.

The LFV in the rare lepton decays occurs in the slepton sector, either generated via charged slepton mixing and mediated by neutralinos or caused by sneutrino

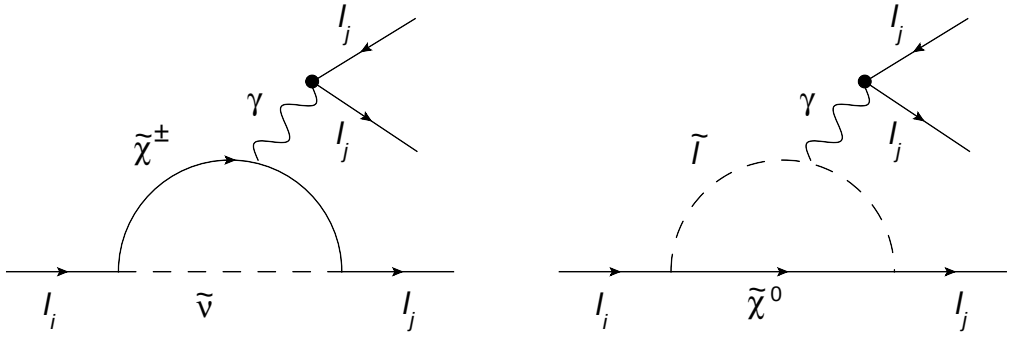

Figure 5.3: The analogon to Fig. 5.2 for the three-body decays.

mixing involving charginos in the loop. The 1-loop diagrams are shown in Fig. 5.2 for the two-body and Fig. 5.3 for the three-body decays. Like for the superpartners the sneutrino mixing is in general large compared to the charged slepton mixing, so that the diagrams including sneutrinos give the dominant contributions.

5.3 Mass insertion approximation

Assuming the off-diagonal entries to be small compared to the diagonal ones, the flavor mixing can be parametrized at the low scale via the mass insertion approximation, independently from the exact source. As we will see later on, this allows to do analytical calculations using a simplified approach. The Feynman graphs in this approximation are shown in Fig. 5.4, the three-body decays are analogous.

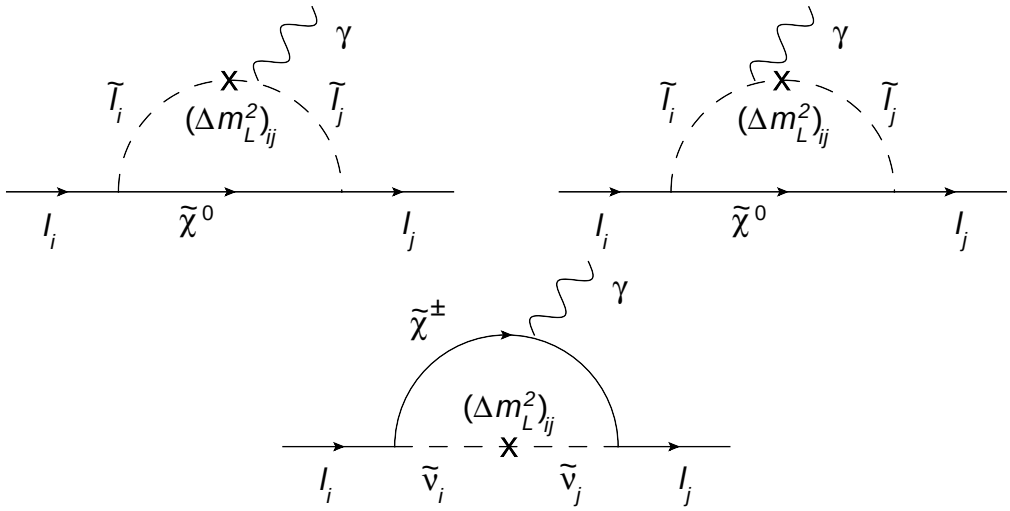

Figure 5.4: Dominating 1-loop graphs for BR($l_i \to l_j\gamma$) corresponding to Fig. 5.2; the LL type mass insertion is denoted by a cross.

The mass insertions

$$(\Delta m^2_L)_{ij} = \widetilde{m}^2 \delta^l_{ij} \tag{5.1}$$

with the mass insertion factor δ^l_{ij} and the average slepton mass $\widetilde{m}$ are the off-diagonal entries in the left slepton squared mass matrix $(m^2_L)_{ij}$. As long as $|\delta| < 1$ the mass insertion approximation works well. According to the chirality of the respective superpartners of the sleptons, there are LL, LR, RL and RR type mass insertions. The dominant part for the considered processes is the LL mass insertion, especially the diagram including charginos, leading to the following rough scaling of the rare lepton decays [19, 48]:

$$\mathrm{BR}(l_i \to l_j \gamma) \approx \frac{\alpha^3}{G_F^2} \frac{\left|\delta^l_{ij}\right|^2}{m^4_{\mathrm{SUSY}}} \tan^2\beta \approx \frac{\alpha^3}{G_F^2} \frac{\left|(\Delta m^2_L)_{ij}\right|^2}{m^8_{\mathrm{SUSY}}} \tan^2\beta \tag{5.2}$$

α is the electroweak coupling constant and G_F the Fermi constant. m_{SUSY} is a typical SUSY breaking mass like the slepton or gaugino masses; so we assumed $\widetilde{m} \approx m_{\mathrm{SUSY}}$. Since these masses enter here in high inverse powers and the seesaw type III has a lighter sparticle spectrum (cf. section 4.4) this – together with typically larger Yukawa couplings (from the larger seesaw scale) – leads to larger LFV branching ratios compared to the type I model [54]. For the complete computation we have to take into account also the other types of mass insertions – especially the RR type. There could basically exist regions in the parameter space with accidental cancellations between these terms [48]. However, in this work the focus is only on the effects of the dominating LL type insertions; the topic of chapter 6 is the search after such suppressed regions only by cancellations between different terms within that type. The numerical calculations will show that this is a well-working approximate description of LFV in our models.

Via a one-step integration of the RGEs in the leading log approximation we get for the mass insertions in the slepton squared mass and the trilinear coupling matrices the following expressions with the mSUGRA parameters specified in chapter 3 [19]

$$(\Delta m^2_L)_{ij} \cong -\frac{9}{5}\frac{1}{8\pi^2}(3m_0^2 + A_0^2)(Y_W^\dagger L Y_W)_{ij} \tag{5.3}$$

$$(\Delta A_e)_{ij} \cong -\frac{9}{5}\frac{3}{16\pi^2}A_0(Y_e Y_W^\dagger L Y_W)_{ij} \tag{5.4}$$

Here we used a basis where the leptonic Yukawa coupling Y_e is diagonal. L is a diagonal matrix specified by

$$L = \mathrm{diag}\left(\ln\left(\frac{M_{\mathrm{GUT}}}{M_1}\right), \ln\left(\frac{M_{\mathrm{GUT}}}{M_2}\right), \ln\left(\frac{M_{\mathrm{GUT}}}{M_3}\right)\right) \tag{5.5}$$

for three generations resp.

$$L = \mathrm{diag}\left(\ln\left(\frac{M_{\mathrm{GUT}}}{M_1}\right), \ln\left(\frac{M_{\mathrm{GUT}}}{M_2}\right)\right) \tag{5.6}$$

for two generations of **24**-plets with the masses M_1, M_2, M_3 and the GUT scale M_{GUT}.

Like in the other seesaw types the flavor violation in the right-slepton sector is negligible:

$$(\Delta m_e^2)_{ij} \cong 0 \tag{5.7}$$

The previous approximations work quite well for the seesaw type I. For types II and III, especially for regions with low m_0 and large $m_{1/2}$ that we will use later on, they are bad approximations concerning the absolut scale of the matrix elements [48]. However, the general behavior and the cancellation points are described very good by these formulae.

Since in this approximative description both the $l_i \to l_j\gamma$ and the $l_i \to 3l_j$ decays are driven by the same mass insertions (cf. Figs. 5.2, 5.3 and 5.4) they are expected to show a similar behavior in the parameter scans. There are also other processes that are dominated by this effect. At the LHC for example the lepton flavor violating decays of the next-to-lightest neutralino $\widetilde{\chi}_2^0 \to \widetilde{\chi}_1^0 l_i l_j$ are interesting phenomena. The investigation of these decays and their phenomenological properties at the LHC will be the subject of chapter 7.

Chapter 6

Studies of the parameter space

To get a first overview of the regions in the parameter space where the branching ratios of the lepton flavor violating μ- and τ-decays are compatible with the experimental constraints, we do at first some analytical studies of the LFV branching ratios, that allow us to check the influence of different parameters quickly without calculating the whole spectrum for every point. Of course this can only be done in an approximative way which was motivated in chapter 5.3, using Eq. 5.2 with $(\Delta m_L^2)_{ij}$ expressed by Eq. 5.4 leading to the proportionality

$$\mathrm{BR}(l_i \to l_j \gamma) \propto \left|(\Delta m_L^2)_{ij}\right|^2 \propto \left|(Y_W^\dagger L Y_W)_{ij}\right|^2 \equiv \Delta_{ij}^2. \tag{6.1}$$

The Yukawa couplings Y_W are expressed by the Casas-Ibarra [37] formula Eq. 4.26 (or Eq. 4.35 for the two **24**-plet case) in terms of the R matrix, the neutrino and **24**-plet masses and the PMNS matrix U.

The physically cleanest way of analytical studies is the consideration of the squared ratios of the BRs as this was done in [55]. The favorable feature of this quantity is the independence of the SUSY parameters and other prefactors, which do not cause any problems because of the division. However, for our investigations it seems to be easier to consider the corresponding off-diagonal entries of the slepton mass matrix $|(\Delta m_L^2)_{ij}|^2$ or, without prefactors, the Δ_{ij}^2 itselves, since they correspond directly to the branching ratios of $\mathrm{BR}(l_i \to l_j \gamma)$ and other processes with the same flavor change. As long as the mass insertion approximation works well, we state good accordance in the behavior of these quantities. Of course, the absolute size of the Δ_{ij}^2 is no longer an experimentally approachable physical value; but for the search for cancellations and the observation of general properties as a first hint for further numerical studies prefactors are not of major interest.

After receiving an overview of the interesting regions, the second step is to calculate the exact values numerically to get the absolut size of the branching ratios to compare them with the experimental constraints presented in section 5.1. These calculations have been done with the LFV version of the program package `SPheno` [56, 57] in a numerical procedure as done e. g. in [19]. At first we use the Yukawa couplings calculated like before from the inverted seesaw formulae Eq. 4.26 and Eq. 4.35. They

are inserted at the seesaw scale and also affected by the RGE running to the low energy scale where neutrino data is measured. The neutrino masses and mixing angles obtained this way usually deviate from the current experimental values (cf. chapter 2). To fit them to data, we vary the input values for the Yukawas in a simple iteration that converges in a few steps if they are small compared to 1. Because of the stronger RGE running already mentioned in section 4.4 the differences can be larger in type II and type III seesaws and thus in general more steps are required than in type I. This neutrino data fit is implemented in the front end program `FrontEndSPheno` [58], that was used to scan over various input parameters. We use 2-loop RGES unless stated otherwise, calculated with the package `SARAH` [59–61].

If not specified otherwise, the PMNS matrix is taken in the tri-bi-maximal form (Eq. 2.6), the **24**-plet masses degenerate and the R matrix as the unity matrix $R = \mathbb{1}$ to calculate the input values for the Y_ν. In many scans both possible neutrino mass hierarchies (cf. chapter 2) have been tested; if not stated explicitly the calculations are for normal hierarchy. In all our studies the Majorana phases α_1 and α_2 are assumed to be zero. Based on the studies done in [19], the mSUGRA parameter are taken at

$$m_0 = m_{1/2} = 1000 \text{ GeV}, \; A_0 = 0 \text{ GeV}, \; \tan(\beta) = 10, \; \text{sgn}(\mu) = +1. \tag{6.2}$$

Of course, the following plots depend on these parameters. However, the main properties investigated in this chapter are effects of the neutrino and seesaw parameters, whereas the mSUGRA parameters change the scale only weakly. Their influence is considered in chapter 7.

6.1 Effects of the seesaw scale

In section 4.4 we stated the large effects on the mass spectrum produced by the seesaw particles and their dependence on the seesaw scale. Fig. 6.1 shows this compared to type I for some mass parameters of the MSSM, without fixing neutrino data. Since the branching ratios of the LFV decays scale like the SUSY masses to the inverse power eigth, the mass spectrum and thus M_{seesaw} must have substantial impact on $\text{BR}(\mu \to e\gamma)$ etc. This was tested numerically to compare the different types of seesaw mechanism (Fig. 6.2), each with a degenerate spectrum of the seesaw particles. The viable range of M_{seesaw} is restricted from below by the effects mentioned in section 4.4. The upper limit is given by the fact that for larger seesaw scales the fit to neutrino data does not converge. However, a hierarchy between the heavy masses can shift this limit.

As already mentioned, the seesaw type III has a lighter sparticle spectrum, leading with Eq. 5.2 to larger BRs. The allowed range of M_{seesaw} strongly depends on the seesaw type, with a quite short interval for the seesaw III model. Comparing this to the low energy constraints stated in section 5.1, we see that the type III model in this configuration is not compatible because the predicted value for $\text{BR}(\mu \to e\gamma)$ is

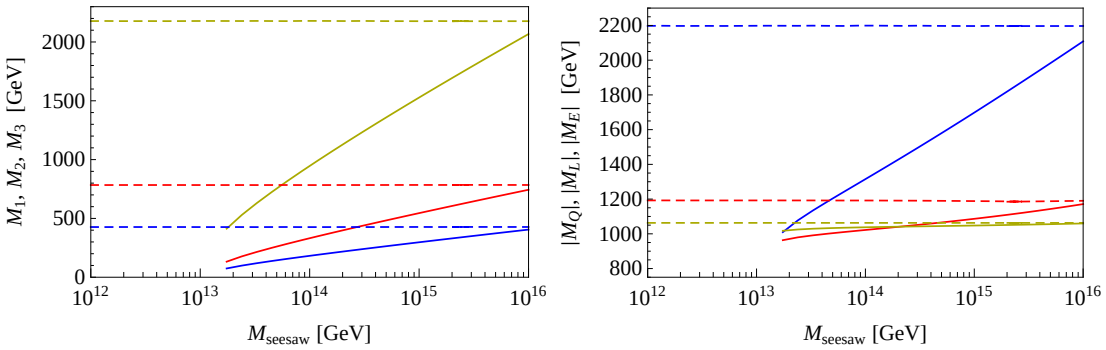

Figure 6.1: Mass parameters M_1 (blue), M_2 (red), M_3 (yellow) on the left resp. $|M_Q|$ (blue), $|M_L|$ (red), $|M_E|$ (yellow) on the right panel versus the seesaw scale for the type III (solid lines) compared to type I (dashed lines). The mSUGRA parameter are as given in Eq. 6.2, neutrino data is not fitted.

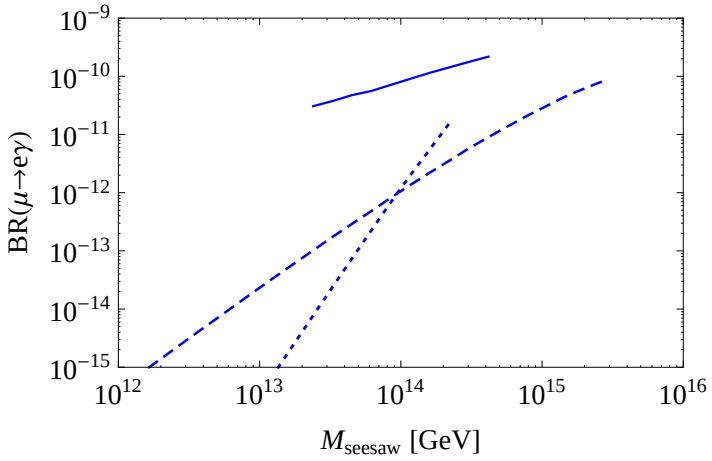

Figure 6.2: BR($\mu \to e\gamma$) versus the seesaw scale for the seesaw type I (dashed), type II (dotted) and type III (solid).

above the limit of $2.4 \cdot 10^{-12}$ everywhere. Therefore, we have to go to special regions in the parameter space where this value is suppressed.

Also the two and the three **24**-plet case have been compared (Fig. 6.3). Here one can clearly see the advantages of the two **24**-plet scenario: the viable range of M_{seesaw} is considerably larger than in the three generation case due to the smaller RGE coefficients; the size of the BRs is also reduced because of the heavier mass spectrum. This means that the reduction to the two generation scenario is one possibility to reach viable regions of the parameter space. Since the dependence is nearly linear, the seesaw scale can be used to fit BR($\mu \to e\gamma$) to a certain value by a simple iteration, which will be done in chapter 7.

In section 4.4 we noted the important 2-loop effects in this model. Thus, we also compared also the calculations at 1-loop and 2-loop level (Fig. 6.4). The 2-loop

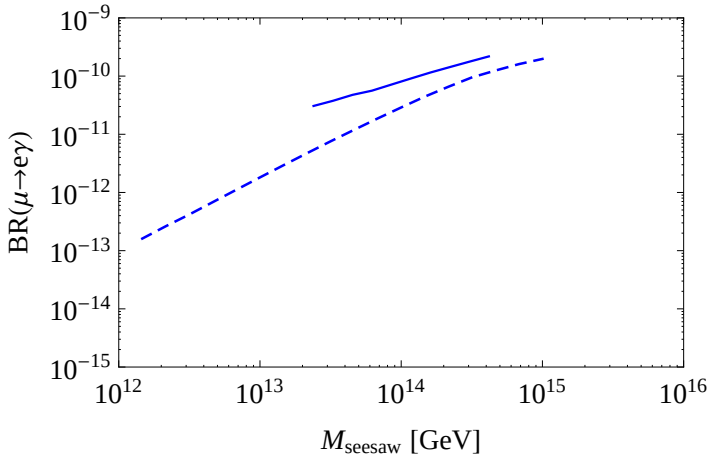

Figure 6.3: BR($\mu \to e\gamma$) versus the seesaw scale for the two (dashed) and the three (solid) **24**-plet scenario; mSUGRA parameters like in Eq. 6.2.

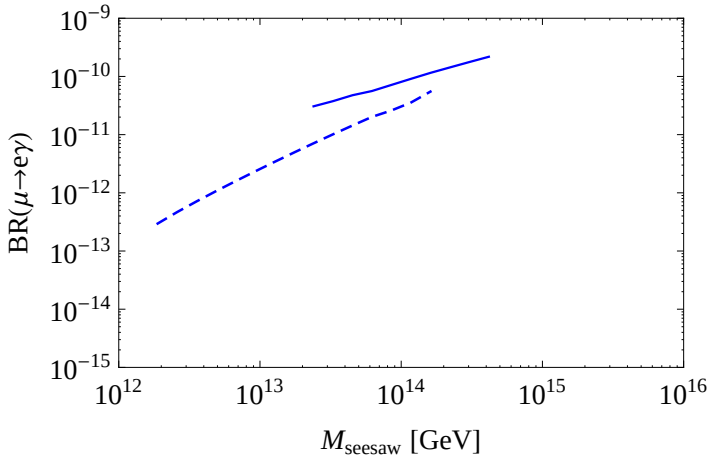

Figure 6.4: BR($\mu \to e\gamma$) versus the seesaw scale calculated with 1-loop (dashed) and 2-loop (solid) RGEs.

effects do have an important impact and lead both to larger BRs because of the stronger RGE runnings as well as to a shift and a decrease of the viable range for the fit to neutrino data.

6.2 The reactor angle θ_{13} and the Dirac phase δ

The first studies are treating the neutrino mixing parameters. Starting from tri-bi-maximal mixing (Eq. 2.6) we fix the solar and the atmospheric mixing angle to

$$\cos(\theta_{12}) = \sqrt{\frac{2}{3}}\ ,\ \cos(\theta_{23}) = \frac{1}{2}\sqrt{2} \tag{6.3}$$

and observe the influence of the variation of the reactor angle from $\theta_{13} = 0$ as this was done in [19].

As stated in chapter 2, there are recent hints to a non-zero reactor angle from the T2K experiment [22]. However, since this is only a first evidence which is yet to be confirmed by other experiments in the near future, studies varying this angle are certainly of major interest, so that the range investigated in this section is from zero to the 3σ limit given in [24] ($0 < \sin^2(\theta_{13}) < 0.035$). Furthermore, the value of the Dirac phase δ is important which can also cause complex parameters (if $\delta \neq n * \pi$, $n \in \mathbb{N}$) in the neutrino mixing matrix U. Since the experimentally allowed range for δ is quite large (see Tab. 2.1), we will not constrain our studies of this phase. The mSUGRA parameters are chosen as in Eq. 6.2, and $R = \mathbb{1}$. In this section we consider only normal neutrino mass hierarchy.

The results in Fig. 6.5 show a good agreement between the Δ_{ij} and the branching ratios calculated by numerics, only slightly changing the point of the cancellation at about $\sin(\theta_{13})^2 = 7 \cdot 10^{-3}$. Taking the prefactors into account can change the relation between the absolute sizes of the different BRs. For a Dirac phase $\delta = 0$ we observe a cancellation in $\mathrm{BR}(\tau \to e\gamma)$. Changing δ to π switches the behavior of Δ_{12}^2 and Δ_{13}^2 resulting in a cancellation for $\mathrm{BR}(\mu \to e\gamma)$. When going to complex parameters, i.e. for values $\delta = 3\pi/4$, we see these cancellations turning incomplete. Because of this complementary behavior, a cancellation in $\mu \to e\gamma$ and $\tau \to e\gamma$ is not possible at the same time by varying the reactor angle; of course the bound for the latter process is clearly weaker. The process $\tau \to \mu\gamma$ is evidently insensitive to variations of θ_{13} for all Dirac phases δ.

Considering the absolute size of $\mathrm{BR}(\mu \to e\gamma)$, we state that there are regions around the cancellation point for $\delta = \pi$ that are in agreement with the experimental constraint of $2.4 \cdot 10^{-12}$. The θ_{13} value at this point is nearly at the lower end of the 1σ region given in Tab. 2.1. Further experimental results on this issue are expected soon.

Apart from this, there is an interesting possibility to move the cancellation point if we go to parameter points with non-degenerate **24**-plet masses (see Fig. 6.6). Proceeding from the point shown in Fig. 6.5 with $\delta = \pi$, changing M_1 has no effect, whereas the hierarchy between M_2 and M_3 is quite important: Setting $M_3 > M_2$ shifts the cancellation to higher $\sin^2(\theta_{13})$ values, while $M_2 > M_3$ does the opposite. The overall scaling of M_2 and M_3 shifts the absolute value of Δ_{12}^2 in a way similar to Fig. 6.3 and does not affect the position of the cancellation.

For the two **24**-plet scenario, it is also possible to achieve cancellations by variation of the reactor angle. Numerical scans on this issue are shown in Fig. 6.7. As in the other case, the cancellation point can also be shifted by varying the mass hierarchy between the two masses M_1 and M_2. However, in this model the search for cancellation points is not that important, because it is already possible to reach viable ranges of $\mathrm{BR}(\mu \to e\gamma)$ by pushing the seesaw scale to sufficiently low values (cf. Fig. 6.3).

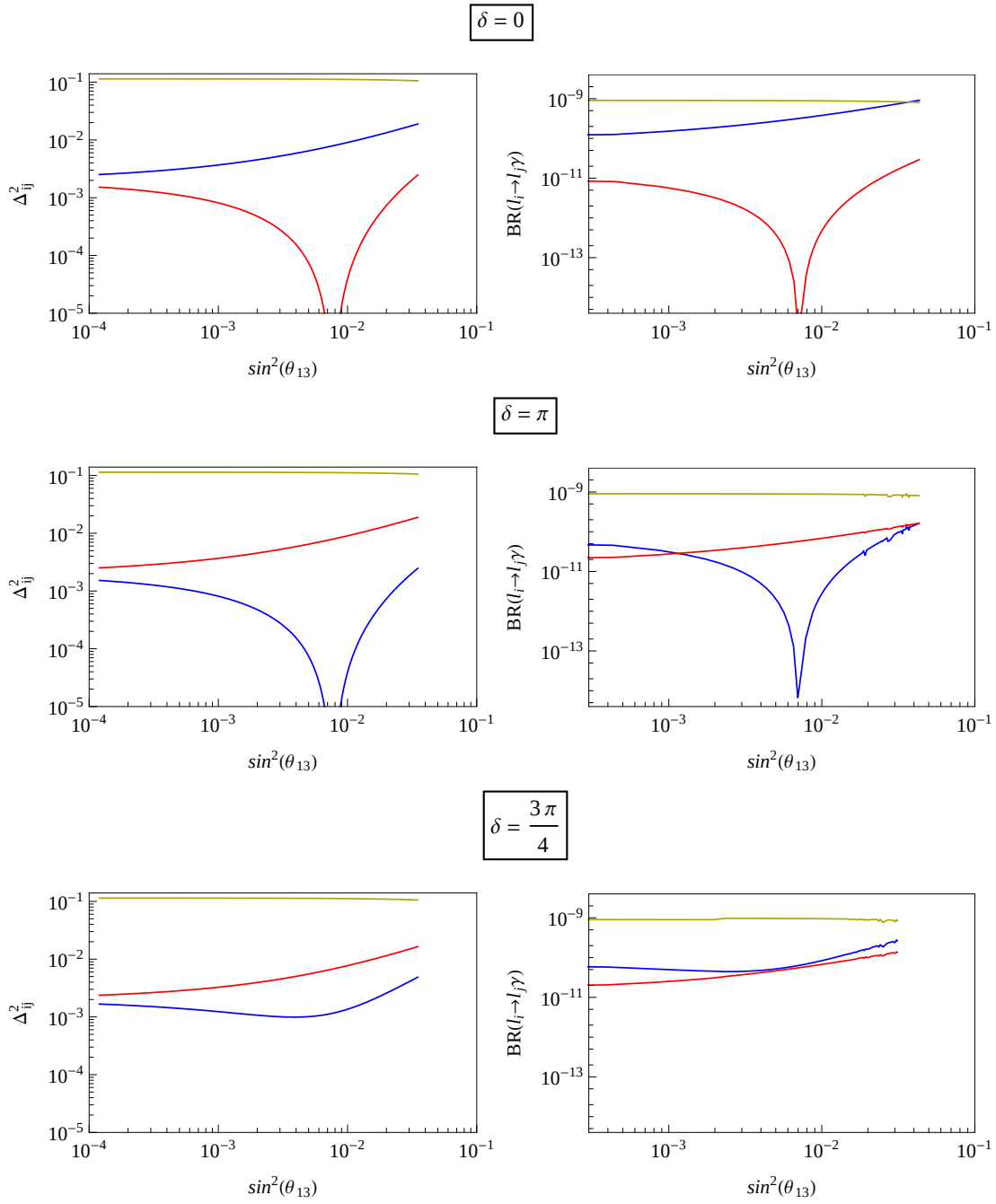

Figure 6.5: Δ^2_{12} (blue), Δ^2_{13} (red), Δ^2_{23} (yellow) to the left and the corresponding $\mathrm{BR}(\mu \to e\gamma)$ (blue), $\mathrm{BR}(\tau \to e\gamma)$ (red) and $\mathrm{BR}(\tau \to \mu\gamma)$ (yellow) to the right over the reactor angle θ_{13} for real parameters with Dirac phases $\delta = 0$ (upper panels), $\delta = \pi$ (mid panels) and $\delta = 3\pi/4$ (lower panel). The M_W are degenerate at $M_1 = M_2 = M_3 = 10^{14}$ GeV. Small fluctuations in the BRs arised due to numerical effects.

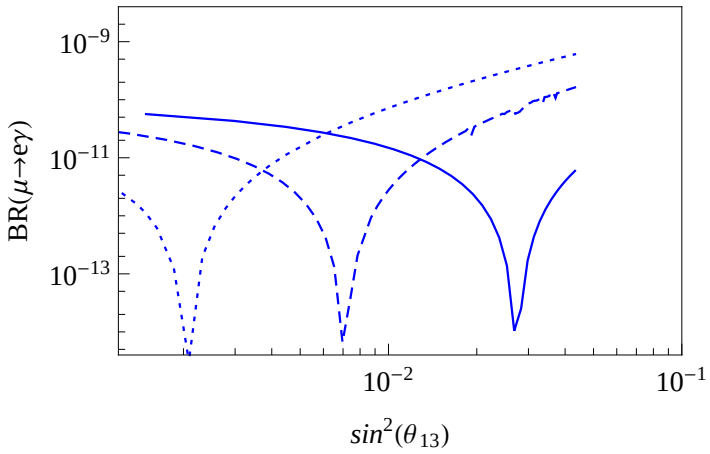

Figure 6.6: BR($\mu \to e\gamma$) for three **24**-plets and $\delta = \pi$ with different hierarchies $M_1 = M_2 = 10^{14}$ GeV, $M_3 = 2 \cdot 10^{14}$ GeV (solid), $M_3 = 1 \cdot 10^{14}$ GeV (dashed) and $M_3 = 5 \cdot 10^{13}$ GeV (dotted); other parameters like in Fig. 6.5.

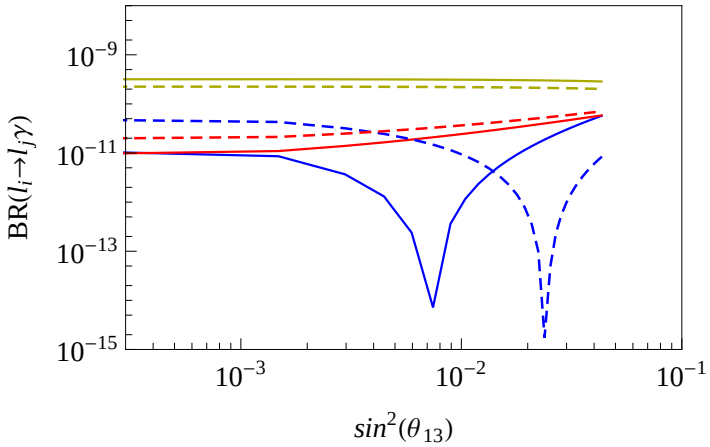

Figure 6.7: BR($\mu \to e\gamma$) (blue), BR($\tau \to e\gamma$) (red) and BR($\tau \to \mu\gamma$) (yellow) at two **24**-plets and $\delta = \pi$ for degenerate masses $M_1 = M_2 = 10^{14}$ GeV, (solid lines) and hierarchical masses $M_1 = 2 \cdot 10^{14}$ GeV, $M_2 = 10^{14}$ GeV, (dashed lines).

6.3 Influence of the R matrix

Since the reactor angle θ_{13} will be measured or at least constrained to a smaller region in the near future and additionally a CP violating phase $\delta = \pi$ is required to produce a BR($\mu \to e\gamma$) cancellation, it is of particular interest to find such cancellations also by varying other (seesaw) parameters. For this, especially the R matrix introduced in Eq. 4.25 (resp. Eq. 4.34 for two **24**-plets) is a promising candidate, as it is not specified by experimentally approachable neutrino data and only restrained by the condition $R^T R = \mathbb{1}$. This can be realized, for example, with the parametrizations

presented in section 4.3, depending on three complex angles in the three **24**-plet scenario and one complex angle in the two **24**-plet scenario.

Though R is not a mixing matrix of the seesaw masses, changing the R angles produces such an effect on the product

$$\rho = R^\dagger \sqrt{M_W} L \sqrt{M_W} R \tag{6.4}$$

appearing in the approximative formula Eq. 6.1

$$\mathrm{BR}(l_i \to l_j \gamma) \propto \frac{5}{2v_u^2} U \sqrt{\widehat{m}_\nu} \left(R^\dagger \sqrt{M_W} L \sqrt{M_W} R \right) \sqrt{\widehat{m}_\nu} U^\dagger, \tag{6.5}$$

and thus on the Δ_{ij}^2. For $s_1 = s_2 = s_3 = 0$ it is given by

$$\rho = \mathrm{diag}\left(M_1 \ln\left(\frac{M_{\mathrm{GUT}}}{M_1}\right), M_2 \ln\left(\frac{M_{\mathrm{GUT}}}{M_2}\right), M_3 \ln\left(\frac{M_{\mathrm{GUT}}}{M_3}\right)\right). \tag{6.6}$$

Changing one of the s_i from 0 to 1 yields a flip between the other two diagonal entries; in case of $s_1 = 1$ this looks like

$$\rho = \mathrm{diag}\left(M_1 \ln\left(\frac{M_{\mathrm{GUT}}}{M_1}\right), M_3 \ln\left(\frac{M_{\mathrm{GUT}}}{M_3}\right), M_2 \ln\left(\frac{M_{\mathrm{GUT}}}{M_2}\right)\right). \tag{6.7}$$

Setting $s_1 = s_2 = s_3 = 1$ acts on the Δ_{ij}^2 like inverting the ordering of the three **24**-plet masses. Correspondingly, values of the s_i different from 0 or 1 provide mixings of the M_W contributions in this matrix. Therefore, as the R matrix produces flippings or mixings, variations of the ϕ angles will change the branching ratios only if the M_W are non-degenerate. On the other hand, with three **24**-plet masses there are even six possible mass hierarchies which in general have to be tested. In the two **24**-plet scenario the situation is sizably easier because of only two possible hierarchies.

6.3.1 Real case

At first we consider real values for the ϕ angles only; complex ones are treated in section 6.3.2. The neutrino mixing angles are fixed to tri-bi-maximal values from Eq. 2.6 and for the time being also the Dirac phase δ is set to zero. The neutrino masses are set to the best fit values given in Tab. 2.1 with a small but non-zero $m_1 = 10^{-4}$ eV $< 1\% \cdot m_3$, which may be of important impact as we will see later on. Here we start with the seesaw III model with two **24**-plets where the situation is less complicated since there is only one angle ϕ parametrizing the 2×3 R matrix (cf. section 4.3.2), together with two possible neutrino mass hierarchies and two possible orderings of the $M_{W,i}$. Fig. 6.8 shows the Δ_{ij}^2 and the corresponding $\mathrm{BR}(l_i \to l_j \gamma)$ for normal hierarchy. The expected accordance of the behavior up to overall scalings motivates the study of the first quantity instead of calculating the whole BRs and spectra for every case. Fig. 6.9 shows these elements for inverse hierarchy where the quantities Δ_{12}^2 and Δ_{13}^2 are degenerate. Certain symmetries which show the effect of ϕ as a kind of mixing angle between the heavy masses can be realized. We find cancellations for the μ–e as well as for the τ–e combination in different constellations.

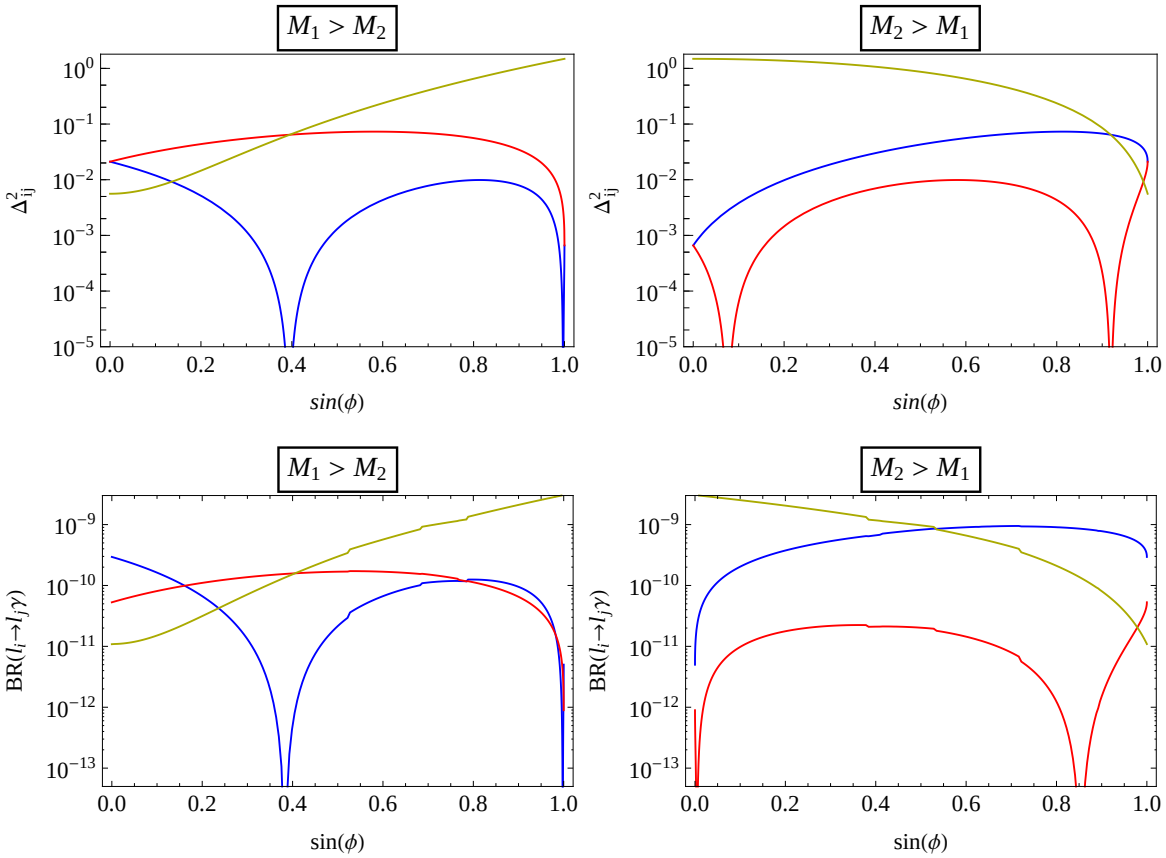

Figure 6.8: Δ^2_{12} (blue), Δ^2_{13} (red) and Δ^2_{23} (yellow) compared to the corresponding $\mathrm{BR}(l_i \to l_j\gamma)$ (lower panels) for two **24**-plets by variation of $\sin(\phi)$ at normal neutrino mass hierarchy, Dirac phase $\delta = 0$ and a **24**-plet hierarchy $M_1 > M_2$ and the two possible **24**-plet mass orderings.

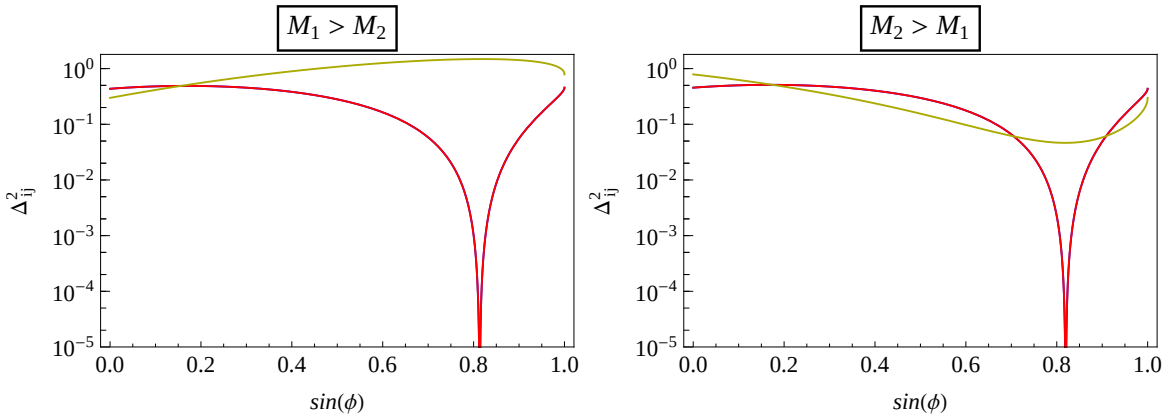

Figure 6.9: Like Fig. 6.8 for inverse hierarchy.

In the next step we treat the realization with three generations of **24**-plet. Their masses are chosen for different hierarchies, but the heaviest one will always take

10^{15} GeV, the mid-one 10^{14} GeV and the lightest one 10^{13} GeV.[1] Here, only normal neutrino mass hierarchy is considered. As in the previous case, we assume good accordance between Δ^2_{ij} and $\mathrm{BR}(l_i \to l_j\gamma)$, which was probed numerically for different parameter combinations. Examples for scans over the ϕ_1 and the ϕ_3 angle are shown in 6.10. Large deviations in the general behavior as well as in the positions of the cancellation points have not been found. Therefore we only show Δ^2_{ij} in the following.

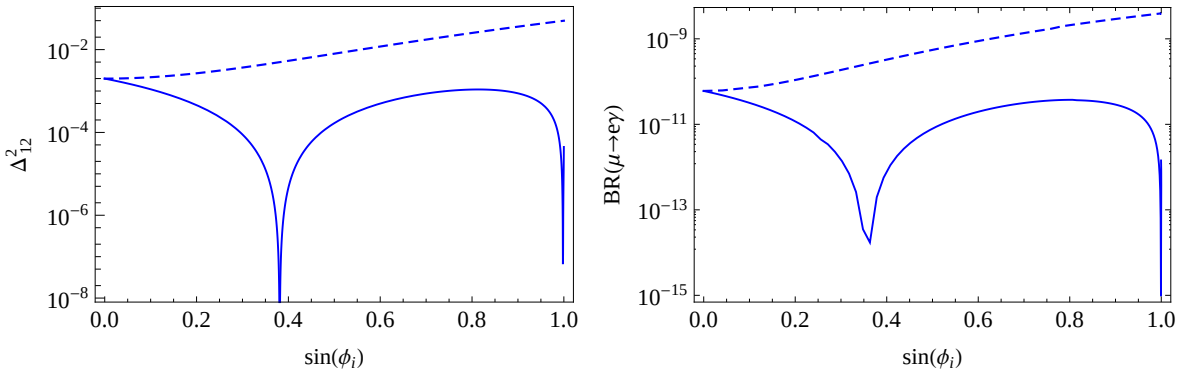

Figure 6.10: Comparison of analytical Δ^2_{12} and numerical $\mathrm{BR}(\mu \to e\gamma)$ calculation, respectively, for variation of $\sin(\phi_1)$ (solid) and $\sin(\phi_3)$ (dashed) with the other angles set to zero, for normal neutrino mass hierarchy, Dirac phase $\delta = 0$ and a **24**-plet hierarchy $M_1 > M_2 > M_3$.

Varying initially only one of the ϕ_i with the other ones set to zero, one will already have $6 \cdot 3 = 18$ plots considering all possible hierarchies and angles. Figures 6.11 and 6.12 show 9 selected ones, three for each ϕ_i angle.

[1] Note that the observations of section 6.1 are only for degenerate $M_{W,i}$; in the non-degenerate case also values outside the given ranges are allowed if the mean value is roughly within the viable range.

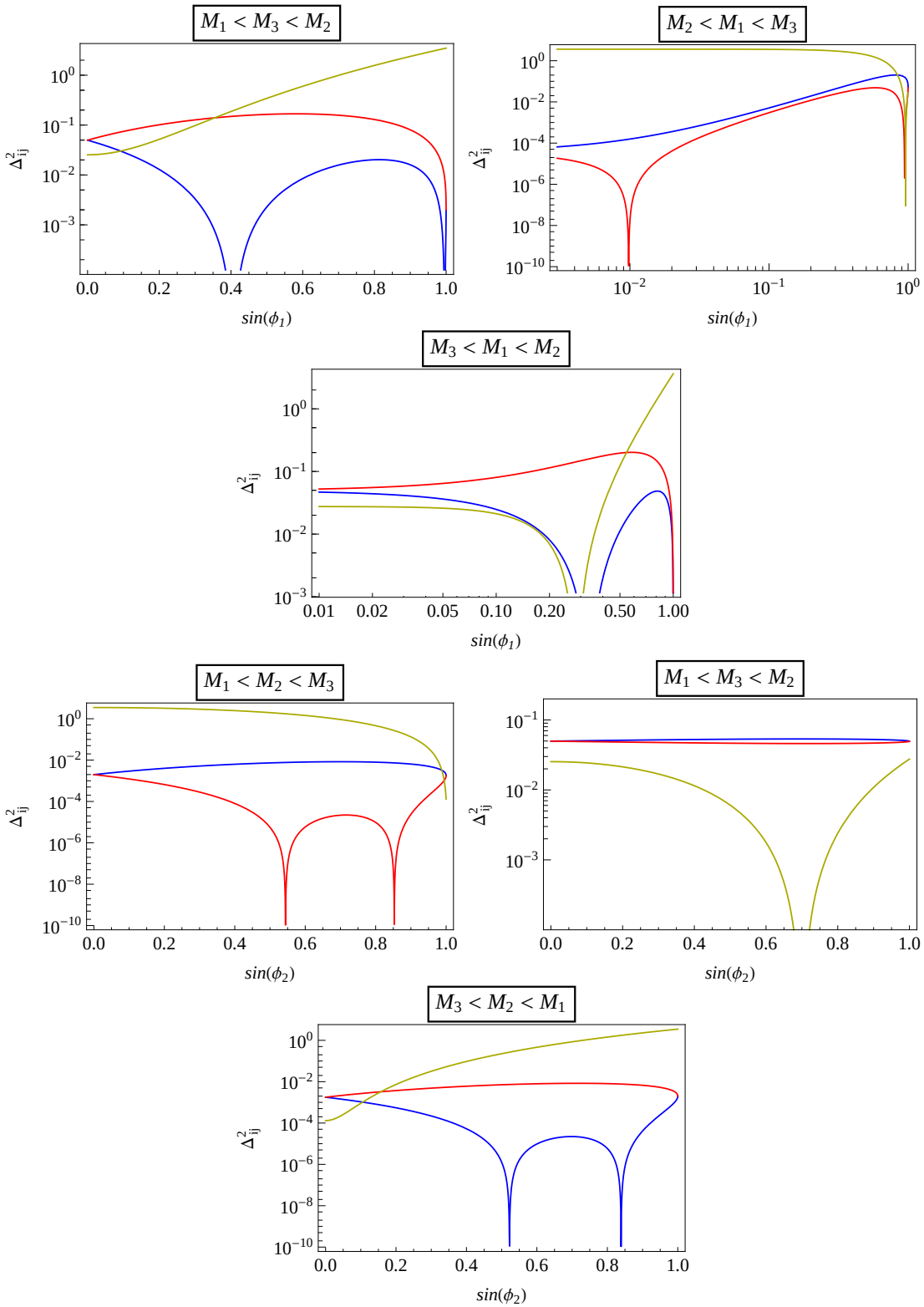

Figure 6.11: Δ^2_{12} (blue), Δ^2_{13} (red) and Δ^2_{23} (yellow) versus $\sin(\phi_1)$ and $\sin(\phi_2)$, respectively, with real ϕ_1 values for different hierarchies of the **24**-plet masses M_1, M_2 and M_3.

There are several combinations of mass hierarchies and ϕ_i angle variations shown in the plot that provide cancellations in the Δ^2_{ij}; for Δ^2_{12} corresponding to $\mu \to e\gamma$, one can find them e. g. for $M_1 < M_3 < M_2$ or $M_3 < M_2 < M_1$ by varying ϕ_1.

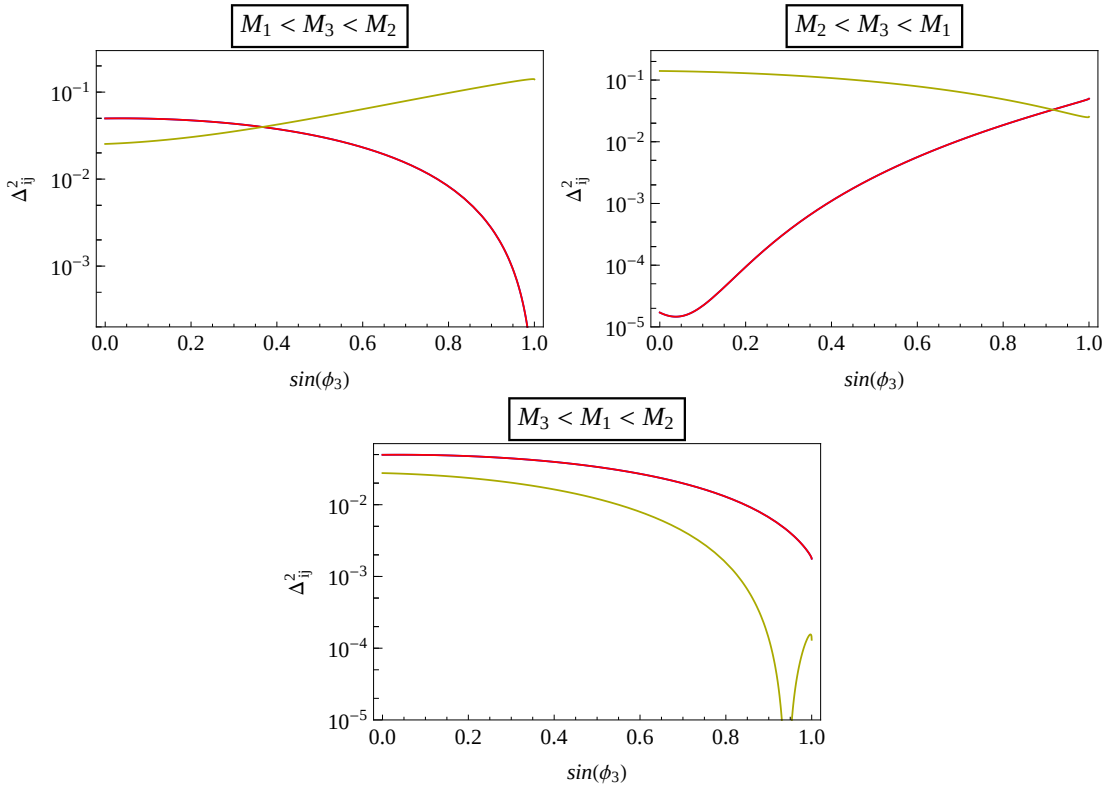

Figure 6.12: Like Fig. 6.11 for variation of ϕ_3.

To generate these cancellations, variation of the ϕ_3 angle seems to be less interesting. In total, the situation does not show any obvious systematics as especially the hierarchy of the $M_{W,i}$ plays an important role.

Of course, in general all ϕ_i angles must be considered to be non-zero. To study this issue, we built 3-dimensional plots by variation of two angles ϕ_i, ϕ_j while holding ϕ_k at a fixed value. A few selected of the many possible combinations are shown in Fig. 6.13 where one indeed can see interesting cancellation regions with more than one angle not equal zero. Since it will not be a study of manageable size to check every possible combination of ϕ_i values and no evident systematics could be identified, we confine ourselves to demonstrating the possibility of such cancellation regions. Of course, we can do the numerical BR($\mu \to e\gamma$) calculation also for these 3-dimensional plots. However, to reach a satisfying resolution, this requires quite time- and data-consuming scans so that we probed that for selected cases only.

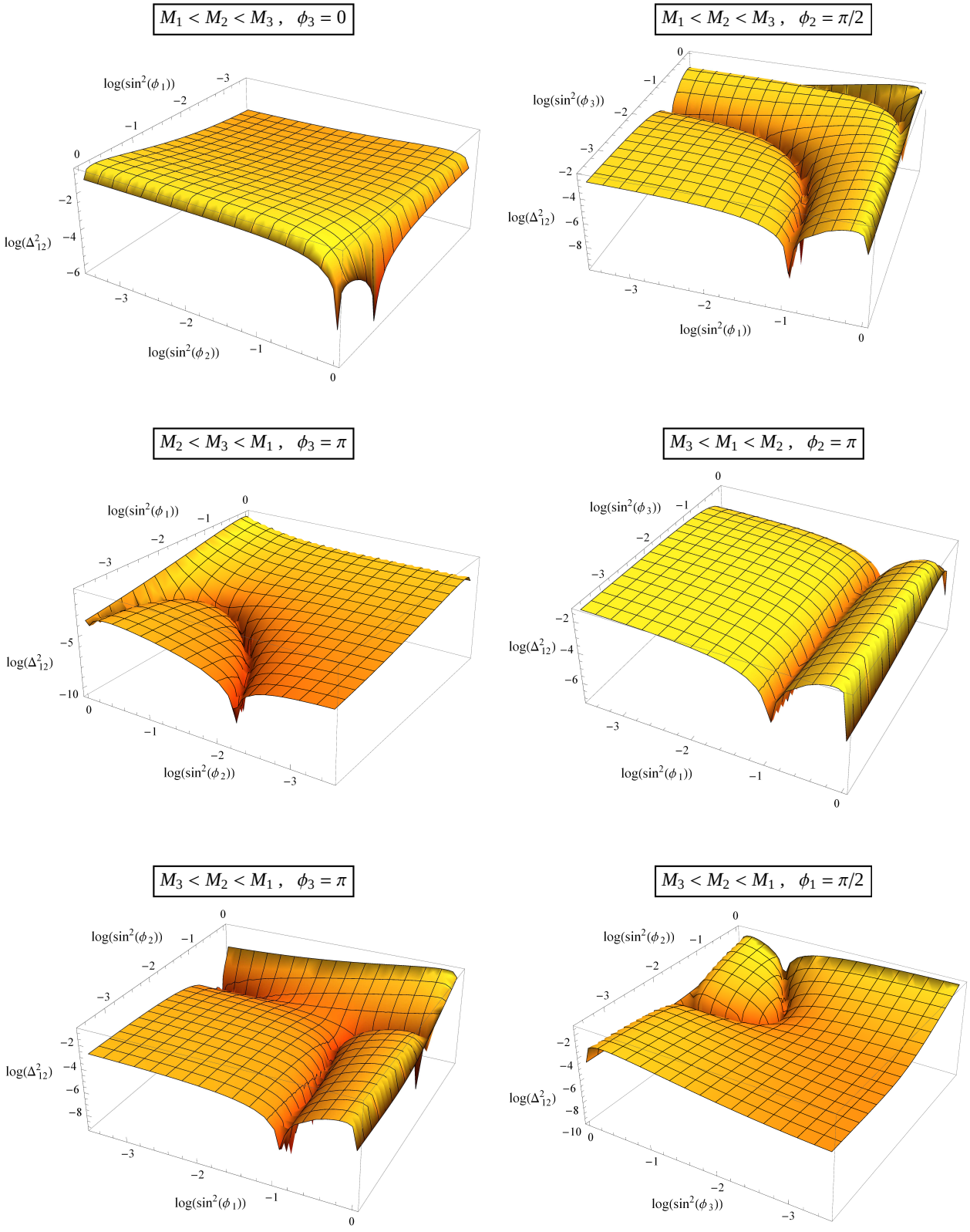

Figure 6.13: 3-dimensional graphs of Δ^2_{12} by varying two ϕ_i angles at a fixed value of the third one for different mass hierarchies of the **24**-plets.

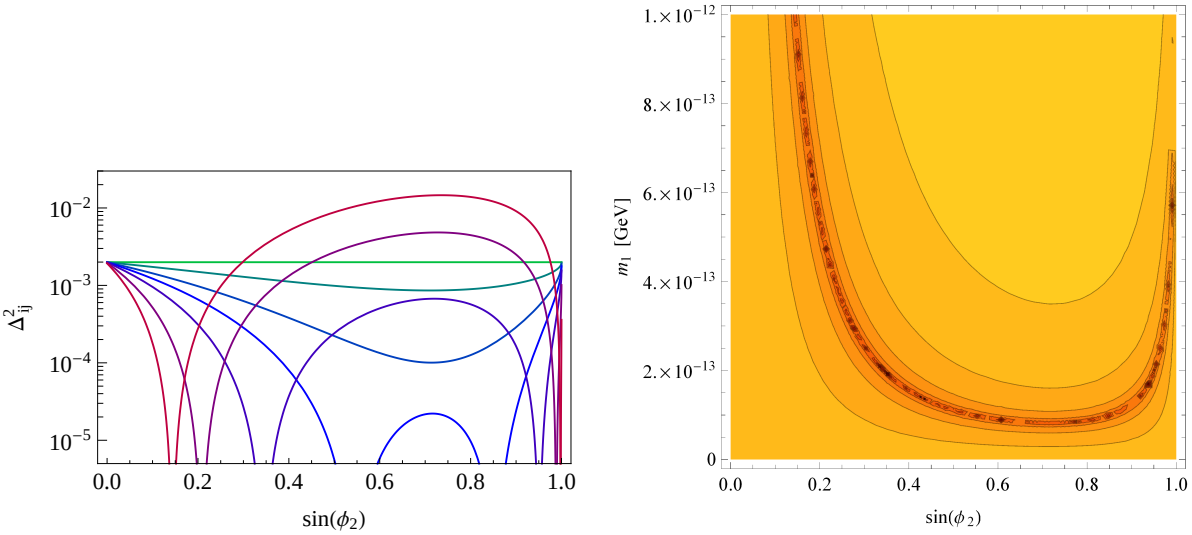

Figure 6.14: Δ^2_{12} for different m_1 values from 0 GeV (green) to 10^{-12} GeV (violet) on the left panel resp. as contour plot on the right panel.

In section 2.2 we remarked the uncertainty of the absolute value of the smallest neutrino mass. In a few special graphs a striking deviation for $m_1 = 0$ (resp. $m_3 = 0$) could be determined. One of these cases for the three **24**-plet model and normal hierarchy is shown in Fig. 6.14 where the cancellation depends strongly on m_1 and only appears for a non-zero value. Hence, one has to check also for the influence of this value in general.

6.3.2 Complex case

For general situations one has to consider the angles parametrizing the R matrix to be complex. However, for the case of three seesaw particles this means an observation of six ϕ parameters (three angles and three phases) together with the already mentioned six possible hierarchy combinations; additionally, the two possible neutrino mass hierarchies as well as the neutrino mixing parameters – especially the reactor angle θ_{13} and the Dirac phase δ – have to be considered. Thus, a complete study of all different parameter combinations would hardly be of manageable size. In [62], an overview of many parameter combinations was given for the seesaw type I.

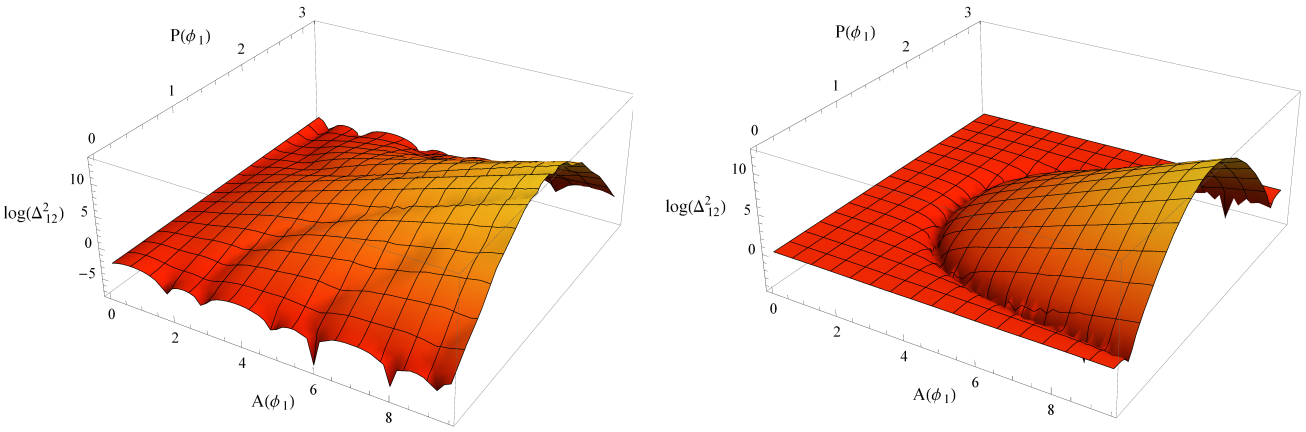

Figure 6.15: Complex parameter scans of Δ^2_{12} over modulus $A(\phi_1)$ and phase $P(\phi_1)$ of the R parametrization angle ϕ_1 at normal (left panel) resp. inverse (right panel) neutrino mass hierarchy, tri-bi-maximal neutrino mixing and $M_3 > M_2 > M_1$.

As we already demonstrated in the previous sections, there are many potential parameter combinations to produce cancellations in the LFV decays. Therefore, we will restrict ourselves to only show the possibility to generate such cancellations for complex angles. Indeed, a certain selection of analytical parameter studies including complex R matrix entries was done, but without finding any systematics in the behavior. Generally, the scenarios with inverse neutrino mass hierachy are somewhat more interesting to find cancellation at complex R parameters. Two exemplary graphs for the three **24**-plet scenario are shown in Fig. 6.15

6.4 Three-body decays

So far we have only discussed the lepton flavor violating two-body decays $l_i \to l_j\gamma$. However, there are other low energy processes concerning the lepton sector which are constrained by experiments. In chapter 5.1 we already mentioned the three-body decays $l_i \to 3l_j$ which also need to be tested in general. Nevertheless, as stated in section 5.3, the decays $l_i \to l_j\gamma$ and $l_i \to 3l_j$ in the mass insertion approximation are driven by the same mass insertion factor $(m_L^2)_{ij}$, given by Eq. 5.4. So we expect the three-body decays to behave roughly like the two-body analogs under variation of the neutrino mixing or the seesaw parameters. This was tested by several numerical scans.

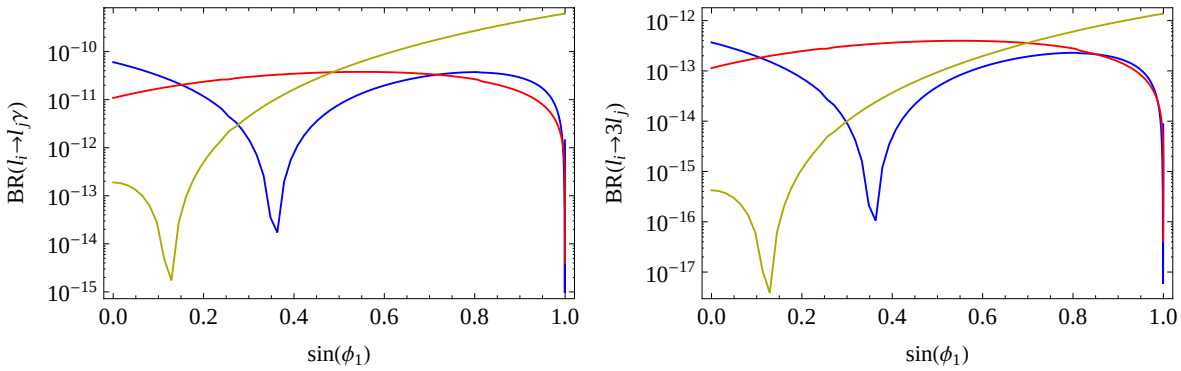

Figure 6.16: Comparison of the two-body decays $l_i \to l_j\gamma$ (left panel) and the-three body decays $l_i \to 3l_j$ (right panel) for variation of $\sin(\phi_1)$ at normal neutrino mass hierarchy, Dirac phase $\delta = 0$ and a **24**-plet hierarchy $M_1 > M_2 > M_3$; l_i, $l_j = \mu$, e (blue); τ, e (red); τ, μ (yellow).

One example is shown in Fig. 6.16 where this assumption is confirmed distinctly. Hence we also conclude that possible contributions from box diagrams including either neutralinos and charged sleptons or charginos and sneutrinos are negligible. These and other diagramms contributing to LFV three-body decays are discussed in [63]. Since the absolute size of the branching ratios in Fig. 6.16 is more than two orders of magnitude smaller than for the corresponding two-body decays and the scaling is quite similar, we do not run into problems with the experimental bounds given in Tab. 5.1 as long as our model agrees with the BR($\mu \to e\gamma$) bound.

6.5 Other low energy observables

Further experimental constraints on low energy observables related to lepton flavor violation have also been tested by the numerical calculations. One of particular interest is the electric dipole moment of the electron, which appears if we go to complex Yukawa couplings like in section 6.3.2. We found that it is roughly correlated to BR($\mu \to e\gamma$). However, at all tested parameter points, this value was smaller than $\mathcal{O}(10^{-33})$ e cm and thus is far below the current experimental bound of $10.5 \cdot 10^{-28}$ e cm given in [64].

The overall result of the parameter studies does not show any striking systematics concerning the appearance of accidental cancellations and the number of parameters makes it difficult to study all possible combinations in a comprehensive way. Hence, we conclude that the realization with two **24**-plets is the more interesting scenario, not only because of the reduced number of input parameters, but especially from the fact that, in the case of an appropriate seesaw scale, no cancellation is required as long as BR($\mu \to e\gamma$) will not be constrained to even smaller values of $\mathcal{O}(10^{-13})$ in the near future. Nevertheless, if three massive neutrinos are realized in nature, this model is no longer a valid description. Then we will have to consider three generations of the **24**-plet in which case the situation is more complicated because of the larger number of parameters. Still we found various possibilities to generate cancellations for both models by variation of neutrino mixing parameters like θ_{13} or the neutrino mass hierarchy as well as seesaw specific quantities like the R matrix or the **24**-plet masses. Moreover, interesting tendencies produced by shifting the seesaw scale or varying the hierarchy of the heavy masses could be identified and used to move the cancellation points to other parameter values which will be interesting if certain quantities will be measured or more constrained in the future. So, even if in some cases a special fine-tuning should be required, there are several methods to find parameter regions in accordance with experimental constraints.

Chapter 7

LHC phenomenology of lepton flavor violating decays

The LFV processes discussed in the previous chapters take place at low energies. However, we expect such flavor mixing effects to also arise at the high energy scale where the masses of supersymmetric particles supposedly are located. The aim of this work is therefore to identify LFV decays within a SUSY seesaw III scenario, which are in accordance with the low energy constraints and measurable in the 14 TeV run at the LHC [1]. For this, we will mainly treat the seesaw III model with two **24**-plet generations where the branching ratios of all rare lepton decays are below the respective constraints at certain values of M_{seesaw} without the requirement of any special cancellation regions in the parameter space.

7.1 Lepton flavor violating decays of the $\widetilde{\chi}_2^0$

Since the sparticle mass spectrum is quite heavy and we presume a proton-proton center of mass energy $\sqrt{s} = 14$ TeV at the LHC, which is of course reduced at the parton level, it is clear that the probability to see sparticles and their decays is largest for the lightest sparticles. In section 3.6 we already mentioned the special impact of the LSP – in our case the lightest neutralino $\widetilde{\chi}_1^0$ – in R-parity conserving models. For this reason, the most interesting processes should be LFV decays of other light sparticles into the LSP and other products, including two leptons of different flavor. As neutrinos cannot be detected directly by the LHC experiments (especially [2, 3]), only charged leptons in the final state are considered. In this work, we study the decay of the next-to-lightest neutralino $\widetilde{\chi}_2^0$ into the LSP $\widetilde{\chi}_1^0$ and two charged leptons $l_i^{\pm}$, $l_j^{\mp}$ with distinct flavor and opposite charge. This process is mediated by charged sleptons, given at tree level by the Feynman graph shown in Fig. 7.1. We use the narrow-width-approximation [65, 66] to factorize the BRs of the cascade decays. In general the contributions of all six sleptons have to be considered. However, if some of them are off-shell, i.e. heavier than the neutralino $\widetilde{\chi}_2^0$, the respective diagrams will be strongly suppressed, leading to a reduced branching ratio $\text{BR}(\widetilde{\chi}_2^0 \to \widetilde{\chi}_1^0 l_i l_j)$. This

quantity is summed over all intermediate sleptons and charges, including also the BR of the direct three-body decay:

$$\begin{aligned}\mathrm{BR}(\widetilde{\chi}_2^0 \to \widetilde{\chi}_1^0 l_i l_j) &= 2 \cdot \mathrm{BR}(\widetilde{\chi}_2^0 \to \widetilde{\chi}_1^0 l_i^+ l_j^-) \\ &+ 2 \cdot \sum_{k=1}^{6} \left(\mathrm{BR}(\widetilde{\chi}_2^0 \to l_i^+ \widetilde{l}_k^-) \mathrm{BR}(\widetilde{l}_k^- \to l_j^- \widetilde{\chi}_1^0) + \mathrm{BR}(\widetilde{\chi}_2^0 \to l_j^- \widetilde{l}_k^+) \mathrm{BR}(\widetilde{l}_k^+ \to l_i^+ \widetilde{\chi}_1^0) \right).\end{aligned} \tag{7.1}$$

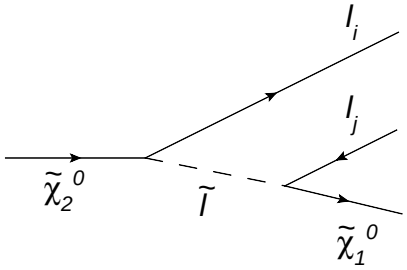

Figure 7.1: Tree-level diagram for the process $\widetilde{\chi}_2^0 \to \widetilde{\chi}_1^0 l_i l_j$, mediated by charged sleptons.

In the mass insertion approximation introduced in section 5.3, this graph can be described like in Fig. 7.2. Of course, the mass insertion $(\Delta m_L^2)_{ij}$ in this diagram is the same as in the low energy processes of Fig. 5.4:

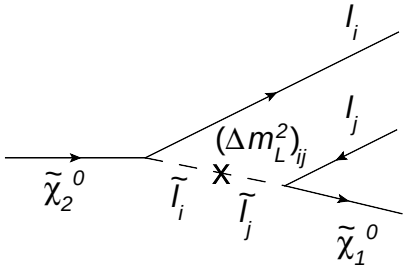

Figure 7.2: The diagram of Fig. 7.1 in the mass insertion approximation.

Thus we expect $\mathrm{BR}(\widetilde{\chi}_2^0 \to \widetilde{\chi}_1^0 l_i l_j)$ to scale roughly like the branching ratios of the rare lepton decays $l_i \to \ l_j \gamma$ and $l_i \to 3 l_j$. This was probed numerically by various scans, varying different parameters like in chapter 6. Figs. 7.3, 7.4 and 7.5 show this behavior for various scenarios. One can see that the general trend is the same; however, the ratios between the different flavor combinations as well as the overall scales behave in a distinct way. The small magnitude of $\mathrm{BR}(\widetilde{\chi}_2^0 \to \widetilde{\chi}_1^0 l_i l_j)$ originates from the fact, that for the chosen mSUGRA parameters all sleptons are off-shell. Also for complex ϕ angles in the R matrix the cancellations are similar. This behavior restricts us to get regions with small $\mathrm{BR}(\mu \to e\gamma)$ as long as we like to achieve large branching ratios for the LFV neutralino $\widetilde{\chi}_2^0$ decay or at least at the

μ-e-version of this decay. Nevertheless, one could use some of the cancellation points in the parameter space to get a sufficiently small BR($\mu \to e\gamma$) together with an also small BR($\widetilde{\chi}_2^0 \to \widetilde{\chi}_1^0 \mu e$), but, at the same time, sizable branching ratios of the other LFV $\widetilde{\chi}_2^0$ decays.

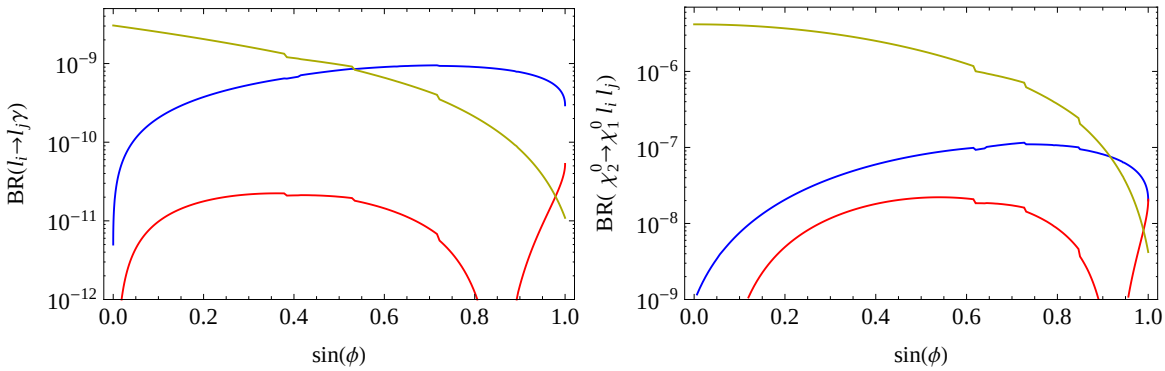

Figure 7.3: BR($l_i \to l_j\gamma$) (left panel) and BR($\widetilde{\chi}_2^0 \to \widetilde{\chi}_1^0 l_i l_j$) (right panel) versus the real R parametrization angle ϕ for two **24**-plets; mSUGRA parameters as given by Eq. 6.2, $M_2 > M_1$, U tri-bi-maximal, CP phase $\delta = 0$ and normal neutrino mass hierarchy. $i, j = \mu, e$ (blue); τ, e (red), τ, μ (yellow).

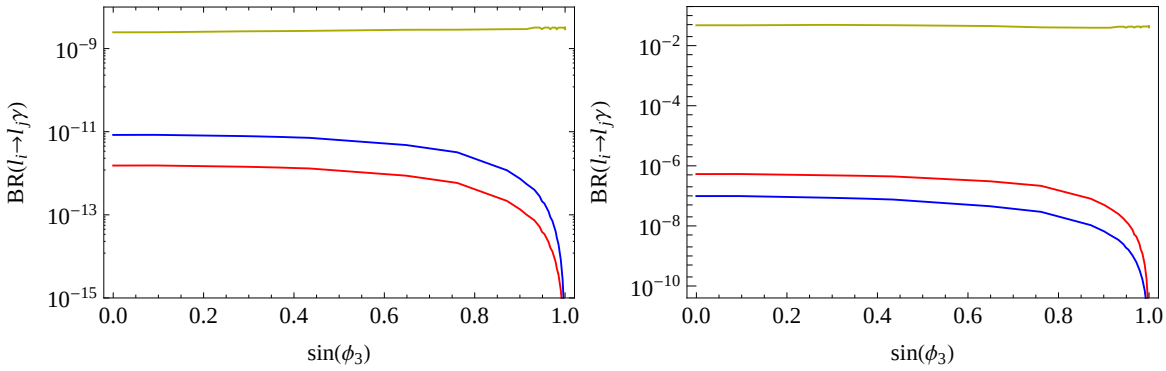

Figure 7.4: Like Fig. 7.3 for three **24**-plets with $M_3 > M_2 > M_1$, $m_0 = 250$ GeV and $m_{1/2} = 1800$ GeV and variation of ϕ_3 while $\phi_1 = \phi_2 = 0$.

Since the LHC is a proton collider, the preferred particles produced in the collisions are colored particles. Among the sparticles of the MSSM only squarks and the gluino show this characteristic. Neutralinos are mainly produced in squark decays like

$$\widetilde{q} \to q\widetilde{\chi}_2^0, \tag{7.2}$$

leading to final states with the particles of Fig. 7.1 plus a jet. Gluinos decay only into quark-squark-pairs where the squarks again can decay into neutralinos, including one more jet in the final state. Since we postulate R-parity conservation, sparticles can be produced only in pairs, and so at least two jets are required; even more jets might appear in decay chains including gluinos.

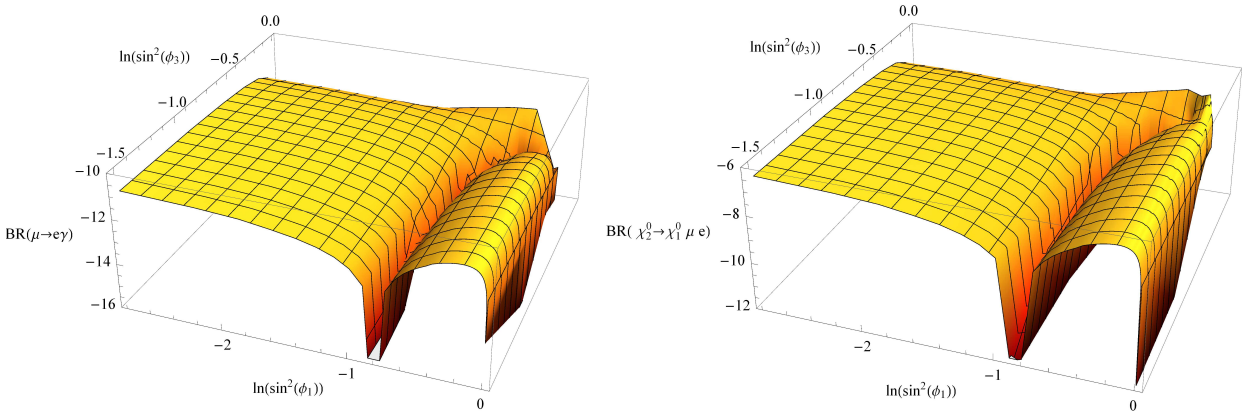

Figure 7.5: 3-dimensional plot for BR($\mu \to e\gamma$) (left panel) and BR($\widetilde{\chi}_2^0 \to \widetilde{\chi}_1^0 \mu e$) (right panel) by variation of ϕ_1 and ϕ_3.

7.2 Parameter scans at fixed BR($\mu \to e\gamma$)

In the previous section we have seen that the branching ratios of the LFV neutralino $\widetilde{\chi}_2^0$ decays scale very similarly to the rare lepton decays. Hence, we can conclude that regions with small BR($l_i \to l_j\gamma$) are not interesting for phenomenological studies on the resp. neutralino decays. So, we took the strongest of these constraints, namely the one on BR($\mu \to e\gamma$) and fixed this quantity to a short interval below the experimental constraint given in Tab. 5.1:

$$2.2 \cdot 10^{-12} < \text{BR}(\mu \to e\gamma) < 2.4 \cdot 10^{-12} \tag{7.3}$$

This was done by varying the seesaw scale using a simple Newton iteration, implemented in the FrontEnd program [58]. Since the dependence of BR($\mu \to e\gamma$) on M_{seesaw} is nearly linear, convergence is usually reached within a few steps.

We already mentioned that BR($\widetilde{\chi}_2^0 \to \widetilde{\chi}_1^0 l_i l_j$) depends on the mass spectrum, especially on the relation between the neutralino and the slepton masses. To find regions in the parameter space where the contribution of the sleptons and thus the whole branching ratio is largest, we performed parameter scans over the m_0-$m_{1/2}$-plane while fixing BR($\mu \to e\gamma$). The results of this scans are shown in Fig. 7.6 for BR($\widetilde{\chi}_2^0 \to \widetilde{\chi}_1^0 \mu e$), Fig. 7.7 for BR($\widetilde{\chi}_2^0 \to \widetilde{\chi}_1^0 \tau e$) and Fig. 7.8 for BR($\widetilde{\chi}_2^0 \to \widetilde{\chi}_1^0 \tau \mu$). We see that there is a clear threshold where the branching ratios come up to sizable orders of magnitude in the range of a few percent. The reason for that one finds by looking at the mass spectrum: When the left charged sleptons become lighter than the neutralino $\widetilde{\chi}_2^0$ and thus get on-shell in the diagram of Fig. 7.1, the branching ratio for the decay becomes large. This level crossing effect is illustrated in Fig. 7.9. Here we see that the critical influence comes from the left sleptons which go on-shell at $m_{1/2}$ values of about 1550 GeV – exactly the point where the LFV branching ratios become sizable. This confirms the assumption of section 5.3 where we considered in

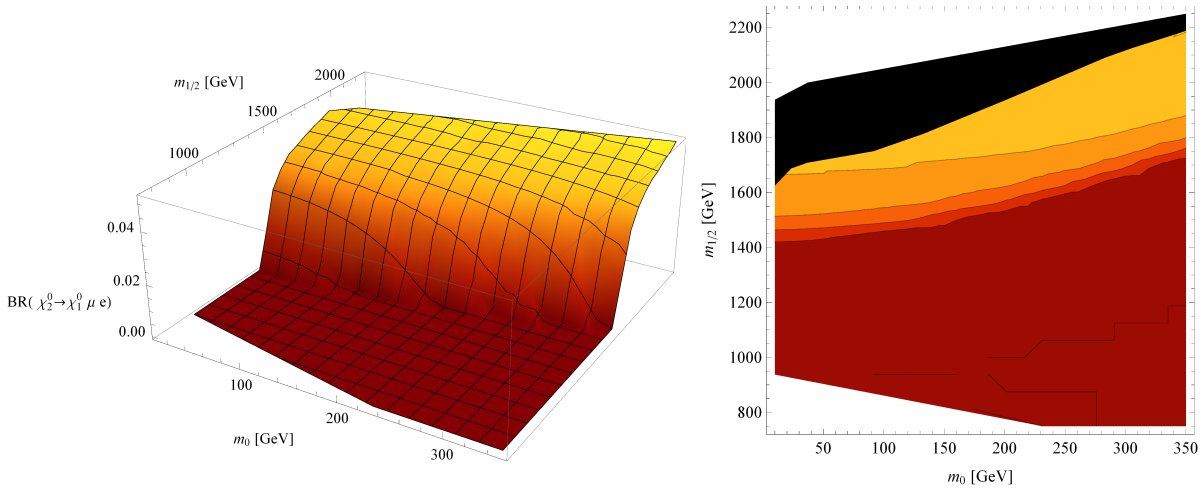

Figure 7.6: BR($\widetilde{\chi}_2^0 \to \widetilde{\chi}_1^0 \mu e$) at fixed BR($\mu \to e\gamma$) for variation of m_0 and $m_{1/2}$. The neutrino mixing parameters are at tri-bi-maximal values, $A_0 = 0$ GeV, $\tan(\beta) = 10$, $\mathrm{sgn}(\mu) = +1$, $R = \mathbb{1}$. The contour levels from red to yellow are (0.00, 0.01, 0.02, 0.03, 0.04). The black region in the contour plot is excluded by a charged LSP.

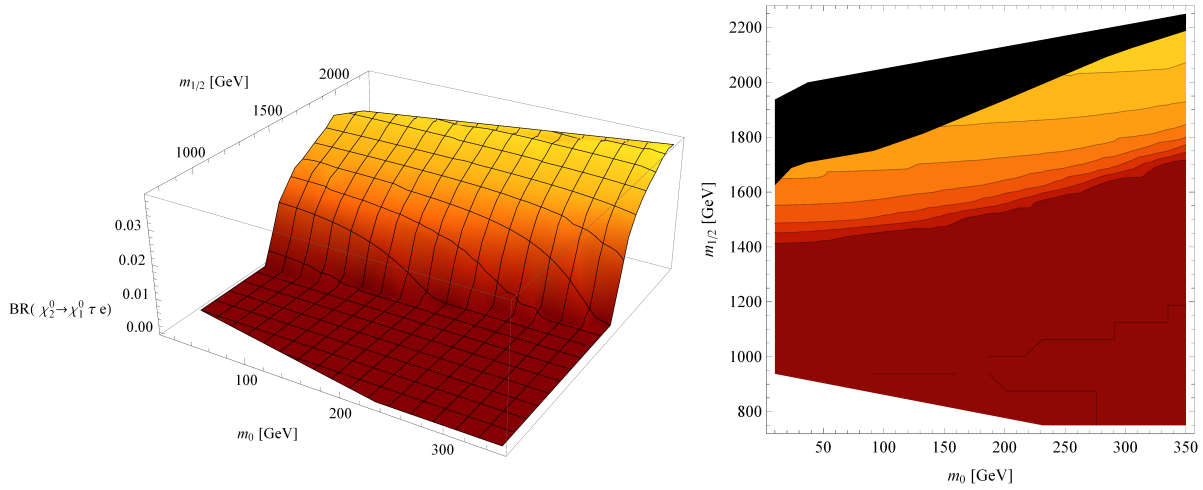

Figure 7.7: BR($\widetilde{\chi}_2^0 \to \widetilde{\chi}_1^0 \tau e$) corresponding. Fig. 7.6. The contour levels from red to yellow are (0.00, 0.005, 0.01, 0.015, 0.02, 0.025, 0.03, 0.035).

a first approximation only the LL type mass insertions for the left-handed sleptons. The masses of the involved particles at an examplary mSUGRA point are shown in Tab. 7.1 where one can see that the left sleptons are significantly heavier than the right ones, carrying very similar masses among themselves, respectively.

From Figs. 7.6, 7.7 and 7.8 we notice that the threshold depends strongly on the gaugino mass parameter $m_{1/2}$ but varies only slightly with the scalar mass parameter

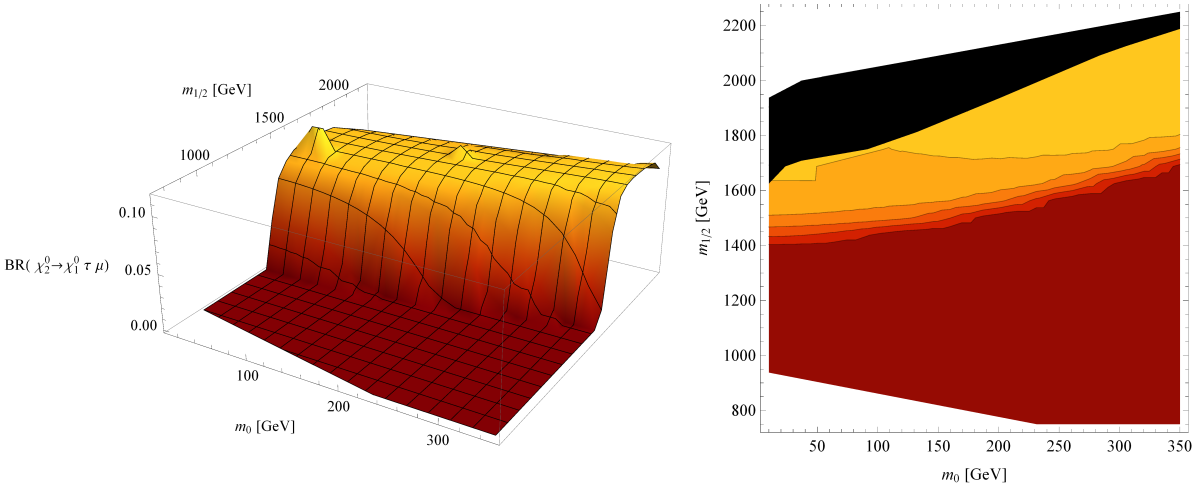

Figure 7.8: BR($\widetilde{\chi}_2^0 \to \widetilde{\chi}_1^0 \tau\mu$) corresponding. Fig. 7.6. The contour levels from red to yellow are (0.00, 0.02, 0.04, 0.06, 0.08, 0.1).

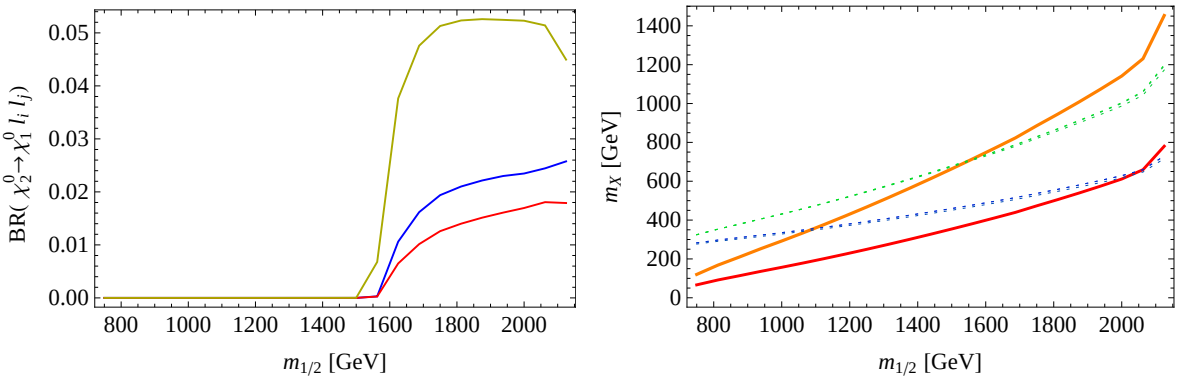

Figure 7.9: BR($\widetilde{\chi}_2^0 \to \widetilde{\chi}_1^0 l_i l_j$) (left panel) for $m_0 = 250$ GeV compared to the mass spectrum of the neutralinos $\widetilde{\chi}_2^0$ (orange), $\widetilde{\chi}_1^0$ (red) and the charged sleptons (dashed lines); the right sleptons $\widetilde{l}_1$, $\widetilde{l}_2$, $\widetilde{l}_3$ (blue) are lighter than the left ones $\widetilde{l}_4$, $\widetilde{l}_5$, $\widetilde{l}_6$ (green). The neutrino parameters are at tri-bi-maximal values, normal neutrino mass hierarchy and $R = \mathbb{1}$; M_{seesaw} varies to fit BR($\mu \to e\gamma$) to the bound.

m_0. Especially the asymmetric regions in the m_0-$m_{1/2}$-plane are interesting, preferring large $m_{1/2}$ and rather small m_0 values. After crossing this limit, the branching ratios aproach some kind of saturation, i.e. they increase only slightly with larger $m_{1/2}$, so we reach up to 4% for BR($\widetilde{\chi}_2^0 \to \widetilde{\chi}_1^0 \mu e$), 3% for BR($\widetilde{\chi}_2^0 \to \widetilde{\chi}_1^0 \tau e$) and 8% for BR($\widetilde{\chi}_2^0 \to \widetilde{\chi}_1^0 \tau\mu$). However, at $m_{1/2}$ values this large, the right sleptons do soon become lighter than the neutralino $\widetilde{\chi}_1^0$. Therefore it is no longer the LSP, but one of the charged leptons takes its place, and so these regions are no longer interesting (cf. 3.6). Therefore, we assume the most promising parameter points to be close to

sparticle	mass [GeV]	main character
$\widetilde{\chi}_1^0$	484.58	$\widetilde{B}^0$
$\widetilde{l}_1$	539.64	$\widetilde{\tau}_R$
$\widetilde{l}_2$	549.78	$\widetilde{\mu}_R$
$\widetilde{l}_3$	549.82	$\widetilde{e}_R$
$\widetilde{l}_4$	839.53	$\widetilde{\tau}_L$
$\widetilde{l}_5$	847.54	$\widetilde{\mu}_L$
$\widetilde{l}_6$	849.59	$\widetilde{e}_L$
$\widetilde{\chi}_2^0$	906.38	$\widetilde{W}^0$

Table 7.1: Masses of the sleptons and lighter neutralinos for an exemplary point of Fig. 7.9: $m_0 = 250$ GeV, $m_{1/2} = 1800$ GeV, $M_{\text{seesaw}} = 6.57 \cdot 10^{13}$ GeV and $\text{BR}(\mu \to e\gamma) = 2.25 \cdot 10^{-12}$. The right column gives the dominating particle character of each mass eigenstate as given by the respective mixing matrices.

the thresholds. The regions excluded by featuring a charged slepton LSP are drawn black in the contour plots.

Since the influence of the mass spectrum is crucial, the variation of the trilinear coupling parameter A_0 has also been tested. In Fig. 7.10 the contour plot of Fig. 7.6 for $\text{BR}(\widetilde{\chi}_2^0 \to \widetilde{\chi}_1^0 \mu e)$ is repeated twice for $A_0 = -1000$ GeV and $A_0 = +1000$ GeV, respectively. The limit is shifted to higher $m_{1/2}$ values in both cases, though only slightly for positive A_0 and clearly more for negative A_0. Here, the maximum BR values after crossing the threshold hardly change; only $\text{BR}(\widetilde{\chi}_2^0 \to \widetilde{\chi}_1^0 \tau\mu)$ increases at $A_0 = +1000$ GeV up to 12%. Indeed, this effect is small and does not change the overall order of magnitude compared to the values at $A_0 = 0$ GeV, but it also has effects on the mass spectrum, allowing also regions that are excluded for $A_0 = 0$ GeV because of a slepton LSP. Fig. 7.11 displays the variation of the $\text{BR}(\widetilde{\chi}_2^0 \to \widetilde{\chi}_1^0 l_i l_j)$ with A_0, reaching a maximum at about 300 GeV.

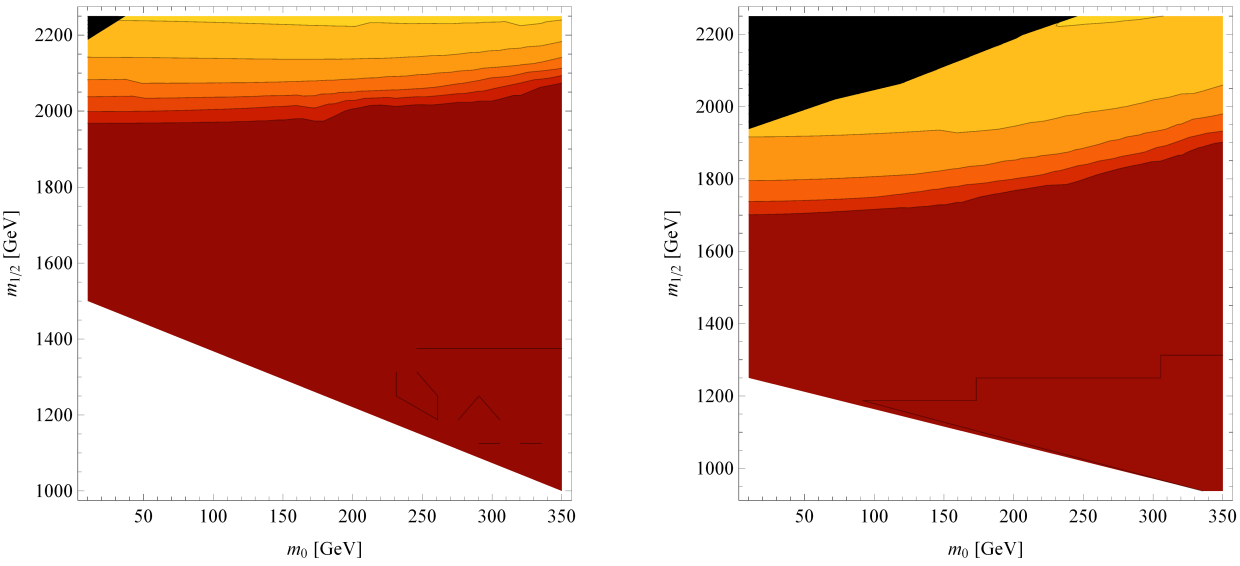

Figure 7.10: Contour plots like in Fig. 7.6 for various A_0 parameter values: $A_0 = -1000$ GeV (left panel) and $A_0 = +1000$ GeV (right panel). The contour levels from red to yellow are (0.00, 0.01, 0.02, 0.03, 0.04, 0.05) for the left and (0.00, 0.005, 0.01, 0.015, 0.02, 0.025, 0.03) for the right plot.

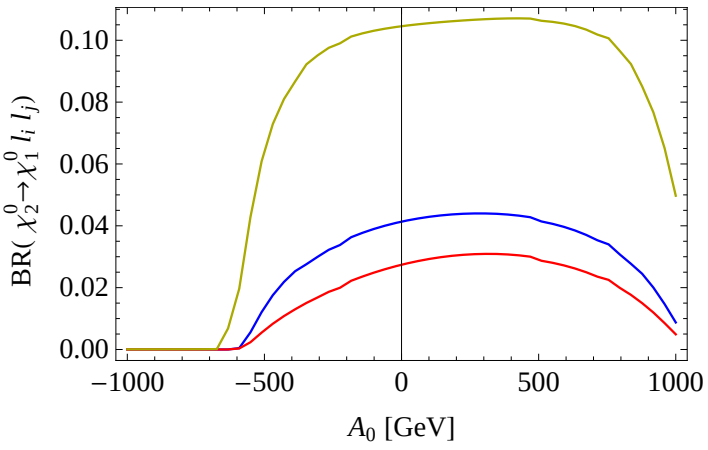

Figure 7.11: BR($\widetilde{\chi}_2^0 \to \widetilde{\chi}_1^0 \mu e$) (blue), BR($\widetilde{\chi}_2^0 \to \widetilde{\chi}_1^0 \tau e$) (red) and BR($\widetilde{\chi}_2^0 \to \widetilde{\chi}_1^0 \tau \mu$) (yellow) versus the trilinear mSUGRA parameter A_0 for two **24**-plets, $m_0 = 250$ GeV, $m_{1/2} = 1800$ GeV and the basic tri-bi-maximal neutrino mixing parameters.

7.3 Branching ratios and cross sections

In the next step we calculated the production cross section σ of the neutralino $\widetilde{\chi}_2^0$ for a $\sqrt{s} = 14$ TeV proton-proton collision times the branching ratio of the

respective LFV decay for promising regions of the parameter space. In the narrow-width-approximation [65, 66], one can to this to simplify the complexity of scattering amplitudes by assuming that the cross section for a process factorizes into a production cross section of an unstable particle and the branching ratio of its decay into the final state particles:

$$\sigma = \sigma_{\text{prod}} \times \frac{\Gamma}{\Gamma_{\text{tot}}} = \sigma_{\text{prod}} \times \text{BR} \tag{7.4}$$

The calculation of the production cross section of the neutralino $\widetilde{\chi}_2^0$ was done in the same way as in [67] using the package `LHC FASER` [68]. This program interpolates for a given spectrum the production cross sections of the colored sparticles between certain points that have been calculated before with `PROSPINO` [69] at 1-loop order.

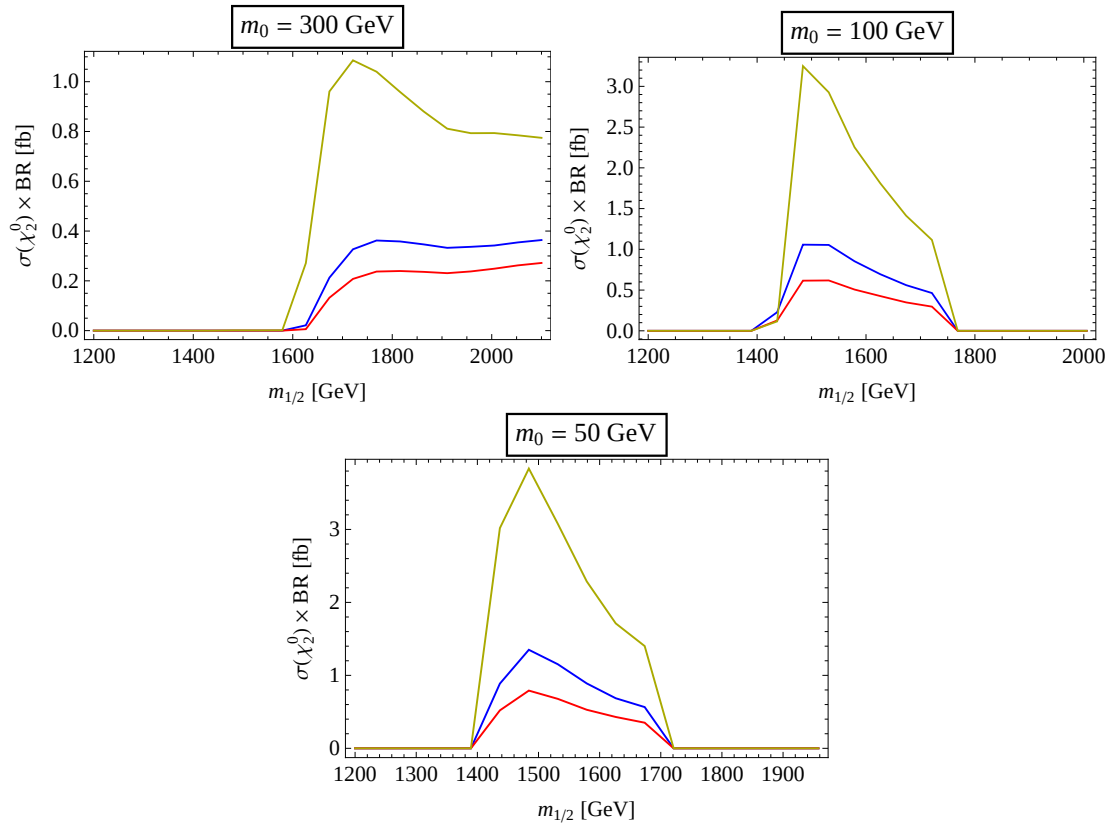

Figure 7.12: Grid calculation of $\sigma(\widetilde{\chi}_2^0) \times \text{BR}(\widetilde{\chi}_2^0 \to \widetilde{\chi}_1^0 \mu e)$ (blue), $\sigma(\widetilde{\chi}_2^0) \times \text{BR}(\widetilde{\chi}_2^0 \to \widetilde{\chi}_1^0 \tau e)$ (red) and $\sigma(\widetilde{\chi}_2^0) \times \text{BR}(\widetilde{\chi}_2^0 \to \widetilde{\chi}_1^0 \tau \mu)$ (yellow) in femtobarn over $m_{1/2}$ for different values of m_0; all other parameters are fixed at the values of e. g. Fig. 7.11. The edges arise from a finite resolution.

Fig. 7.12 shows this calculation for variation of $m_{1/2}$ and three different fixed m_0 values. Obviously, $\sigma \times$BR gets into sizable orders of magnitude at the same thresholds as observed in the previous section. For $m_0 = 50$ GeV and $m_0 = 100$ GeV one can state a sudden decrease above a certain $m_{1/2}$ value where the neutralino

$\widetilde{\chi}_1^0$ becomes heavier than the lightest slepton, leading to a charged LSP, which is excluded by dark matter constraints. $\sigma\times$BR is largest for the decay $\widetilde{\chi}_2^0 \to \widetilde{\chi}_1^0 \tau\mu$ with values up to a few femtobarn. With

$$n = \sigma(\widetilde{\chi}_2^0) \times \mathrm{BR}(\widetilde{\chi}_2^0 \to \widetilde{\chi}_1^0 l_i l_j) \cdot L \tag{7.5}$$

we get the result that, with an expected luminosity of $L = 100$ fb^{-1} for the $\sqrt{s} =$ 14 TeV LHC run, at least a few hundred events could be seen. We suspect that the observed points with the highest $\sigma\times$BR are near to the maximum. With an even finer and more extensive parameter study these values could be increased a little bit. However, since the calculation of the production cross sections has an uncertainty up to 20%, this effort is not appropriate.

The appearance of a large τ–μ flavor violation could be observed in many models that include LFV [70]. Of course it arises mainly from the fact that the other flavor combinations (especially μ–e) are constrained strongly from low energy data. As shown in the previous sections, these constraints also lead to suppressed neutralino decays with the same flavor violation. However, since the τ leptons decay already in the detector, they cannnot be measured as good as muons or electrons, so the potential to find $\widetilde{\chi}_2^0 \to \widetilde{\chi}_1^0 e\mu$ may be higher than for the decays including τ leptons in the final state.

7.4 Monte Carlo study

For the last step of our phenomenological studies we chose the most promising parameter point from the previous studies (cf. Fig. 7.12)

$$m_0 = 50 \text{ GeV},\ m_{1/2} = 1484 \text{ GeV},\ A_0 = 0 \text{ GeV},\ \tan_\beta = 10 \text{ and } \mu > 0 \tag{7.6}$$

and performed a Monte Carlo simulation for the LFV $\widetilde{\chi}_2^0$ decays using the program `WHIZARD` [71, 72]. The `WHIZARD` model file for the seesaw III as well as the parameter input file were generated with `SARAH` [59–61] resp. `SUSY Tool Box` [73]. A Les Houches Accord input file to calculate the spectrum for this point is shown in the appendix A. From the calculations in section 7.3 we obtained for this point the values

$$\sigma(\widetilde{\chi}_2^0) \times \mathrm{BR}(\widetilde{\chi}_2^0 \to \widetilde{\chi}_1^0 \mu e) = 1.35037 \text{ fb} \Rightarrow n_{\mu e} = 135 \text{ events} \tag{7.7a}$$

$$\sigma(\widetilde{\chi}_2^0) \times \mathrm{BR}(\widetilde{\chi}_2^0 \to \widetilde{\chi}_1^0 \tau e) = 0.79119 \text{ fb} \Rightarrow n_{\tau e} = 79 \text{ events} \tag{7.7b}$$

$$\sigma(\widetilde{\chi}_2^0) \times \mathrm{BR}(\widetilde{\chi}_2^0 \to \widetilde{\chi}_1^0 \tau\mu) = 3.83413 \text{ fb} \Rightarrow n_{\tau\mu} = 383 \text{ events} \tag{7.7c}$$

for a luminosity $L = 100$ fb^{-1}. These cross sections are calculated at 1-loop level, whereas the Monte Carlo study only considers tree-level diagrams. However, since we also know the tree-level cross section from the `PROSPINO` interpolation, we can scale the simulation results by the so-called K factor

$$K = \frac{\sigma_{\mathrm{NLO}}}{\sigma_{\mathrm{LO}}} \tag{7.8}$$

to get an approximation for the 1-loop values. Since the K factor depends on the colored particles involved in the cascade, it is equal for the different lepton combinations in the final state and given by

$$K \approx 1.18. \tag{7.9}$$

For each process we simulated the number of events given by Eq. 7.7 as expected from the 1-loop calculations. However, for these numbers of events the expected edge structure [74] could not be observed well because of large statistical fluctuations. So we increased them by a factor 3, assuming a high-luminosity LHC run with 300 fb^{-1} that is still under discussion.

The detector signal is specified by two leptons with distinct flavor and charge $l_i^{\pm}$, $l_j^{\mp}$, two hadronic jets from the squark decays Eq. 7.2 and missing transverse energy $\not{E}_T$ from the escaping neutralino LSPs $\widetilde{\chi}_1^0$. Assuming narrow width approximation, we considered only the cascade decays

$$pp \to \widetilde{q}_{L/R}\widetilde{q}_{L/R} \to q\widetilde{\chi}_1^0 + q\widetilde{\chi}_2^0 \to qq\widetilde{\chi}_1^0\widetilde{\chi}_1^0 l_i l_j \tag{7.10}$$

and neglected the small contributions from gluino pair or gluino-squark pair production. We summed over all charges and flavors expect for top quarks in the final states since they have to be reconstructed in a special way. For the last step of Eq. 7.10, we did not use narrow width approximation but considered all contributing diagrams. Therefore, also off-shell particles are allowed, with the respective consequences for kinematics.

To distinguish the signal from possible background processes it is convenient to look at the mass distribution of the two leptons in the final state. The invariant mass is given by

$$m_{l_i l_j}^2 = (p_{l_i} + p_{l_j})^2. \tag{7.11}$$

Considering the kinematics of such two body decays as was done in [74], we expect characteristic edges in the invariant di-lepton mass spectra. Their positions depend on the mass of the intermediate slepton $\widetilde{l}_k$

$$\left(m_{l_i l_j}^{\text{edge}}\right)^2 = \frac{(m_{\widetilde{\chi}_2^0}^2 - m_{\widetilde{l}_k}^2)(m_{\widetilde{l}_k}^2 - m_{\widetilde{\chi}_1^0}^2)}{m_{\widetilde{l}_k}^2}. \tag{7.12}$$

For the spectrum at the chosen point we get the values listed in Tab. 7.2 where also the neutralino masses are shown. From Tab. 7.1 and Fig. 7.9 we know that the contributions from the right sleptons can be neglected, since the channels including these particles have tiny BRs. We expect the main edge at about 140 GeV; here the differences between the $m_{l_i l_j}^{\text{edge}}$ of the different channels including left sleptons can lead to a less sharp edge. However, statistics can produce single events between this threshold and the $m_{l_i l_j}^{\text{edge}}$ value of the right sleptons at about 230 GeV.

For τ leptons in the final state, we have to consider the effects of subsequent decays: Since the neutrinos cannot been seen in the detector, leptonic decay channels

sparticle	mass [GeV]	$m_{l_i l_j}^{\text{edge}}$ [GeV]
$\widetilde{\chi}_1^0$	344.58	
$\widetilde{l}_1$	376.92	213.07
$\widetilde{l}_2$	385.95	233.86
$\widetilde{l}_3$	385.98	232.93
$\widetilde{l}_4$	621.94	148.32
$\widetilde{l}_5$	625.05	139.27
$\widetilde{l}_6$	625.89	136.72
$\widetilde{\chi}_2^0$	646.96	

Table 7.2: Mass spectrum of the involved neutralinos and the sleptons at the chosen parameter point Eq. 7.6; the right column shows the respective values of $m_{l_i l_j}^{\text{edge}}$ for the different slepton channels.

cannot be distinguished from primary electrons or muons. Thus, only the hadronic jet-like τ decays can be considered to detect it. For this reason the edges will become less sharp for the final states including τ leptons. This smearing arises from neutrino emission. Therefore, the process with μ–e in the final state is very interesting in spite of the fact that less events are expected than for τ–μ.

Figs. 7.13, 7.14 and 7.15 show the results of the signal studies where one can state the characteristic edges in the distribution over the invariant mass of the leptons. For μ–e in the final state, we observe these edges at the expected values. As we expected, the main contributions stem from $\widetilde{l}_5$ and $\widetilde{l}_6$ which are mainly $\widetilde{\mu}$- and $\widetilde{e}$-like, respectively. The τ–e case shows a similar behavior but is harder to evaluate due to the smaller number of events. We state that the mostly $\widetilde{\tau}$-like slepton $\widetilde{l}_4$ gives a small contribution compared to $\widetilde{l}_6$. For τ–μ scenario, we can guess the characteristic double edge structure. The first edge stems from cascades including $\widetilde{l}_5$, whereas the other one at about 148 GeV comes from the $\widetilde{l}_4$ contribution. A few events exceed this threshold; this effect arises due to the off-shell particles.

To estimate the potential for the discovery of the LFV $\widetilde{\chi}_2^0$ decays, we need the ratio of signal to possible background events. In this work, this could not be done in a satisfactory manner. However, when we set suitable cuts for the search – especially for missing transverse energy $\not{E}_T$ –, we strongly can reduce the SM background that arises mostly from neutrinos escaping the detector. This was discussed in [70] for τ–μ in the final state where also a detector simulation for the ATLAS experiment [2] can be found. For our simulation we chose a cut of

$$\not{E}_T > 75 \text{ GeV}. \tag{7.13}$$

Together with a limit on the detection angle θ between the beam axis and the

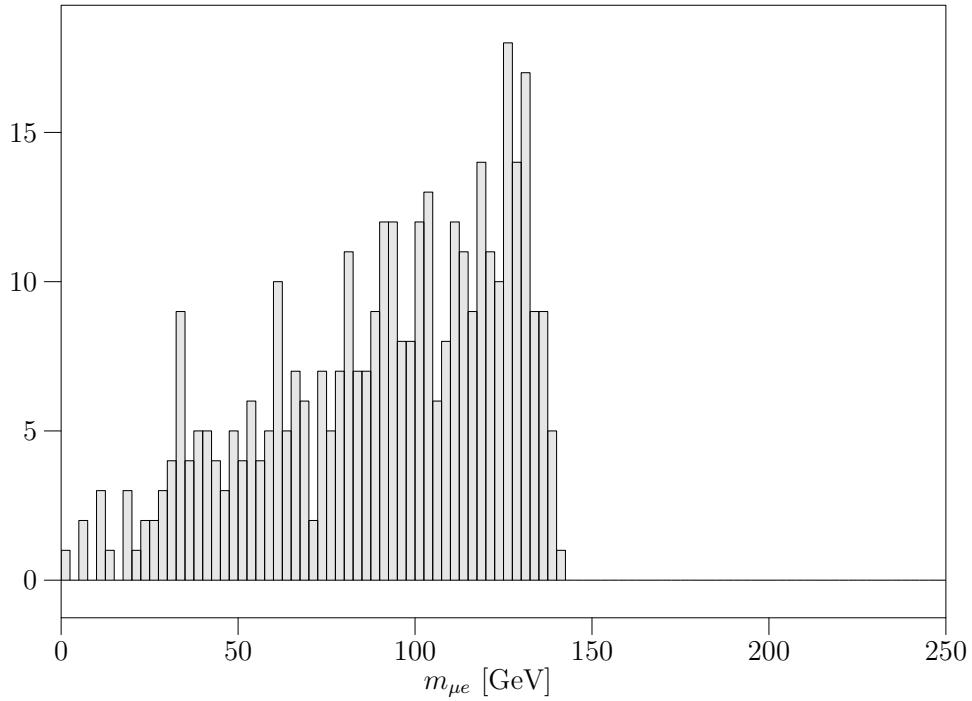

Figure 7.13: Invariant mass distributions for $\widetilde{\chi}_2^0 \to \widetilde{\chi}_1^0 \mu e$ for 405 simulated events assuming a luminosity of 300 fb^{-1}; 378 events passed the cuts.

momentum direction of the respective particle

$$|\eta| = |-\ln \tan(\theta/2)| < 2.5, \tag{7.14}$$

this cut only threw away less than 7% of the simulated signal events leading to the total numbers of events shown in the respective figures.

The largest SM contributions stem from $t\bar{t}$ production. Nevertheless, a more important issue are the background reactions from the decay of supersymmetric particles, arising from different decay cascades of the squarks and the gluino. In particular, the production of chargino pairs that decay into pairs of W bosons and neutralinos can generate a sizable number of background events, since the W bosons can decay into $l_i^{\pm}\nu_i^{\mp}$ with different flavor. Stemming from different decay chains, the charged leptons in such processes are uncorrelated. Therefore, we expect the invariant mass distributions of the charged leptons in these processes to be relatively flat or even slightly decreasing with increasing $m_{l_i l_j}$ [74]. Hence, there is a justified hope that the triangular edge structure of the LFV signal can still be observed over this flat background, but this needs to be tested in the future.

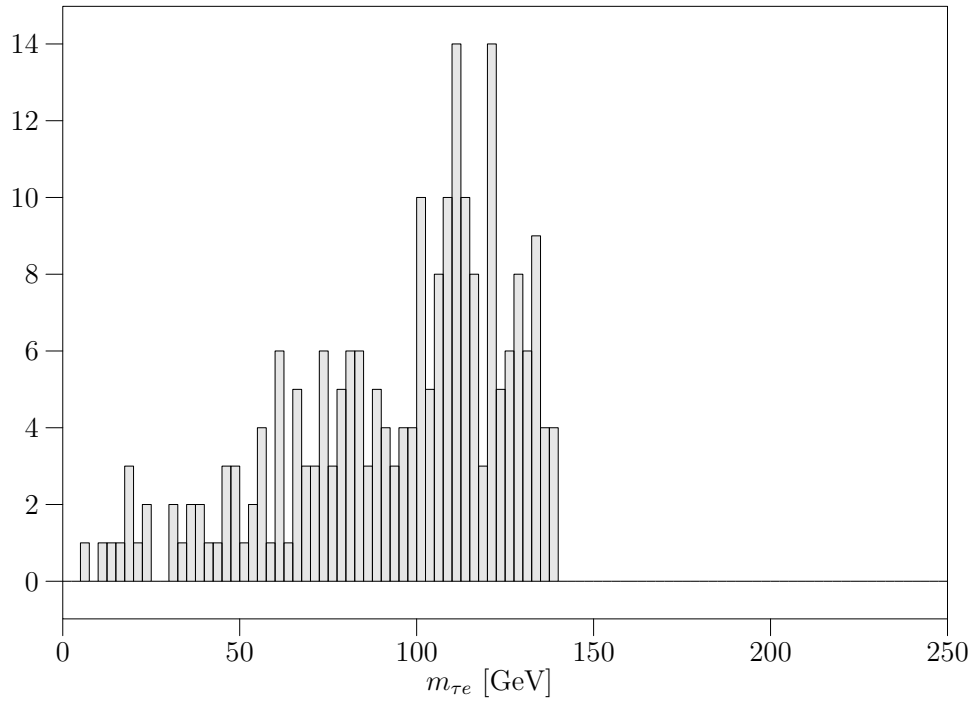

Figure 7.14: Invariant mass distributions for $\widetilde{\chi}_2^0 \to \widetilde{\chi}_1^0 \tau e$ for 237 simulated events; 224 events passed the cuts.

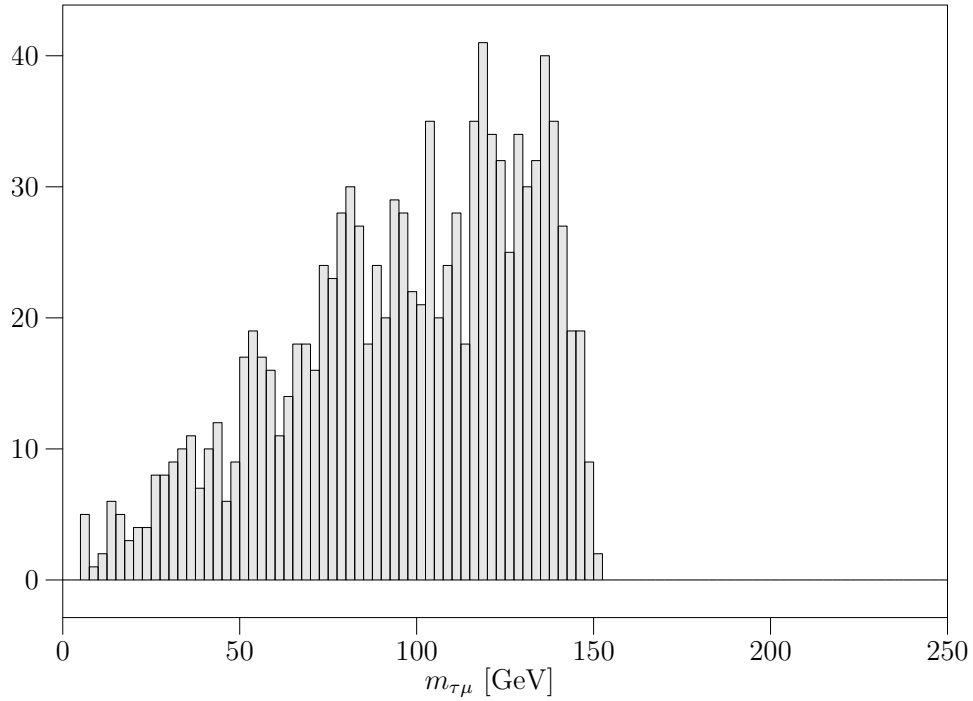

Figure 7.15: Invariant mass distributions for $\widetilde{\chi}_2^0 \to \widetilde{\chi}_1^0 \tau \mu$ for 1149 simulated events; 1099 events passed the cuts.

Chapter 8

Summary and outlook

In this work we have studied the phenomenological properties of the supersymmetric seesaw type III. This mechanism introduces at least two heavy fermionic triplets belonging to the adjoint representation of $SU(2)_L$ to the particle spectrum of the MSSM. These new states generate the neutrino masses and mixings required to explain neutrino oscillation measurements. To maintain gauge coupling unification, the triplets are embedded in **24**-plets under $SU(5)$. After breaking this symmetry to the SM gauge group at the scale M_{GUT}, these **24**-plets decompose into different representations of $SU(3)_C \times SU(2)_L \times U(1)_Y$. Two of these components have the same quantum numbers as the aforementioned fermionic triplet and the singlet right-handed neutrino. Therefore, the **24**-plet always produces a combination of type I and type III seesaw.

According to present data one massless or very light neutrino is still possible. For that case, the realization with two **24**-plets also leads to a viable model. To describe three similar neutrino masses, we need three generations of **24**-plets in general. Since the new particles are charged under the SM gauge group, they also contribute to the β coefficients of the RGEs, leading to a stronger running of the gauge couplings and thus a lighter sparticle spectrum than in the type I model. The new heavy states also induce off-diagonal entries in the left slepton squared mass matrix. This can produce large contributions to the branching ratios of rare lepton decays like $l_i \to l_j \gamma$ and $l_i \to 3l_j$ via 1-loop diagrams including charged sleptons and sneutrinos. Compared to the seesaw type I, these BRs are increased in the type III for similar mSUGRA parameters: On the one hand, this is due to the lighter sparticles, since the BRs scale like high inverse powers of SUSY masses. The other reason is that the off-diagonal entries induced by the seesaw mechanism are larger in the type III model.

However, these branching ratios are constrained to tiny values by direct searches, especially $\mathrm{BR}(\mu \to e\gamma)$ where the current experimental bound is $2.4 \cdot 10^{-12}$. So, the first aim of this work was to study the parameter space with respect to these experimental constraints. In order to do so, we have used the mass insertion approximation which allowed us to calculate first estimates to understand the behavior of the BRs. Then we have tested these results by numerically calculating the spectra and branching ratios. Indeed, we found that the BRs behave in the same way as the

mass insertions.

For two generations of **24**-plets, we obtain a working model by choosing a sufficiently low seesaw scale. However, we have shown that a higher M_{seesaw} also can be realized as soon as we achieve special cancellations arising between different contributions to the off-diagonal entries in the slepton squared mass matrix. These cancellations appear for various combinations of mass hierarchies and mixing angles. In the three-generation model we find a different situation: As long as no accidental cancellation arises, we find $\text{BR}(\mu \to e\gamma)$ to be above the experimental bound in general – for all allowed values of the seesaw scale. Nevertheless, we have found that such cancellations appear in distinct parameter constellations. We have investigated them for both real and complex non-zero values of the seesaw specific parameters and the neutrino mixing parameters within the range allowed by experiment. Another important role is played by the hierarchies of the heavy masses (degenerate or hierarchical) and of the neutrino masses and the value of the lightest neutrino mass. Altogether, there are many different parameter points where the three **24**-plet model has not yet been excluded by experiment, even if $\text{BR}(\mu \to e\gamma)$ is constrained to values a few orders of magnitude smaller than the current bound. Then, of course, an even more precise fine tuning is required. The bounds for other LFV decays like $l_i \to 3l_j$ do not produce additional strong constraints on our models: We have investigated these decays and stated that their BRs behave similarly to $\text{BR}(l_i \to l_j\gamma)$, thus not leading to further conflicts with data as long as the latter ones are sufficiently suppressed.

In the next step we have considered lepton flavor violating decays of the supersymmetric particles that can potentially be observed at the LHC, with a focus of the decay of the next-to-lightest neutralino $\widetilde{\chi}_2^0$ into two leptons with different flavor and the lightest neutralino $\widetilde{\chi}_1^0$, in regions where $\widetilde{\chi}_1^0$ is the LSP. This process is mediated by sleptons and thus its branching ratio becomes large as soon as they are the only on-shell particles. In general, we have found that these decays behave similarly to the rare lepton decays mentioned above, especially concerning the cancellation points. Therefore, we have used an iterative calculation to fix $\text{BR}(\mu \to e\gamma)$ to values close to the experimental bound by varying the seesaw scale. With this procedure we have tested the influence of the mSUGRA parameters on the LFV $\widetilde{\chi}_2^0$ decay in the two **24**-plet model. We could identify regions where the branching ratios are in the order of several percent – up to 10% for $\text{BR}(\widetilde{\chi}_2^0 \to \widetilde{\chi}_1^0\tau\mu)$. For these interesting points we have estimated the cross sections (resp. $\sigma\times\text{BR}$) for the flavor violating cascade decays with the result that at least a few hundred events can be found at a $\sqrt{s} = 14$ TeV LHC with a luminosity of $L = 100\ \text{fb}^{-1}$. Finally, we have done a Monte Carlo simulation on this issue for three different lepton signals. Studies on possible background processes, especially on SUSY background reactions, still have to be done. Also signals including more than two jets in the final state arising from cascades including gluinos have to be tested. In total, we expect that there is a good chance to see flavor violating processes at the LHC if a scenario of the supersymmetric seesaw type III is realized in nature.

For further studies it would be interesting to check the LHC phenomenology also for the three-generation model. To do this, one has to consider a cancellation point where $\mathrm{BR}(\mu \to e\gamma)$ is suppressed, followed by a search for the most suitable mSUGRA parameters to achieve large BRs for the LFV neutralino decays, at least for $\mathrm{BR}(\widetilde{\chi}_2^0 \to \widetilde{\chi}_1^0 \tau e)$ and $\mathrm{BR}(\widetilde{\chi}_2^0 \to \widetilde{\chi}_1^0 \tau \mu)$. Similar to the case of two **24**-plets where $\mu \to e\gamma$ was suppressed naturally for a suitable seesaw scale, we also expect large $\mathrm{BR}(\widetilde{\chi}_2^0 \to \widetilde{\chi}_1^0 \mu e)$ if we go near a cancellation so that $\mathrm{BR}(\mu \to e\gamma)$ is below but close to the bound again.

If $\mu \to e\gamma$ or other rare lepton decays could be measured in the near future, the parameter space of the model could be determined more precisely. On the other hand, if the bound should be shifted to even lower values, special cancellations would turn out to be even more necessary.

Appendix A

Input file

SUSY Les Houches Accord input file LesHouches.in for the data point Eq. 7.6 to run the program `SPheno` [56, 57].

```
Block MODSEL                # Select model
 3    10                     # mSugra
 5    2                      # CP violation
 6    1                      # switching on flavour violation
12    1000                   # Q Scale
Block SMINPUTS              # Standard Model inputs
 2   1.166390E-05       # G_F, Fermi constant
 3   1.190000E-01       # alpha_s(MZ) SM MSbar
 4   9.118760E+01       # Z-boson pole mass
 5   4.200000E+00       # m_b(mb) SM MSbar
 6   1.712000E+02       # m_top(pole)
 7   1.777000E+00       # m_tau(pole)
Block MINPAR                # Input parameters
 1   5.000000000E+01      # m0
 2   1.48421050E+03       # m12
 4   1                  # sign(mu)
 5   0.000000E+00       # A0
Block EXTPAR                # Input parameters
25   1.000000E+01       # tanb
Block SPhenoInput       # SPheno specific input
 1  -1                 # error level
 2   1                 # SPA conventions
11   1                 # calculate branching ratios
12   1.00000000E-04    # write only branching ratios larger than this value
21   0                 # calculate cross section
38   2                 # gives loop level used in the RGEs
39   1                 # writes additional SLHA file SPheno_1.spc
Block YB3IN             #
   1  1    -5.25194830E-02   # Re[Y_(b,1,1)]
   1  2    -5.25194830E-02   # Re[Y_(b,1,2)]
   1  3     5.25194830E-02   # Re[Y_(b,1,3)]
   2  1     0.00000000E+00   # Re[Y_(b,2,1)]
   2  2    -1.54748190E-01   # Re[Y_(b,2,2)]
   2  3    -1.54748190E-01   # Re[Y_(b,2,3)]
   3  1     6.00000000E-06   # Re[Y_(b,3,1)]
   3  2     0.00000000E+00   # Re[Y_(b,3,2)]
   3  3     0.00000000E+00   # Re[Y_(b,3,3)]
```

```
Block ImYB3IN          #
 1   1   0.00000000E+00 # Re[Y_(b,1,1)]
 1   2   0.00000000E+00 # Re[Y_(b,1,2)]
 1   3   0.00000000E+00 # Re[Y_(b,1,3)]
 2   1   0.00000000E+00 # Re[Y_(b,2,1)]
 2   2   0.00000000E+00 # Re[Y_(b,2,2)]
 2   3   0.00000000E+00 # Re[Y_(b,2,3)]
 3   1   0.00000000E+00 # Re[Y_(b,3,1)]
 3   2   0.00000000E+00 # Re[Y_(b,3,2)]
 3   3   0.00000000E+00 # Re[Y_(b,3,3)]
Block MWMIN            #
 1   1  2.50113000E+13      #
 2   2  2.50113000E+13      #
 3   3  1.00000000E+17      #
```

References

[1] L. Evans and P. Bryant, "LHC Machine", *J. Instrum.* **3** (2008), abridged version of the LHC Design Report (CERN-2004-003), S08001. 164 p.

[2] G. Aad et al., "The ATLAS Experiment at the CERN Large Hadron Collider", *JINST* **3** (2008), S08003.

[3] R. Adolphi et al., "The CMS experiment at the CERN LHC", *JINST* **3** (2008), S08004.

[4] J. Wess and B. Zumino, "A Lagrangian Model Invariant Under Supergauge Transformations", *Phys. Lett.* **B49** (1974), 52.

[5] B. Cleveland et al., "Measurement of the solar electron neutrino flux with the Homestake chlorine detector", *Astrophys. J.* **496** (1998), 505–526.

[6] Y. Fukuda et al., "Evidence for oscillation of atmospheric neutrinos", *Phys. Rev. Lett.* **81** (1998), 1562–1567, arXiv:hep-ex/9807003.

[7] K. Eguchi et al., "First results from KamLAND: Evidence for reactor anti-neutrino disappearance", *Phys. Rev. Lett.* **90** (2003), 021802, arXiv:hep-ex/0212021.

[8] Q. Ahmad et al., "Direct evidence for neutrino flavor transformation from neutral current interactions in the Sudbury Neutrino Observatory", *Phys. Rev. Lett.* **89** (2002), 011301, arXiv:nucl-ex/0204008.

[9] P. Adamson et al., "Measurement of the neutrino mass splitting and flavor mixing by MINOS", *Phys. Rev. Lett.* **106** (2011), 181801, arXiv:1103.0340 [hep-ex].

[10] E. Ma, "Pathways to naturally small neutrino masses", *Phys. Rev. Lett.* **81** (1998), 1171–1174, arXiv:hep-ph/9805219.

[11] M. Gell-Mann, P. Ramond, and R. Slansky, "Complex spinors and unified theories", *Conf. Proc.* **C790927** (1979), 315–321.

[12] T. Yanagida, "Horizontal symmetry and masses of neutrinos", *Conf. Proc.* **C7902131** (1979), 95.

[13] R. N. Mohapatra and G. Senjanovic, "Neutrino Mass and Spontaneous Parity Violation", *Phys. Rev. Lett.* **44** (1980), 912.

[14] R. Foot, H. Lew, X. G. He, and G. C. Joshi, "Seesaw neutrino masses induced by a triplet of leptons", *Z. Phys.* **C44** (1989), 441.

[15] J. Adam et al., "New limit on the lepton-flavour violating decay $\mu^+ \to e^+\gamma$", *Phys. Rev. Lett.* **107** (2011), 171801, arXiv:1107.5547 [hep-ex].

[16] K. Hayasaka et al., "New search for $\tau \to \mu\gamma$ and $\tau \to e\gamma$ decays at Belle", *Phys. Lett.* **B666** (2008), 16–22, arXiv:0705.0650 [hep-ex].

[17] B. Aubert et al., "Searches for Lepton Flavor Violation in the Decays $\tau^\pm \to e^\pm\gamma$ and $\tau^\pm \to \mu^\pm\gamma$", *Phys. Rev. Lett.* **104** (2010), 021802, arXiv:0908.2381 [hep-ex].

[18] K. Hayasaka, "Recent Tau Decay Results at B Factories: Lepton Flavor Violating Tau Decays", *Conf. Proc.* **C100715** (2010), arXiv:1010.3746 [hep-ex].

[19] J. Esteves et al., "Supersymmetric type-III seesaw: lepton flavour violating decays and dark matter", *Phys. Rev.* **D83** (2011), 013003, arXiv:1010.6000 [hep-ph].

[20] B. Pontecorvo, "Mesonium and anti-mesonium", *Sov. Phys. JETP* **6** (1957), 429.

[21] K. Nakamura and others (Particle Data Group), "Review of Particle Physics", *Journal of Physics G* **37, 075021** (2010).

[22] K. Abe et al., "Indication of Electron Neutrino Appearance from an Accelerator-produced Off-axis Muon Neutrino Beam", *Phys. Rev. Lett.* **107** (2011), 041801, arXiv:1106.2822 [hep-ex].

[23] T. Schwetz, M. Tortola, and J. Valle, "Where we are on θ_{13}: addendum to 'Global neutrino data and recent reactor fluxes: status of three-flavour oscillation parameters'", *New J. Phys.* **13** (2011), 109401, arXiv:1108.1376 [hep-ph].

[24] T. Schwetz, M. Tortola, and J. Valle, "Global neutrino data and recent reactor fluxes: status of three-flavour oscillation parameters", *New J. Phys.* **13** (2011), 063004, arXiv:1103.0734 [hep-ph].

[25] P. Preuss, http://www.lbl.gov/Science-Articles/Archive/sabl/2006/Jul/03.html.

[26] P. F. Harrison, D. H. Perkins, and W. G. Scott, "Tri-bimaximal mixing and the neutrino oscillation data", *Phys. Lett.* **B530** (2002), 167, arXiv:hep-ph/0202074.

[27] M. Hirsch, S. Morisi, and J. Valle, "Modelling tri-bimaximal neutrino mixing", *Phys. Rev.* **D79** (2009), 016001, arXiv:0810.0121 [hep-ph].

[28] S. Glashow, "Partial Symmetries of Weak Interactions", *Nucl. Phys.* **22** (1961), 579–588.

[29] A. Salam, "Renormalizability of gauge theories", *Phys. Rev.* **127** (1962), 331–334.

[30] S. Weinberg, "A Model of Leptons", *Phys. Rev. Lett.* **19** (1967), 1264–1266.

[31] S. P. Martin, "A Supersymmetry primer", *Perspectives on supersymmetry II*, ed. by G. L. Kane, World Scientific Pub. Co., 1997, pp. 1–153, arXiv:hep-ph/9709356.

[32] J. Bagger and J. Wess, "Supersymmetry and supergravity", *Supersymmetry and Supergravity*, Princeton Univ. Press, 1990.

[33] I. Aitchison, "Supersymmetry and the MSSM: An Elementary introduction", (2005), Notes of Lectures for Graduate Students in Particle Physics Oxford, 2004 and 2005, arXiv:hep-ph/0505105.

[34] M. Drees, "An Introduction to supersymmetry", (1996), arXiv:hep-ph/9611409.

[35] M. Drees, R. Godbole, and P. Roy, *Theory and phenomenology of sparticles: An account of four-dimensional N=1 supersymmetry in high energy physics*, World Scientific, 2004.

[36] A. Redelbach, "SUSY seesaw model and phenomenological implications for leptonic processes at low energies and leptogenesis", Doktorarbeit, Universität Würzburg, 2009.

[37] J. Casas and A. Ibarra, "Oscillating neutrinos and $\mu \to e\gamma$", *Nucl. Phys.* **B618** (2001), 171–204, arXiv:hep-ph/0103065.

[38] W. Porod, "LHC phenomenology of supersymmetric models beyond the MSSM", *J. Phys. Conf. Ser.* **259** (2010), 012002, arXiv:1010.4737 [hep-ph].

[39] S. Weinberg, "Baryon and Lepton Nonconserving Processes", *Phys. Rev. Lett.* **43** (1979), 1566–1570.

[40] S. Weinberg, "Varieties of Baryon and Lepton Nonconservation", *Phys. Rev.* **D22** (1980), 1694.

[41] F. Borzumati and T. Yamashita, "Minimal supersymmetric SU(5) model with nonrenormalizable operators: Seesaw mechanism and violation of flavour and CP", *Prog. Theor. Phys.* **124** (2010), 761–868, arXiv:0903.2793 [hep-ph].

[42] A. Rossi, "Supersymmetric seesaw without singlet neutrinos: Neutrino masses and lepton flavor violation", *Phys. Rev.* **D66** (2002), 075003, arXiv:hep-ph/0207006.

[43] M. R. Buckley and H. Murayama, "How can we test seesaw experimentally?", *Phys. Rev. Lett.* **97** (2006), 231801, arXiv:hep-ph/0606088.

[44] P. Minkowski, "$\mu \to e\gamma$ at a Rate of One Out of 1-Billion Muon Decays?", *Phys. Lett.* **B67** (1977), 421.

[45] J. Schechter and J. W. F. Valle, "Neutrino Masses in $SU(2) \otimes U(1)$ Theories", *Phys. Rev.* **D22** (1980), 2227.

[46] T. P. Cheng and L. F. Li, "Neutrino Masses, Mixings and Oscillations in $SU(2) \otimes U(1)$ Models of Electroweak Interactions", *Phys. Rev.* **D22** (1980), 2860.

[47] M. Hirsch, S. Kaneko, and W. Porod, "Supersymmetric seesaw type II. LHC and lepton flavour violating phenomenology", *Phys. Rev.* **D78** (2008), 093004, arXiv:0806.3361 [hep-ph].

[48] A. Masiero, S. Vempati, and O. Vives, "Massive neutrinos and flavor violation", *New J. Phys.* **6** (2004), Focus Issue on 'Neutrino Physics' edited by F. Halzen, M. Lindner and A. Suzuki, 202, arXiv:hep-ph/0407325.

[49] A. Ibarra and G. G. Ross, "Neutrino phenomenology: The Case of two right-handed neutrinos", *Phys. Lett.* **B591** (2004), 285–296, arXiv:hep-ph/0312138.

[50] P. H. Chankowski et al., "Patterns of lepton flavor violation motivated by decoupling and sneutrino inflation", *Nucl. Phys.* **B690** (2004), 279–301, arXiv:hep-ph/0403180.

[51] B. Dutta and R. N. Mohapatra, "Lepton flavor violation and neutrino mixings in a 3×2 seesaw model", *Phys. Rev.* **D68** (2003), 056006, arXiv:hep-ph/0305059.

[52] M. De Gerone for the MEG Collaboration, "$\mu \to e\gamma$ and $\mu \to eee$ Status and perspectives", *Conf. Proc.* **FPCP2011** (2011), arXiv:1108.2670 [hep-ex].

[53] F. Borzumati and A. Masiero, "Large Muon and electron Number Violations in Supergravity Theories", *Phys. Rev. Lett.* **57** (1986), 961.

[54] A. Abada, A. J. R. Figueiredo, J. C. Romao, and A. M. Teixeira, "Probing the supersymmetric type III seesaw: LFV at low-energies and at the LHC", *JHEP* **1108** (2011), 099, arXiv:1104.3962 [hep-ph].

[55] M. Hirsch et al., "Probing minimal supergravity in type I seesaw with lepton flavour violation at the LHC", *Phys.Rev.* **D78** (2008), 013006, arXiv:0804.4072 [hep-ph].

[56] W. Porod, "SPheno, a program for calculating supersymmetric spectra, SUSY particle decays and SUSY particle production at e^+e^- colliders", *Comput. Phys. Commun.* **153** (2003), 275–315, arXiv:hep-ph/0301101.

[57] W. Porod and F. Staub, "SPheno 3.1: Extensions including flavour, CP-phases and models beyond the MSSM", (2011), arXiv:1104.1573 [hep-ph].

[58] J. Romao, A. del Moral, M. Hirsch, and A. Vicente, "FrontEndSPheno", Private communication; for further information contact jorge.romao@ist.utl.pt.

[59] F. Staub, "SARAH", (2008), arXiv:0806.0538 [hep-ph].

[60] F. Staub, "Automatic Calculation of supersymmetric Renormalization Group Equations and Self Energies", *Comput. Phys. Commun.* **182** (2011), 808–833, arXiv:1002.0840 [hep-ph].

[61] F. Staub, "From Superpotential to Model Files for FeynArts and CalcHep/ CompHep", *Comput. Phys. Commun.* **181** (2010), 1077–1086, arXiv:0909.2863 [hep-ph].

[62] F. F. Deppisch, F. Plentinger, and G. Seidl, "Lepton Flavor Violation in Complex SUSY Seesaw Models with Nearly Tribimaximal Mixing", *JHEP* **1101** (2011), 004, arXiv:1011.1404 [hep-ph].

[63] E. Arganda and M. Herrero, "Testing supersymmetry with lepton flavor violating τ and μ decays", *Phys. Rev.* **D73** (2006), 055003, arXiv:hep-ph/0510405.

[64] J. Hudson et al., "Improved measurement of the shape of the electron", *Nature* **473** (2011), 493–496.

[65] C. F. Uhlemann, "Narrow-width approximation in the MSSM", Diplomarbeit, Universität Würzburg, 2007.

[66] C. F. Uhlemann and N. Kauer, "Narrow-width approximation accuracy", *Nucl. Phys.* **B814** (2009), 195–211, arXiv:0807.4112 [hep-ph].

[67] J. Esteves et al., "Dark matter and LHC phenomenology in a left-right supersymmetric model", *JHEP* **1201** (2012), 095, arXiv:1109.6478 [hep-ph].

[68] H. K. Dreiner, M. Kramer, J. M. Lindert, and B. O'Leary, "SUSY parameter determination at the LHC using cross sections and kinematic edges", *JHEP* **1004** (2010), 109, arXiv:1003.2648 [hep-ph].

[69] W. Beenakker, R. Hopker, and M. Spira, "PROSPINO: A Program for the production of supersymmetric particles in next-to-leading order QCD", (1996), arXiv:hep-ph/9611232.

[70] J. Harz, "Lepton-Flavor-Verletzung am ATLAS-Experiment am Beispiel des Zerfalls $\widetilde{\chi}_2^0 \to \widetilde{\chi}_1^0 \tau\mu$", Masterarbeit, Universität Würzburg, 2010.

[71] W. Kilian, T. Ohl, and J. Reuter, "WHIZARD: Simulating Multi-Particle Processes at LHC and ILC", *Eur. Phys. J.* **C71** (2011), 1742, arXiv:0708.4233 [hep-ph].

[72] M. Moretti, T. Ohl, and J. Reuter, "O'Mega: An Optimizing matrix element generator", (2001), arXiv:hep-ph/0102195.

[73] F. Staub, T. Ohl, W. Porod, and C. Speckner, "A tool box for implementing supersymmetric models", (2011), arXiv:1109.5147 [hep-ph].

[74] A. Bartl et al., "Test of lepton flavor violation at LHC", *Eur. Phys. J.* **C46** (2006), 783–789, arXiv:hep-ph/0510074.

List of Figures

2.1 The possible neutrino mass hierarchies and their flavor composition [25]. 5

3.1 One-loop graphs for the quantum corrections to the Higgs squared mass by a fermion f (left) resp. a scalar S (right). 6

4.1 Principle of the seesaw mechanism [41]. 16
4.2 Seesaw type I. 16
4.3 Seesaw type II. 18
4.4 Seesaw type III. 19

5.1 SM 1-loop graph for BR($l_i \to l_j\gamma$) mediated by neutrinos and W bosons. 25
5.2 1-loop graphs dominating BR($l_i \to l_j\gamma$) via lepton flavor violation in the slepton sector. 25
5.3 The analogon to Fig. 5.2 for the three-body decays. 26
5.4 Dominating 1-loop graphs for BR($l_i \to l_j\gamma$) corresponding to Fig. 5.2; the LL type mass insertion is denoted by a cross. 26

6.1 Mass parameters M_1 (blue), M_2 (red), M_3 (yellow) on the left resp. $|M_Q|$ (blue), $|M_L|$ (red), $|M_E|$ (yellow) on the right panel versus the seesaw scale for the type III (solid lines) compared to type I (dashed lines). The mSUGRA parameter are as given in Eq. 6.2, neutrino data is not fitted. 31
6.2 BR($\mu \to e\gamma$) versus the seesaw scale for the seesaw type I (dashed), type II (dotted) and type III (solid). 31
6.3 BR($\mu \to e\gamma$) versus the seesaw scale for the two (dashed) and the three (solid) **24**-plet scenario; mSUGRA parameters like in Eq. 6.2. . 32
6.4 BR($\mu \to e\gamma$) versus the seesaw scale calculated with 1-loop (dashed) and 2-loop (solid) RGEs. 32
6.5 Δ^2_{12} (blue), Δ^2_{13} (red), Δ^2_{23} (yellow) to the left and the corresponding BR($\mu \to e\gamma$) (blue), BR($\tau \to e\gamma$) (red) and BR($\tau \to \mu\gamma$) (yellow) to the right over the reactor angle θ_{13} for real parameters with Dirac phases $\delta = 0$ (upper panels), $\delta = \pi$ (mid panels) and $\delta = 3\pi/4$ (lower panel). The M_W are degenerate at $M_1 = M_2 = M_3 = 10^{14}$ GeV. Small fluctuations in the BRs arised due to numerical effects. 34

6.6 BR($\mu \to e\gamma$) for three **24**-plets and $\delta = \pi$ with different hierarchies $M_1 = M_2 = 10^{14}$ GeV, $M_3 = 2 \cdot 10^{14}$ GeV (solid), $M_3 = 1 \cdot 10^{14}$ GeV (dashed) and $M_3 = 5 \cdot 10^{13}$ GeV (dotted); other parameters like in Fig. 6.5. 35
6.7 BR($\mu \to e\gamma$) (blue), BR($\tau \to e\gamma$) (red) and BR($\tau \to \mu\gamma$) (yellow) at two **24**-plets and $\delta = \pi$ for degenerate masses $M_1 = M_2 = 10^{14}$ GeV, (solid lines) and hierarchical masses $M_1 = 2{\cdot}10^{14}$ GeV, $M_2 = 10^{14}$ GeV, (dashed lines). 35
6.8 Δ^2_{12} (blue), Δ^2_{13} (red) and Δ^2_{23} (yellow) compared to the corresponding BR($l_i \to l_j\gamma$) (lower panels) for two **24**-plets by variation of $\sin(\phi)$ at normal neutrino mass hierarchy, Dirac phase $\delta = 0$ and a **24**-plet hierarchy $M_1 > M_2$ and the two possible **24**-plet mass orderings. . . . 37
6.9 Like Fig. 6.8 for inverse hierarchy. 37
6.10 Comparison of analytical Δ^2_{12} and numerical BR($\mu \to e\gamma$) calculation, respectively, for variation of $\sin(\phi_1)$ (solid) and $\sin(\phi_3)$ (dashed) with the other angles set to zero, for normal neutrino mass hierarchy, Dirac phase $\delta = 0$ and a **24**-plet hierarchy $M_1 > M_2 > M_3$. 38
6.11 Δ^2_{12} (blue), Δ^2_{13} (red) and Δ^2_{23} (yellow) versus $\sin(\phi_1)$ and $\sin(\phi_2)$, respectively, with real ϕ_1 values for different hierarchies of the **24**-plet masses M_1, M_2 and M_3. 39
6.12 Like Fig. 6.11 for variation of ϕ_3. 40
6.13 3-dimensional graphs of Δ^2_{12} by varying two ϕ_i angles at a fixed value of the third one for different mass hierarchies of the **24**-plets. 41
6.14 Δ^2_{12} for different m_1 values from 0 GeV (green) to 10^{-12} GeV (violet) on the left panel resp. as contour plot on the right panel. 42
6.15 Complex parameter scans of Δ^2_{12} over modulus $A(\phi_1)$ and phase $P(\phi_1)$ of the R parametrization angle ϕ_1 at normal (left panel) resp. inverse (right panel) neutrino mass hierarchy, tri-bi-maximal neutrino mixing and $M_3 > M_2 > M_1$. 43
6.16 Comparison of the two-body decays $l_i \to l_j\gamma$ (left panel) and the-three body decays $l_i \to 3l_j$ (right panel) for variation of $\sin(\phi_1)$ at normal neutrino mass hierarchy, Dirac phase $\delta = 0$ and a **24**-plet hierarchy $M_1 > M_2 > M_3$; l_i, $l_j = \mu$, e (blue); τ, e (red); τ, μ (yellow). 44

7.1 Tree-level diagram for the process $\widetilde{\chi}^0_2 \to \widetilde{\chi}^0_1 l_i l_j$, mediated by charged sleptons. 47
7.2 The diagram of Fig. 7.1 in the mass insertion approximation. 47
7.3 BR($l_i \to l_j\gamma$) (left panel) and BR($\widetilde{\chi}^0_2 \to \widetilde{\chi}^0_1 l_i l_j$) (right panel) versus the real R parametrization angle ϕ for two **24**-plets; mSUGRA parameters as given by Eq. 6.2, $M_2 > M_1$, U tri-bi-maximal, CP phase $\delta = 0$ and normal neutrino mass hierarchy. $i, j = \mu, e$ (blue); τ, e (red), τ, μ (yellow). 48
7.4 Like Fig. 7.3 for three **24**-plets with $M_3 > M_2 > M_1$, $m_0 = 250$ GeV and $m_{1/2} = 1800$ GeV and variation of ϕ_3 while $\phi_1 = \phi_2 = 0$. 48

7.5 3-dimensional plot for BR($\mu \to e\gamma$) (left panel) and BR($\widetilde{\chi}_2^0 \to \widetilde{\chi}_1^0 \mu e$) (right panel) by variation of ϕ_1 and ϕ_3. 49
7.6 BR($\widetilde{\chi}_2^0 \to \widetilde{\chi}_1^0 \mu e$) at fixed BR($\mu \to e\gamma$) for variation of m_0 and $m_{1/2}$. The neutrino mixing parameters are at tri-bi-maximal values, $A_0 =$ 0 GeV, $\tan(\beta) = 10$, $\mathrm{sgn}(\mu) = +1$, $R = \mathbb{1}$. The contour levels from red to yellow are (0.00, 0.01, 0.02, 0.03, 0.04). The black region in the contour plot is excluded by a charged LSP. 50
7.7 BR($\widetilde{\chi}_2^0 \to \widetilde{\chi}_1^0 \tau e$) corresponding. Fig. 7.6. The contour levels from red to yellow are (0.00, 0.005, 0.01, 0.015, 0.02, 0.025, 0.03, 0.035). . . . 50
7.8 BR($\widetilde{\chi}_2^0 \to \widetilde{\chi}_1^0 \tau \mu$) corresponding. Fig. 7.6. The contour levels from red to yellow are (0.00, 0.02, 0.04, 0.06, 0.08, 0.1). 51
7.9 BR($\widetilde{\chi}_2^0 \to \widetilde{\chi}_1^0 l_i l_j$) (left panel) for $m_0 = 250$ GeV compared to the mass spectrum of the neutralinos $\widetilde{\chi}_2^0$ (orange), $\widetilde{\chi}_1^0$ (red) and the charged sleptons (dashed lines); the right sleptons $\widetilde{l}_1$, $\widetilde{l}_2$, $\widetilde{l}_3$ (blue) are lighter than the left ones $\widetilde{l}_4$, $\widetilde{l}_5$, $\widetilde{l}_6$ (green). The neutrino parameters are at tri-bi-maximal values, normal neutrino mass hierarchy and $R = \mathbb{1}$; M_{seesaw} varies to fit BR($\mu \to e\gamma$) to the bound. 51
7.10 Contour plots like in Fig. 7.6 for various A_0 parameter values: $A_0 =$ -1000 GeV (left panel) and $A_0 = +1000$ GeV (right panel). The contour levels from red to yellow are (0.00, 0.01, 0.02, 0.03, 0.04, 0.05) for the left and (0.00, 0.005, 0.01, 0.015, 0.02, 0.025, 0.03) for the right plot. 53
7.11 BR($\widetilde{\chi}_2^0 \to \widetilde{\chi}_1^0 \mu e$) (blue), BR($\widetilde{\chi}_2^0 \to \widetilde{\chi}_1^0 \tau e$) (red) and BR($\widetilde{\chi}_2^0 \to \widetilde{\chi}_1^0 \tau \mu$) (yellow) versus the trilinear mSUGRA parameter A_0 for two **24**-plets, $m_0 = 250$ GeV, $m_{1/2} = 1800$ GeV and the basic tri-bi-maximal neutrino mixing parameters. 53
7.12 Grid calculation of $\sigma(\widetilde{\chi}_2^0) \times$ BR($\widetilde{\chi}_2^0 \to \widetilde{\chi}_1^0 \mu e$) (blue), $\sigma(\widetilde{\chi}_2^0) \times$ BR($\widetilde{\chi}_2^0 \to \widetilde{\chi}_1^0 \tau e$) (red) and $\sigma(\widetilde{\chi}_2^0) \times$ BR($\widetilde{\chi}_2^0 \to \widetilde{\chi}_1^0 \tau \mu$) (yellow) in femtobarn over $m_{1/2}$ for different values of m_0; all other parameters are fixed at the values of e. g. Fig. 7.11. The edges arise from a finite resolution. . . . 54
7.13 Invariant mass distributions for $\widetilde{\chi}_2^0 \to \widetilde{\chi}_1^0 \mu e$ for 405 simulated events assuming a luminosity of 300 fb^{-1}; 378 events passed the cuts. 58
7.14 Invariant mass distributions for $\widetilde{\chi}_2^0 \to \widetilde{\chi}_1^0 \tau e$ for 237 simulated events; 224 events passed the cuts. 59
7.15 Invariant mass distributions for $\widetilde{\chi}_2^0 \to \widetilde{\chi}_1^0 \tau \mu$ for 1149 simulated events; 1099 events passed the cuts. 59

List of Tables

2.1 Experimental best-fit values of global neutrino data from ref. [23]; see also [24]. The values in brackets are deviations for inverse mass hierarchy. 4

3.1 Chiral supermultiplets in the MSSM [31]. 9
3.2 Gauge supermultiplets in the MSSM [31]. 9

5.1 Current experimental bounds for the BRs of low energy two-body (left) and three-body (right) LFV decays. 24

7.1 Masses of the sleptons and lighter neutralinos for an exemplary point of Fig. 7.9: $m_0 = 250$ GeV, $m_{1/2} = 1800$ GeV, $M_{\text{seesaw}} = 6.57 \cdot 10^{13}$ GeV and $\text{BR}(\mu \to e\gamma) = 2.25 \cdot 10^{-12}$. The right column gives the dominating particle character of each mass eigenstate as given by the respective mixing matrices. 52
7.2 Mass spectrum of the involved neutralinos and the sleptons at the chosen parameter point Eq. 7.6; the right column shows the respective values of $m_{l_i l_j}^{\text{edge}}$ for the different slepton channels. 57

Danksagung

An dieser Stelle möchte ich allen danken, die zum Gelingen dieser Diplomarbeit beigetragen haben:

- Prof. Dr. Werner Porod für die Aufnahme in die Arbeitsgruppe, die interessante Themenstellung und jede erdenkliche Hilfe,
- dem Instituto de Física Corpuscular (IFIC) Valencia für einen mehrmonatigen Forschungsaufenthalt im Sommer 2011,
- Dr. Martin Hirsch für eine hervorragende Betreuung während dieser Zeit und eine Vielzahl wertvoller Tipps,
- Prof. Jorge Romao für die Bereitstellung des FrontEnd-Programms,
- Dr. Florian Staub für die geduldige Hilfestellung zu Problemen mit `SARAH` und `WHIZARD`,
- Dr. Ben o'Leary und Dr. Avelino Vicente für die Bereitstellung weiterer nützlicher Hilfsmittel,
- Lukas Mitzka für die Einarbeitung in `WHIZARD` und die Hilfe bei verschiedenen Problemen,
- Enrico Herrmann und Peter Thomassen für sorgfältiges Korrekturlesen dieser Arbeit,
- ihnen und vielen weiteren Kollegen und Kommilitonen für anregende und unverzichtbare physikalische Diskussionen während der Diplomarbeit und des gesamten Studiums,

und nicht zuletzt meiner Familie und allen Freunden und Verwandten, die ihren Teil zur erfolgreichen Durchführung des Studiums beigetragen haben.

Erklärung

Gemäß der allgemeinen Studien- und Prüfungsordung für die Diplomstudiengänge an der Julius-Maximilians-Universität Würzburg erkläre ich hiermit, dass ich diese Arbeit selbstständig verfasst, keine anderen als die angegebenen Quellen und Hilfsmittel benutzt habe und die Arbeit bisher keiner anderen Prüfungsbehörde unter Erlangung eines akademischen Grades vorgelegt habe.

Würzburg, den 1. März 2012

Christof Weiß